Freie Universität Berlin

Fachbereich Geowissenschaften / Institut für Geologische Wissenschaften

und

Deutsches GeoForschungsZentrum GFZ - Helmholtz Zentrum Potsdam

Department 6 Geotechnologien / Setion 6.1 Sedimentbeckenmodellierung

---

Towards a more sustainable utilization of the urban geological subsurface: Insights from 3D thermohydraulic models

Dissertation

zur Erlangung des Doktorgrades der Naturwissenschaften

"doctor rerum naturalium"

(Dr. rer. nat.)

eingereicht am

Fachbereich Geowissenschaften

der Freien Universität Berlin

von

Maximilian Frick

Berlin, November 2018

Erstgutachter:
Prof. Dr. Michael Schneider
Freie Universität Berlin

Zweitgutachterin:
Prof. Dr. Magdalena Scheck-Wenderoth
Rheinisch-Westfälische Technische Hochschule Aachen

Datum der Disputation: 20.12.2018

Remember that all models are wrong; the practical question is how wrong do they have to be to not be useful. - George E. P. Box and Norman R. Draper

Table of Contents

Lists

List of Figures

List of Tables

List of Symbols

Table 0.1.: List of symbols, parameters and abbreviations used in this thesis.

Symbol	Description
Variables	
S	Storage coefficient
p	Pore pressure
t	Time
q	Volumetric flux (Darcy velocity)
$Q^{()}$	Mass source-sink term
k	Permeability tensor
h	Hydraulic head
g	gravitational acceleration
T	temperature
Q_r	heat source function
C	Concentration
$\dot{m}$	Mass flux
Z_∞	Natural hydraulic head
D	Half doublet separation
$rf = 2D$	Final injected fluid radius, well separation
R	Borehole caliber = 0.065 m
a	Plant life time
M	Effective reservoir thickness
W	Lamberts Function
$\dot{Q}$	Heating power
c	mass-specific heat capacity
W	Working power
COP	Coefficient of performance
Greek	
ρ	Density
ϕ	Porosity
η	Viscosity
$\lambda^{()}$	Thermal conductivity
$\gamma(T,p)$	Compressibility of fluid phase
$\alpha(T,C,p)$	Density ratio
ζ	Relative temperature coefficient

Symbol	Description
Greek cont'd	
ω	Mass fraction
τ	Transmissivity
κ	Hydraulic conductivity
Super-/Subscripts	
eff	effective
f	fluid
s	solid
b	bulk
OP	Operation Point
P	Production
I	Injection
diff	Difference
min	Minimum
max	Maximum
Abbreviations	
m(.)a.s.l.	meter above sea level
MW_{th}	MW thermal
NEGB	Northeast German Basin
m b.s.	meter below surface
ES2050	Energy Systems 2050
ATES	Aquifer Thermal Energy Storage
CEBS	Central European Basin System
DEM	Digital Elevation Model
DHDN	Deutsches Hauptdreiecksnetz
MBS	Middle Buntsandstein
SR	Sedimentary Rotliegend
GWL	Groundwater Level
KH	Karolinenhöhe
FEM	Finite Element Method
(HH)BC	(Hydraulic head) Boundary condition

Declaration of Originality

I hereby certify, as the author of this thesis and as one of the main authors of the publications involved, that the work presented in this thesis was composed by and originated from me, except as acknowledged in text and related reference list. The work was not submitted previously to any other institutions.

Place, Date	Maximilian Frick

Acknowledgments

First and foremost I would like to thank Prof. Dr. Michael Schneider from the Freie Universität Berlin and Prof. Dr. Magdalena Scheck-Wenderoth from the German Research Centre for Geoscience GFZ - Helmholtz Centre Potsdam and Rheinisch-Westfälische Technische Hochschule RWTH Aachen for their supervision, the constructive discussions and the continuous support throughout this thesis. At the same time I would like to thank my mentor Dr. Mauro Cacace, for his supervision, continuous support, both scientifically as well as mentally, his patience and great input into all aspects concerning this thesis.

I would like to thank the Senate Department for Urban Development and the Environment of Berlin (SenStadtUm), Berlin waterworks (BWB), Ministry of Rural Development, Environment and Agriculture of the Federal State of Brandenburg (MRDEA) and the Waterways and Shipping Office (WSA) for providing the data and for their support during the preparation of this thesis. Furthermore I would like to thank DHI WASY for providing the academic license for FEFLOW and their constant support.

I would like to thank all former and present members of GFZ German Center for Geosciences section 6.1 (Basin Modeling) for the help, inspiration and support they gave me during this thesis. Thanks to Anna P., Anna T., Antoine, Cameron, Christian, Jessi, Judith, Lew and Nora. Special thanks go out to Ershad with whom I had the honor of sharing an office with during the time of this thesis.

Moreover, I would like to thank Nasrin Haacke with whom I had the pleasure to work with (as part of her Master's thesis) and who inspired and motivated me when I needed it and became a close friend.

I want to express my deep gratitude to all of my close friends who never stopped supporting me and at times put things into perspective when it was necessary. Special thanks in this regard go out to Julia Oschatz and Martin Lang.

My personal thanks also go to my family for their constant support and encouragement.

In the end I would like to thank the Freie Universität Berlin and the German Research Centre for Geoscience GFZ - Helmholtz Centre Potsdam for providing me with the possibility of carrying out this thesis and also the joint initiative Energy Systems 2050 (ES2050) for providing the funding.

Summary

In the context of the provision of clean renewable energy, the utilization of the subsurface of urban areas has been gaining more attention. Especially major urban centers like the city of Berlin, Germany, have moved into focus because of the major share in global CO_2-Emissions. One of the most promising mitigation factors for at least part of these emissions, is to rely on geothermal energy resources.

The subsurface of Berlin is characterized by a complex geological setting beneath which different, coupled heat transport processes interact and are also overprinted by anthropogenic activities to a certain degree. A major challenge herein is the specific present-day utilization scenario, featuring the production of groundwater from the shallow subsurface (drinking water supply) and extraction of shallow geothermal heat from the underground. Therefore, to predict and reconstruct observed temperature, pressure and mass distributions a precise knowledge of the geological configuration and physical parameters of the subsurface is key. In this thesis I attempt to provide answers to the aforementioned issues by relying on numerical modeling studies which are based on a detailed 3D reconstruction of the underground and on physical principles of heat-, fluid- and mass transport. I present models of increasing complexity and detail concerning all physical processes and boundary conditions at work, enabling detailed representations of the present state, and a reconstruction of the natural state of the system, that is, before any human intervention. Based on the understanding gained from these studies, I derive some conclusive asserts on sustainable utilization scenarios in the underground of Berlin, and based on similarities, of other large urban centers.

An initial set of models investigated, for a first time, the effect of major surface water bodies (lakes and rivers) on the thermal and hydraulic configuration of the subsurface. The results of these models show that major surface water bodies significantly modify the shallow to intermediate geothermal and hydrogeological setting especially where connected to areas showing a certain degree of overprinting by human activities. Due to groundwater production and associated lower hydraulic heads near the surface water bodies, forced infiltration from the latter is predicted, which fits observations closely. The thermal modifications are on the order of interest for shallow geothermal installations and also connect to a shift in areas most promising for exploitation.

The second set of models focused on reconstructing the natural state, that is, the state before pumping activities commenced. This step was deemed necessary in order to be able to quantify the modifications to the subsurface hydrothermal configuration as related to human activities. The reconstructed "natural" state shows a complete replenishment of the depression cones, resulting in a shift of recharge and discharge areas, where rivers and lakes display gaining conditions only. In contrast, models that integrate pumping activities, illustrate that the effects of subsurface production is larger, both in magnitudes and areal as well as depth extents, than previously captured by models that relied on fixed hydraulic surface boundary conditions only. The presence of active wells provides a more realistic representation of flow rates, the net

results of which is a sensitive modification of predicted fluid pathways, in agreement with the monitored hydraulics in Berlin (as exemplary demonstrated for the site of Karolinenhöhe).

In a latter stage, I carried out a quantitative study on the energetic potential of the underground, by conducting a systematic analysis of the geothermal potential stored at different levels beneath the city of Berlin. Two approaches were chosen to identify and quantify promising areas for geothermal utilization. The first approach makes direct use of modeled temperature distribution at different depth levels. These highly nonuniform distributions reflect a heterogeneous potential of heat in place in the underground. In the shallow subsurface, utilization for shallow geothermal heat production and storage could be opted for. In the deep subsurface heat and electricity production are deemed possible. Building on this, the second approach investigated two possible deep geothermal target horizons by simulating a hydrothermal power-plant utilizing the predicted temperatures as well as reservoir geometry and physical properties. The connected geothermal potential of the deeper subsurface then shows nominally promising results, depicting up to $\sim 10\,MW_{th}$ for a single virtual power plant at the most promising locality, while locally $0\,MW_{th}$ are encountered as well.

All of these model results show most importantly that the subsurface thermal, hydraulic and mass distribution is highly sensitive to the parameters under study, which highlights the amount of caution that should be given to any planned change in the utilization of this space. This relates to any planned geothermal utilization of the different groundwater compartments which should be studied in depth using the models of this thesis as starting conditions.

Zusammenfassung

Die Nutzung des Untergrundes städtischer Gebiete gewinnt im Rahmen der Bereitstellung sauberer erneuerbarer Energien zunehmend an Bedeutung. Vor allem Großstädte wie z.B. Berlin, Deutschland, sind aufgrund des hohen Anteils an den globalen CO_2-Emissionen in den Fokus gerückt. Einer der vielversprechendsten Minderungsfaktoren für zumindestens einen Teil dieser Emissionen ist die Einbeziehung von geothermischen Energiequellen.

Der Untergrund Berlins ist durch eine komplexe geologische Struktur gekennzeichnet, in der verschiedene, gekoppelte Wärmetransportprozesse interagieren und bis zu einem gewissen Grad auch von anthropogenen Einflüssen überlagert werden. Eine große Herausforderung ist dabei die spezifische heutige Nutzung des Untergrundes durch Förderung von Grundwasser (Trinkwasserversorgung) und Gewinnung von oberflächennaher Erdwärme. Für die Vorhersage und Rekonstruktion der beobachteten Temperatur-, Druck- und Stoffverteilungen ist daher eine genaue Kenntnis der geologischen Struktur und der physikalischen Parameter des Untergrundes entscheidend. In dieser Arbeit versuche ich, Antworten auf die oben genannten Probleme zu geben, indem ich mich auf numerische Modellierungsstudien beziehe, die ihrerseits auf einer detaillierten 3D-Rekonstruktion des Untergrundes und auf physikalischen Prinzipien des Wärme-, Flüssigkeits- und Stofftransports basieren. Ich zeige Modelle mit zunehmender Komplexität und Detailgenauigkeit in Bezug auf alle physikalischen Prozesse und Randbedingungen, welche detaillierte Darstellungen des gegenwärtigen Zustands ermöglichen und den natürlichen Zustand des Systems, d.h. vor jedem menschlichen Eingriff, rekonstruieren. Ausgehend von den Erkenntnissen aus diesen Studien ziehe ich Rückschlüsse zu nachhaltigen Nutzungsszenarien im Berliner Untergrund und in Anbetracht von Ähnlichkeiten auch zu vergleichbaren Ballungszentren.

Die erste Serie von Modellen untersuchte erstmalig den Einfluss großer Oberflächenwasserkörper (Seen und Flüsse) auf die thermische und hydraulische Konfiguration des Untergrundes. Die Ergebnisse dieser Modelle zeigen, dass große Oberflächenwasserkörper die oberflächennahen bis mittleren geothermischen und hydrogeologischen Verhältnisse signifikant beeinflussen, insbesondere wenn sie an Gebiete angrenzen, die einen gewissen Grad an Überprägung durch menschliche Aktivitäten aufweisen. Durch die Grundwasserförderung und der damit verbundenen niedrigeren hydraulischen Druckhöhen in der Nähe der Oberflächengewässer wird erzwungene Uferfiltration aus diesen vorhergesagt, was sich in den Beobachtungen widerspiegelt. Die thermischen Modifikationen sind vor Allem für oberflächennahe Geothermieanlagen von Bedeutung und damit verbunden kommt es auch zu einer Verschiebung in den für die Nutzung vielversprechendsten Bereichen.

Die zweite Serie von Modellen konzentrierte sich auf die Rekonstruktion des natürlichen Zustands, d.h. des Zustands vor Beginn der Grundwasserförderung. Dieser Zwischenschritt wurde für notwendig erachtet, um die Veränderungen der hydrothermalen Konfiguration im Untergrund im Bezug auf menschliche Aktivitäten quantifizieren zu können. Der rekonstruierte natürliche Zustand zeigt eine vollständige Wiederauffüllung der Absenktrichter, was zu einer

Verschiebung der Quell- und Senkgebiete führt, wobei nur grundwasseraufnehmende Flüsse und Seen existieren. Im Gegensatz dazu zeigen die Modelle, die Pumpaktivitäten einbeziehen, dass die Auswirkungen der unterirdischen Förderung sowohl in Größenordnungen als auch in den räumlichen und Tiefenausdehnungen größer sind als die, die bisher von Modellen erfasst wurden, die sich nur auf feste hydraulische Oberflächen-Randbedingungen bezogen haben. Das Berücksichtigen aktiver Brunnen ermöglicht eine realistischere Darstellung der Durchflussmengen, deren Ergebnis eine sensible Modifikation der vorhergesagten Strömungspfade ist, welche in Übereinstimmung mit der beobachteten Hydraulik in Berlin ist (wie exemplarisch für das Gebiet Karolinenhöhe gezeigt).

In der letzten Phase wurde eine quantitative Studie über das energetische Potenzial des Untergrundes durchgeführt, indem eine systematische Analyse des auf verschiedenen Tiefenebenen unterhalb der Stadt Berlin vorhandenen Geothermiepotenzials durchgeführt wurde. Es wurden zwei Ansätze gewählt, um vielversprechende Gebiete für die geothermische Nutzung zu identifizieren und zu quantifizieren. Der erste Ansatz nutzt die modellierte Temperaturverteilung in verschiedenen Tiefenstufen direkt. Diese sehr ungleichmäßigen Verteilungen spiegeln ein heterogenes Wärmepotenzial im Untergrund wider. Im flachen Untergrund sollte die Nutzung zur oberflächennahen geothermischen Wärmeerzeugung und -speicherung bevorzugt werden. Im tiefen Untergrund werden Wärme- und Stromerzeugung als realisierbar erachtet. Darauf aufbauend wurde ein zweiter Ansatz aufgestellt, welcher zwei potenzielle tiefe geothermische Zielhorizonte, durch Simulation eines hydrothermalen Kraftwerks unter Verwendung der vorhergesagten Temperaturen sowie der Lagerstättengeometrie und physikalischen Eigenschaften, untersucht. Das damit verbundene geothermische Potenzial des tieferen Untergrundes zeigt dann nominal vielversprechende Ergebnisse, die bis zu $\sim$ $10\,MW_{th}$ für ein einzelnes virtuelles Kraftwerk an der vielversprechendsten Stelle aufzeigen, während lokal auch $0\,MW_{th}$ angetroffen werden.

Diese Ergebnisse zeigen vor Allem, dass die unterirdische Temperatur-, Fluiddruck- und Massenverteilung sehr sensibel auf die untersuchten Parameter reagiert, woraus sich die besondere Vorsicht bei jeder geplanten Änderung der Nutzung dieses Raumes ergibt. Dies bezieht sich auf eine geplante geothermische Nutzung der verschiedenen Grundwasserstockwerke, die unter Verwendung der Modelle dieser Arbeit als Ausgangsbedingungen eingehend untersucht werden sollten.

1. Introduction

1.1. General Framework

The utilization of the shallow subsurface has been gaining increased attention in the last decades due to relatively new topics including radioactive waste disposal, underground gas storage, and most relevant for this thesis, geothermal energy extraction and usage. These emerging topics are considered promising to reach energy goals while minimizing related greenhouse gas emissions, especially in large urban areas (Reusswig et al., 2014). However, their integration in the current energetic portfolios requires to face a certain amount of challenges mostly related to a proper management of the subsurface resources. Especially the interactions that already arose or might arise in future utilization scenarios is a challenging topic. Following these statements, this thesis opts to gain new insights in these complex interactions, focusing on the utilization for groundwater production and geothermal utilization for the area of Berlin, capital city of the federal state of Germany, specifically.

In Berlin in particular, the provision of renewable, clean energy has gained increased attention in the context of policy changes (e.g. Twidell and Weir, 2015). To enlarge the portion derived from environmentally friendly resources within the total energetic city-wide portfolio is becoming an increasingly relevant point of discussion in the political agenda (Reusswig et al., 2014). Berlin, but in general all large urban areas, are deemed to be one of the major sources responsible for the ever rising emission of greenhouse gases into the atmosphere (Berlin $\frac{CO_2}{yr} = 19.5 * 10^9\, kg$, Doytsher et al., 2010; S. Berlin-Brandenburg, 2018c). The municipality of Berlin and its proximate surroundings host approximately 4 million inhabitants (S. Berlin-Brandenburg, 2018b,a) and have a primary energy consumption of $263 * 10^{15}\, J$ per year (S. Berlin-Brandenburg, 2018c). This energy is provided almost exclusively by non-renewable energy resources such as coal (20%), oil (36%), gas (30%) and imported electricity (largely from fossil resources, 9%, S. Berlin-Brandenburg (2018c)). In comparison, the share of renewables is limited to only 4%, with biofuels and biomass making up the largest share and geothermal energy only accounting for a small proportion (S. Berlin-Brandenburg, 2018c). This picture profiles even more substantially if considering the energy required for private and district heating only, with more than half of the total requirement (amounting to $\sim 44 * 10^{15}\, J$) provided by gas (67%), followed by coal (23%) and waste heat (7%).

Up to now, the energetic potential from heat energy extraction and production has been investigated only to a minor degree, mainly because of the complexity of its exploration and extraction from the underground. Geothermal energy is a kind of energy resource stored within the earths interior and therein heterogeneously distributed. A sustainable use of this type of resource requires a detailed explorative investigation stage, which should enable to characterize the level of heterogeneity of the hydrogeological and thermal configuration as well as the most relevant physical processes occurring in the subsurface. The unique feature of geothermal energy in comparison to other renewables, stems from it being continuously replenished in time

and the fact that it does not undergo drastic intermittent changes (Lior, 2010). Given these reasons, geothermal energy is currently being discussed as one of the most promising sources of energy to accommodate the base load energy demand (Huenges et al., 2013a). Depending on the thermal and pressure ambient conditions in the underground, geothermal reservoirs can be subdivided into two broad main categories, i.e. high and low enthalpy reservoirs. High enthalpy reservoirs represent by far the best studied and most utilized reservoirs. They are normally associated with relatively high natural subsurface temperatures and steam conditions as found in many volcanic areas around the world (e.g. Iceland - (Ragnarsson, 2003), New Zealand - (Boothroyd, 2009)). In contrast, low enthalpy systems show only moderate reservoir temperatures (normal conductive thermal gradient), their fluid is in a liquid state (though possible gas/steam phases might be encountered near wellbore areas), and are associated with porous and/or granitic rocks. These reservoirs are normally hosted in sedimentary basins, which show above average geothermal potential, given their geophysical characteristics. Due to their abundance worldwide, recent research efforts have been targeting the energetic potential of specific sedimentary basins with the goal to develop best practices to harness their vast energy resources. Major urban centers located in this setting are amongst the recently discussed promising areas for geothermal energy production. Especially those located in regions with above average geothermal potential have been identified to be worth further study in the short and long term. One such area is the municipality of Berlin, capital city of Germany. Berlin is located in the Northeast German Basin (NEGB), a sedimentary basin filled up with 10 km of Mesozoic to Cenozoic sedimentary rocks and characterized by an above average geothermal potential (Huenges et al., 2013a).

In terms of harnessing this energy resource, previous studies focused on the shallow subsurface compartments. This was done due to a number of reasons related to the detailed understanding of the subsurface, technical as well as economical limitations and lastly legal limitations (e.g. BBergG, 2016). However, the capacity of installed geothermal heat pumps is steadily increasing (Wedewardt, 2017; Limberg, 2018). These are limited to the shallow subsurface ($\leq 100\,m\,b.s.$) and recent estimates indicate that more than 7000 geothermal heat pumps are currently installed in the subsurface of the municipality of Berlin, producing overall more than $500 * 10^{12}\,J$ (S. Berlin-Brandenburg, 2018c). They are mainly located in depths $\leq 100\,m\,b.s.$, due to legal restrictions in Germany (BBergG, 2016). In this context, a possible utilization of geothermal resources at depths greater than 100 m b.s. can only be considered as a viable option on the base of a detailed risk investigation analysis. Only recently, attention has been moved to the potential of the deeper reservoirs (Kastner et al., 2015). The main outcome of the investigation by Kastner and co-workers was to provide an approximate estimate of the total energetic power extractable from single geothermal power plants (about $6\,MW_{th}$). Despite the intrinsic limitations in the study, their estimate opens for a new energetic perspective complementary to shallow geothermal installations. It is thus of major importance to provide a sound estimate of the energetic potential of the deeper subsurface, therefore addressing open scientific questions related to the distribution of temperature and fluid velocities with depth. With this thesis, I aim to unravel the first order characteristics of these processes by means of

numerical modeling techniques combining details of the 3D hydrogeological configuration of the underground and the coupled and non linear processes occurring in it. Estimating the geothermal potential also connects to the overarching project this thesis is set in: Energy Systems 2050 (ES2050). This joint initiative of the research field energy of the Helmholtz Association aims to improve the current understanding of energy systems and to develop technological solutions. In this context, the share and potential of geothermal energy provision (deep geothermal) as part of the future energy mix is to be quantified. Another aspect of subsurface utilization is aquifer thermal energy storage (ATES), which has been in use for an extended period of time (Sanner et al., 2005) and is proposed to be expanded as an element in the thermal energy sector (Blöcher et al., 2018).

The specific challenge of an envisaged utilization of the shallow and deep subsurface links back to the specific hydrogeological setting beneath the surface of Berlin. This is extremely relevant for the specific case of Berlin given that the drinking water supply is provided almost exclusively from the groundwater resources within the cities boundaries (Limberg and Thierbach, 1997; Möller and Burgschweiger, 2008). This utilization has been shown to influence the groundwater circulation in direct proximity of the water works (i.e. Massmann et al., 2007), but also in the far field (i.e. Möller and Burgschweiger, 2008). Moreover, these man-made (anthropogenic) effects are of special interest since the shallow aquifers from which the water is produced are possibly connected to the deeper aquifers below, which show higher salinities. Whether this is the case and to which degree these two compartments are hydraulically connected remains an open point of discussion, though there is evidence in both isotopic and chemical data pointing to a dynamic connection among the two aquifer compartments (Tesmer et al., 2007). A connected question is to which degree the shallow and deeper aquifers pore fluid mixing has been, and still is, promoted by extensive shallow groundwater pumping activities, the effects of which is still to be quantified on a city-wide scale (Cai et al., 2014). Here, increased concentrations of groundwater pollutants could also be related to riverine load in form of SO_4^{2-} (Graupner et al., 2014), which have been measured in wells of the municipality of Berlin (Maeng et al., 2010). This observation aligns with the general question of the level of hydraulic connectivity between surface water bodies and the groundwater and the possible problematics therein. This is also an important topic when discussing the provision of heat stored in the deeper sedimentary compartments, the possible detrimental effects of which have rarely been investigated so far.

Another manifestation of anthropogenic overprinting is found in increased groundwater and subsurface temperatures below the urban center of Berlin (Henning and Limberg, 2012). These so-called urban heat islands have been identified as a possible source of heat provision (Menberg et al., 2013, 2015), but may also have a significant influence on groundwater quality and ecology (Brielmann et al., 2009, 2011; Kuttler et al., 2017). In connection to this, ongoing and future geothermal applications should be carefully planned and their effects systematically analyzed and quantified. A number of local studies have already been published (i.e. Griebler et al., 2015; Wedewardt, 2017), but a city-wide analysis has not yet been attempted, which poses serious doubts on the correctness of estimations of the potential of shallow geothermal heat (Hirschl et al., 2011; Lange et al., 2017). It is therefore the main goal of this thesis to help in completing

such a risk assessment on the potential detrimental consequences from the use of shallow and also deep seated geothermal resources beneath Berlin in the light of the contributing physical processes as well as in relation to the specific hydrogeological setting of the shallow to deep subsurface. In this respect this study aligns, benefits and complements previous investigations which have been carried out in the study area.

1.2. Objectives of the Thesis

Inspired from the generic introduction above, I thereby pose three scientific questions that I will address and answer with this thesis. These are:

1. Surface Water - Groundwater - Interactions: What are the main hydrogeological characteristics of these interactions at depths of their dynamics and what are the main consequences for groundwater management and sustainability within an urban area? This question is mainly addressed in Chapter 3 as based on Frick et al. (2018a).

2. Natural versus anthropogenic forcing and their influence on the hydraulic and thermal subsurface configuration in urban areas: How to quantify their respective influence? This question is addressed in Chapter 4 as based on Haacke et al. (2018).

3. Geothermal potential and geothermal exploration: Can we make use of numerical models as effective additional tools? This is addressed in Chapter 5 and Chapter 6 as based on Scheck-Wenderoth et al. (2017) and in preparation in Frick et al. (In Preparation).

1.3. Overview over the Thesis

To provide an answer to the questions raised above, newly built 3D models of heat and fluid transport, which progressively integrate more data and focus on different aspects of these questions, will be investigated. Herein, the most important aspects include: (1) the pore pressure distribution and the related fluid velocity field and (2) the temperature distribution in the subsurface as predicted by the different model scenarios.

Before detailing the answers to the aforementioned open questions, I open the thesis with an introductory overview of the study area and the modeling framework (Chapter 2). This was done intentionally to provide the reader with background information (i) on the specific hydrogeological and thermal configuration in the subsurface of Berlin (Sections 2.1 to 2.3); and (ii) on the physics behind all numerical model results presented in the later chapters of the study (Section 2.4). A paragraph (Section 2.5) briefly summarizing the major outcomes of previous investigations done in the area was added with the aim to detail the playground in which the modeling activities of this thesis are centered in, as well as to highlight the novelty of the present study.

In Chapter 3 I address the first major open scientific question, that is, the one dealing with a proper quantification of surface water - groundwater - interactions on the city-wide hydrodynamics and thermal configuration. This was done by running 3D coupled thermohydraulic numerical simulations. These display increasing complexity in terms of integrated and considered elements of the upper hydraulic boundary condition, that is, additionally resolving lakes and rivers as 3D elements. Additionally, the surface geometry was reconstructed with newly available data. Hereby, the goal was to evaluate and quantify the spatial extent and vigor of the resulting coupled dynamics of these two components, both in terms of the regional hydraulics as well as temperatures.

As the first author of this manuscript, I was the main contributor. I constructed all underlying structural models presented and carried out the 3D coupled thermohydraulic simulations. Furthermore, I constructed all the figures and wrote the text. All co-authors, Magdalena Scheck-Wenderoth, Mauro Cacace and Michael Schneider, contributed with fruitful discussions to the interpretation of the modeling results.

Accepted as: Frick, M., Scheck-Wenderoth, M., Schneider, M., and Cacace, M. (2018a). "Surface to Groundwater Interactions beneath the City of Berlin - Results from 3D Models." In: *Geofluids* In Press.

The final publication will be available at:

`https://www.hindawi.com/journals/geofluids/contents/` under the Creative Commons Attribution License. Hindawi is kindly acknowledged since the article is used in this dissertation for non-commercial purposes.

Chapter 4 addresses the second question dealing with the effect of the superimposition of pumping activities on the hydrodynamic state of the system as discussed in the previous chapter. Therefore, I first describe the workflow followed to numerically represent the "natural" hydraulic state (i.e. the hydraulic state before the commissioning of the operating wells) in detail. In a second step, the effects of the pumping activities have been integrated, covering a period of approximately 100 years. Here the goal is not only to arrive at a proper quantification of the effects of human shallow activities on the hydraulic configuration at different depths. Indeed, by relying on physics-based models assisted by detailed information of both the subsurface hydrogeology and pumping histories, the study also enabled to evaluate the nonlinear interactions between natural versus anthropogenic forcing on the city-wide hydraulics, therefore providing a base to quantify the vulnerability of the water resources to human activities.

As the first co-author, I was a major contributor to the manuscript. Together with the first author (Nasrin Haacke) I constructed all models relevant for this paper by building on the models from Chapter 3. I was also equally involved in carrying out the coupled 3D thermohydraulic simulations, as well as drafting the paper including constructing the figures and writing the text. Mauro Cacace helped draft the manuscript. The design of the study was mainly conducted by myself with contributions from Magdalena Scheck-Wenderoth and Michael Schneider. Again, all co-authors contributed with fruitful discussions to the interpretation of the modeling results.

Published as: Haacke, N., Frick, M., Scheck-Wenderoth, M., Schneider, M., and Cacace, M.

(2018). "3-D Simulations of Groundwater Utilization in an Urban Catchment of Berlin, Germany." In: *Advances in Geosciences*. European Geosciences Union General Assembly 2018, EGU Division Energy, Resources & Environment (ERE) - EGU General Assembly 2018, Vienna, Austria, 8–13 April 2018. Vol. 45. Copernicus GmbH, pp. 177–184. DOI: 10.5194/adgeo-45-177-2018.

The final publication is openly accessible at: https://www.adv-geosci.net/45/177/2018/ under the Creative Commons Attribution License 3.0. Elsevier is kindly acknowledged since the article is used in this dissertation for non-commercial purposes.

Chapter 5 addresses the third question of the thesis by proposing and describing a workflow unifying models at different scales with the aim to optimize the predictability of numerical approaches for geothermal utilization prospects. Here a two stage approach is outlined, where an investigation of the results as based on the models by Frick et al. (2016b) and Scheck-Wenderoth et al. (2017) is carried out first, also comparing them to the ones obtained by the most advanced models produced for this thesis (Chapter 6). Based on this approach I thereby identify sites most suited for possible geothermal utilization and exploitation based on (a) predicted temperatures at selected depth levels and (b) an updated and modified investigation of operational geothermal potential along the lines of Kastner et al. (2013) and Kastner et al. (2015).

As the first co-author, I was a major contributor to the manuscript. I constructed the underlying 3D thermohydraulic and structural model and was largely involved in the construction of the figures. As first co-author I contributed to the manuscript and approved of the final draft.

As the first author of the paper in preparation I carried out all relevant calculations, prepared the underlying models and the manuscript. Björn Lewerenz contributed by writing useful tools and translating the code.

Part 1 is published as: Scheck-Wenderoth, M., Frick, M., Cacace, M., and Sippel, J. (2017). "Overcoming Spatial Scales in Geothermal Modeling for Urban Areas." In: *Energy Procedia* 125, pp. 98–105. DOI: 10.1016/j.egypro.2017.08.080.

The final publication is openly accessible at:

https://www.sciencedirect.com/science/article/pii/S1876610217335622 under the Creative Commons Attribution Non-Commercial No Derivatives License. Elsevier is kindly acknowledged since the article is used in this dissertation for non-commercial purposes.

Part 2 is in preparation as: Frick, M., Lewerenz, B., Kastner, O., Scheck-Wenderoth, M., Schneider, M., and Cacace, M. (In Preparation). "The Geothermal Potential of the Subsurface of Berlin."

Chapters 7 and 8 serve the purpose of aggregating the overall scientific findings of this thesis concerning the general merit and implications for groundwater safety as well as geothermal energy wherein the limitations of the models and methods presented in this theses and possible future work is examined.

2. Modeling Workflow

2.1. Geological Setting and Structural Model

This section focuses on the specific geological setting below Berlin, within the regional tectonic and geological basinal framework.

The study area is located in the Northeast German Basin (NEGB), a sub basin of the intracontinental Central European Basin System (CEBS, Bayer et al. (1997)). The sedimentary infill of these basins of Permian to Neogene age consist mainly of clastics, carbonates and rock salt (Bayer et al., 1997), underlain by variably thick volcanics of Permocarboniferous age (Scheck and Bayer, 1999) and a layer of highly compacted Permian sediments. The depth of the basement varies between -10,000 m a.s.l. in the basinal center and 0 m a.s.l. towards the southern margin, where the crystalline crust is close to the surface (Scheck-Wenderoth and Lamarche, 2005). The geological structure of the basin infill is depicted by variably thick Pre-Permian sediments (Maystrenko and Scheck-Wenderoth, 2013), followed by Permocarboniferous volcanics and highly compacted sandstones of Permian age (Sedimentary Rotliegend). The overlying Permian Zechstein unit consists mostly of rock salt and has been mobilized during several stages from the late Middle Triassic onward (Scheck et al., 2003), resulting in heterogeneous thickness distributions between 4,200 m (salt diapirs) and complete withdrawal. Consequently, the post Zechstein succession shows some extent of restructuration due to salt tectonics as expressed by increased thicknesses where the salt unit withdrew. This is evident in strongly thinned or pierced deposits of most Post-Zechstein strata, observable in most parts of the NEGB (Kaiser et al., 2011). These strata are mainly composed of clastics or carbonates of varying thicknesses. The thickness variations relate to two major processes: (1) the aforementioned salt mobilization and (2) glacial erosion (Sonntag, 2005; Kaiser et al., 2013b). The model area underwent numerous glacial and interglacial periods in the recent geological history, which strongly modified the geometry of the sedimentary units (Kaiser et al., 2013b; Noack et al., 2013). This is most clearly manifested in numerous glacial erosional channels of Elsterian age, locally cutting down through the base of the Oligocene Rupelian unit. This regional clay-rich unit therefore displays a discontinuous nature.

In this general geological frame, the 3D structural model used for this thesis was compiled from a large database mostly used to constrain the uppermost sedimentary sequence (Fig. 2.1), assisted by existing regional 3D structural models for the deeper geological strata (Frick et al., 2016b). This local database consists of 57 geological cross-sections which differentiate the different glacial cycles in high detail. These structural data were implemented in the geological model, resolving the top and base of the associated geological age (Zech and Stoltmann, 2012; Frick, 2015). Additionally, more than 620 well logs have been used to construct the structural model. Most of these wells and available cross sections are limited in their depth coverage (Fig. 2.1, less than -400 *m a.s.l.*). Three local deep seismic profiles were also implemented, depicting a depth coverage down to more than -4000 *m a.s.l.*, whereas the oldest resolved unit is of Permian age (Sedimentary

Rotliegend, Moeck et al. (2015)). To construct the geological surface of the Holocene, a high resolution DEM was utilized (Geodäsie, 2012). These data fail to resolve lake and river bottom surfaces (geological surface) and were therefore combined with water depth data for the surface water bodies to derive the elevation distribution of the top Holocene (see also Chapter 3, Frick et al. (2018a)). On top of these data, a previously existing model (Sippel et al., 2013) was utilized, which in turn is based on larger scale models incorporating regional trends outside of the model area boundaries. These are: (1) the gravity constrained lithosphere-scale 3D geological model of CEBS (grid resolution = 16x16 km, Maystrenko and Scheck-Wenderoth (2013)), (2) the 3D hydrostratigraphical model of the Cenozoic units in Berlin (grid resolution 500x500 m, Jaroch (2006), heavily revised), (3) larger scale 3D models of the shallow to intermediate subsurface based partly on (1), namely Noack et al. (2013) and Kaiser et al. (2013a), and (4) stratigraphic and lithological data from four deep boreholes (Sippel et al., 2013). All these data were digitized, processed, interpolated and integrated into the structural model used for this thesis via the modeling software Petrel©. The resulting structural model is depicted in Fig. 2.2, differentiating 20 geological units up to a depth of -6000 m.a.s.l., wherein 18 represent the sedimentary succession (2 Paleozoic, 8 Mesozoic and 8 Cenozoic) and 2 represent the underlying basement.

In order to help the reader to get accustomed to the local geology, but not to overwhelm the present description, the following description focuses on units of particular interest for (a) geothermal utilization and (b) groundwater utilization wherein they are not mutually exclusive. The focus will also be placed on the sedimentary succession, as the crustal structure has little influence on the processes and investigated depths of this thesis. The interested reader can refer to previous publications for more detailed information (Frick et al., 2015, 2016b).

Starting from the basement, the first unit of interest is namely the Permian Sedimentary Rotliegend, a geological unit composed of consolidated clastics with a porosity and permeability high enough to be considered as a potential target horizon for geothermal installations (Huenges and Ledru, 2011). The top of this unit is depicted by an elevation increase from NW to SE from -3800 m a.s.l. to -2800 m a.s.l. (Fig. 2.3f). The thickness of the unit displays its minima ($\geq 90\,m$) in the central model domain and increasing thicknesses towards the outer bounds with up to 450 m (Fig. 2.4f). Moving up in the sedimentary sequence, the second important unit is represented by the Zechstein Salt, acting as a hydraulic cap rock to the Rotliegend reservoir. This unit displays a very heterogeneous thickness and elevation distribution which derives from its mobilization during the early Mesozoic stages in the evolution of the NEGB and largely influences the geometry of all units above. The elevation of the top of this unit ranges from -150 m a.s.l. to -3200 m a.s.l. (Fig. 2.3e), with thickness maxima expressed in various salt diapirs (Fig. 2.4e 1-2, $max = 3450\,m$) and pillows (Fig. 2.4e 3-5) distributed around areas of strong salt withdrawal (Fig. 2.4e 6-10, $min = 0\,m$). The next unit of regional interest is represented by the Tertiary Middle Buntsandstein. This units consists predominantly of clastics showing relatively high poro-perm values in the range typically considered for viable geothermal installations (Huenges and Ledru, 2011). In comparison to the Sedimentary Rotliegend it depicts much shallower elevations between -150 m a.s.l. and -2500 m a.s.l. with minima and maxima spatially correlating with those of the Permian

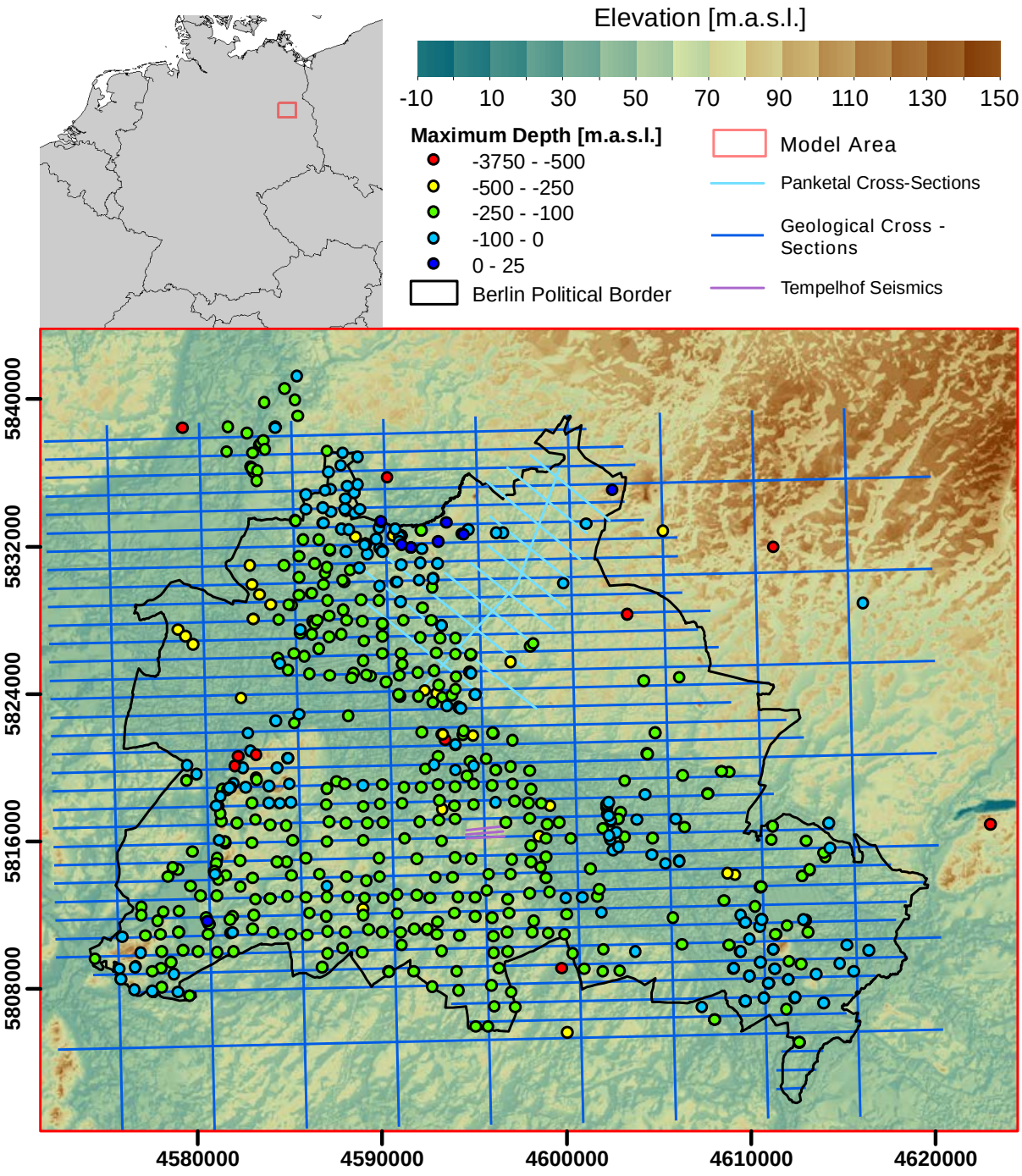

Figure 2.1.: Location of the model area in central Europe and database. As indicated, colored dots represent well positions inside the model area, dark blue lines show locations of the geological cross-sections (light blue lines show cross-sections cutting the Panketal aquifer), m.a.s.l.: meters above sea level; Coordinates [m] in Gauß-Krüger DHDN Zone 4. Please note, that larger scale 3D gravity constrained geological models were also utilized, especially, where no well data are available. After Frick et al. (2018a).

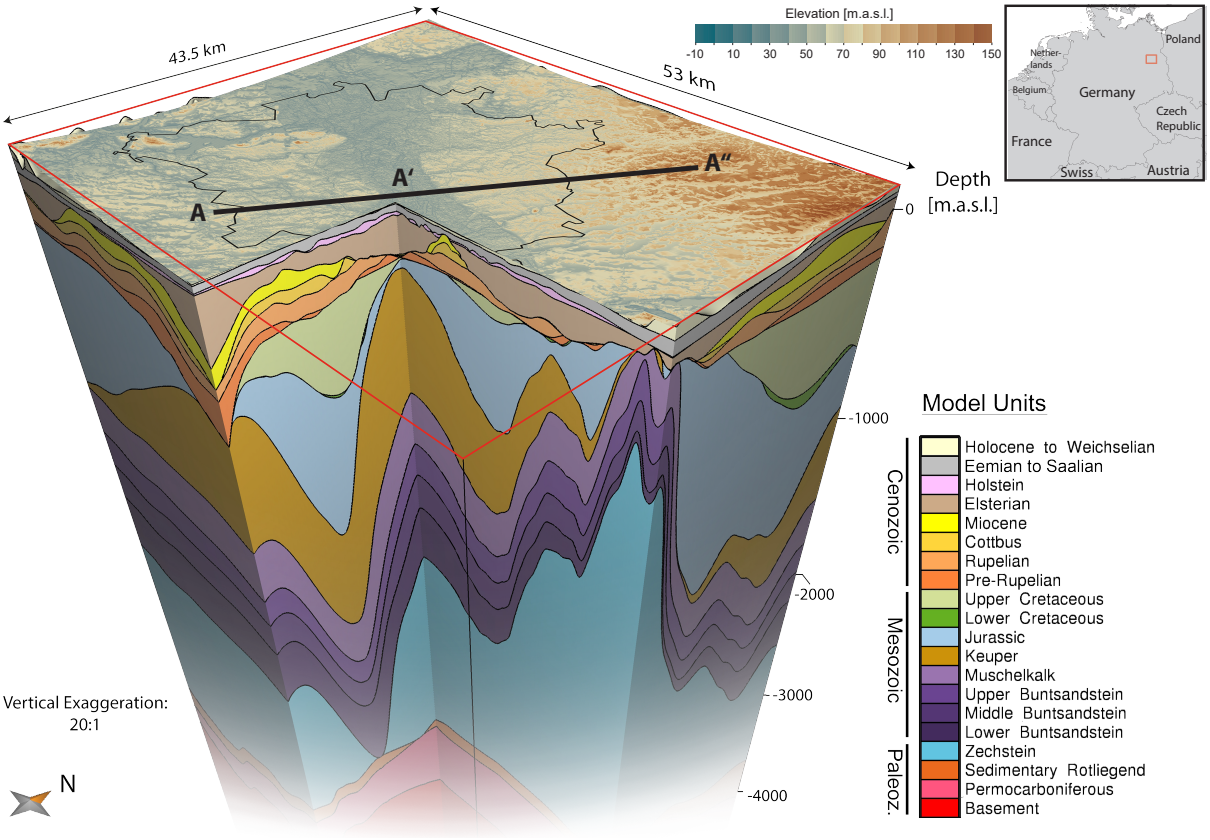

Figure 2.2.: Structural model as used for all simulations. The elevation distribution of the uppermost layer is depicted on top. Thin black line indicates political border of Berlin. Thick black line indicates location of schematic cross section (Fig. 2.5), Modified after Frick et al. (2018a).

Zechstein (Fig. 2.3d,e), and a thickness distribution showing an increase from 100 m in the SE to 240 m in the NW (Fig. 2.4d). Locally this unit has been pierced by the Zechstein diapirs, while its maximum thickness is reached along the southern domain beneath Tempelhof (∼400 m, Fig. 2.4d). The upper Tertiary Muschelkalk has been considered as acting as a hydraulic cap for the Buntsandstein reservoir for a long time. This is due to its lithology which mainly comprises tight carbonates (Noack et al., 2013). However, recent petrophysical investigation performed in the Muschelkalk formation in the neighboring Danish Basin demonstrated an internal regional tripartition of this unit consisting of a regional aquitard sandwiched between two more permeable layers (Pöppelreiter et al., 2005). Based on these results, the Muschelkalk has been subdivided into three main lithological layers, each of similar thickness whose maxima and minima once again spatially correlate with those of the Permian Salt (Fig. 2.4e). The thickness distribution shows a ridge striking N-S with maximum values of 120 m sloping towards E and W with minima of 70 m and locally shows zero thickness, where it has been pierced (Fig. 2.4c). The most important post Mesozoic unit is the Neogene Rupelian. This unit underwent modifications from both, salt movement from below as well as glacial erosion from above. The resulting geometry depicts an elevation distribution where minima of -570 m a.s.l. are located in the ring depression around the NW Zechstein diapir and maxima of 30 m a.s.l. in numerous spots throughout the model domain (Fig. 2.3b). Depressions are also encountered where glacial erosional channels are located, i.e. crossing the center of the model domain striking NNE-SSW (Fig. 2.3b), correlating well with the thickness distribution of the Elsterian deposits (Fig. 2.4a). This is also evident in the thickness distributions where a maximum thickness of ∼400 m is located in the NW and average thicknesses of ∼ 100 m are only perturbed by the erosional channels, where locally the Rupelian is removed entirely (Fig. 2.4a,b).

2.2. Hydrogeological Setting

Numerous studies on the hydrogeology of the region were published throughout the last decades (i.e. Verleger, 1988; Limberg and Thierbach, 1997; Limberg and Thierbach, 2002; Tesmer et al., 2007; Hannapel et al., 2007; Cai et al., 2015; Liu, 2017). However, a number of open questions remains, owing to the complexity of the subsurface and the difficulty posed by the sparsity of data on hydraulic parameters and structure.

In general, the hydrogeological setting can be differentiated into three compartments of regional extent: (a) deep, (b) intermediate and (c) shallow with distinct water type content, i.e. from salty to brackish to fresh water moving from depth to surface. The deep groundwater compartment comprises mainly the Sedimentary Rotliegend, a strongly compacted sandstone unit which is underlain by low permeability volcanics and Pre-Permian sediments, followed up by an impermeable crystalline basement (upper crust). The Rotliegend is overlain by the Permian Zechstein unit, which consists mostly of evaporites and is therefore considered as the boundary between the deep and the intermediate aquifers. The pore water content of this compartment is highly saline and shows signatures of seawater evaporation as main source

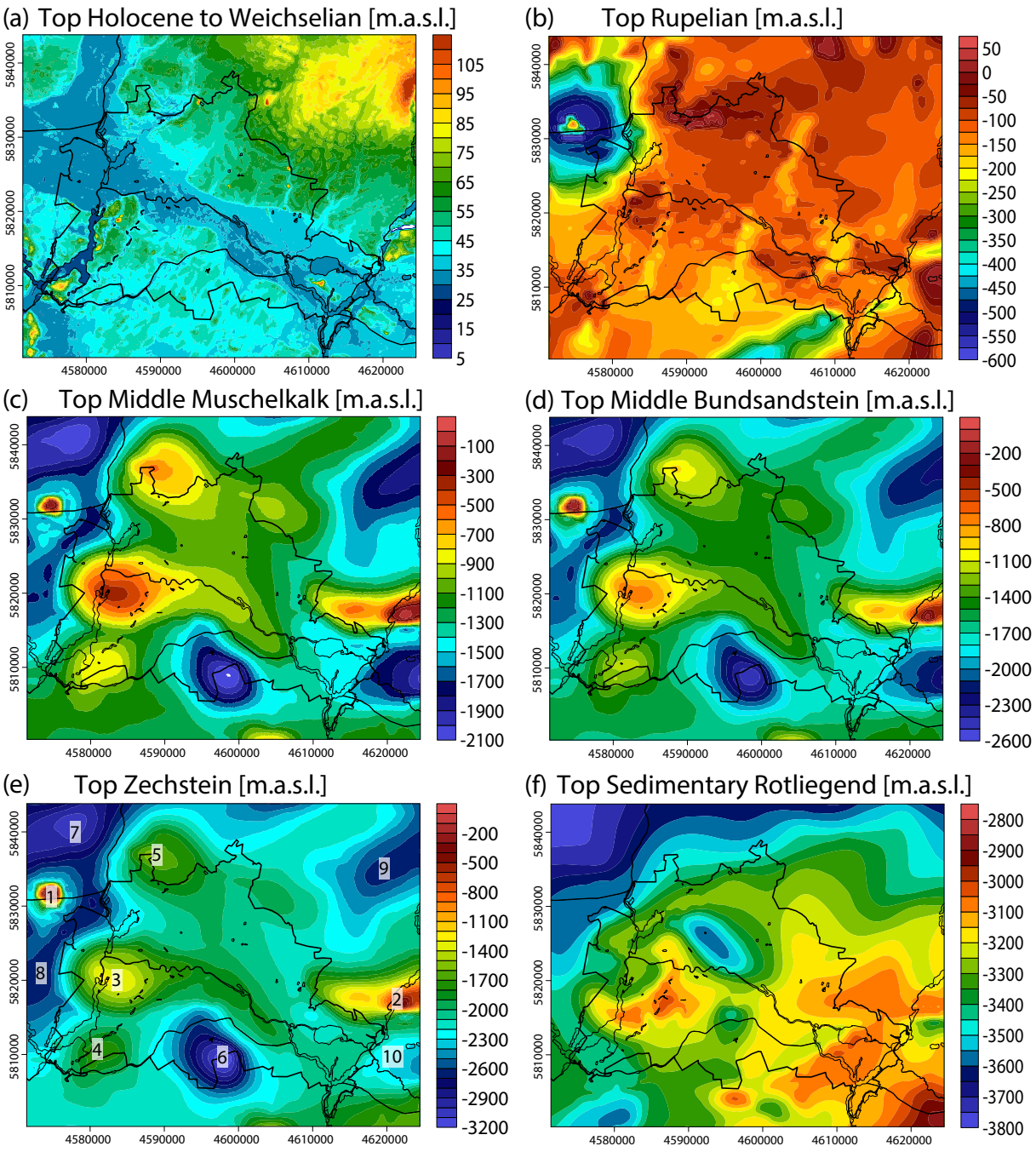

Figure 2.3.: Elevation distribution of the top of important geological (model) units. Coordinates [m] in Gauß-Krüger DHDN Zone 4. (a) Topography, (b) Paleogene Rupelian, (c) Triassic Middle Muschelkalk, (d) Triassic Middle Buntsandstein, (e) Permian Zechstein, (f) Permian Sedimentary Rotliegend.

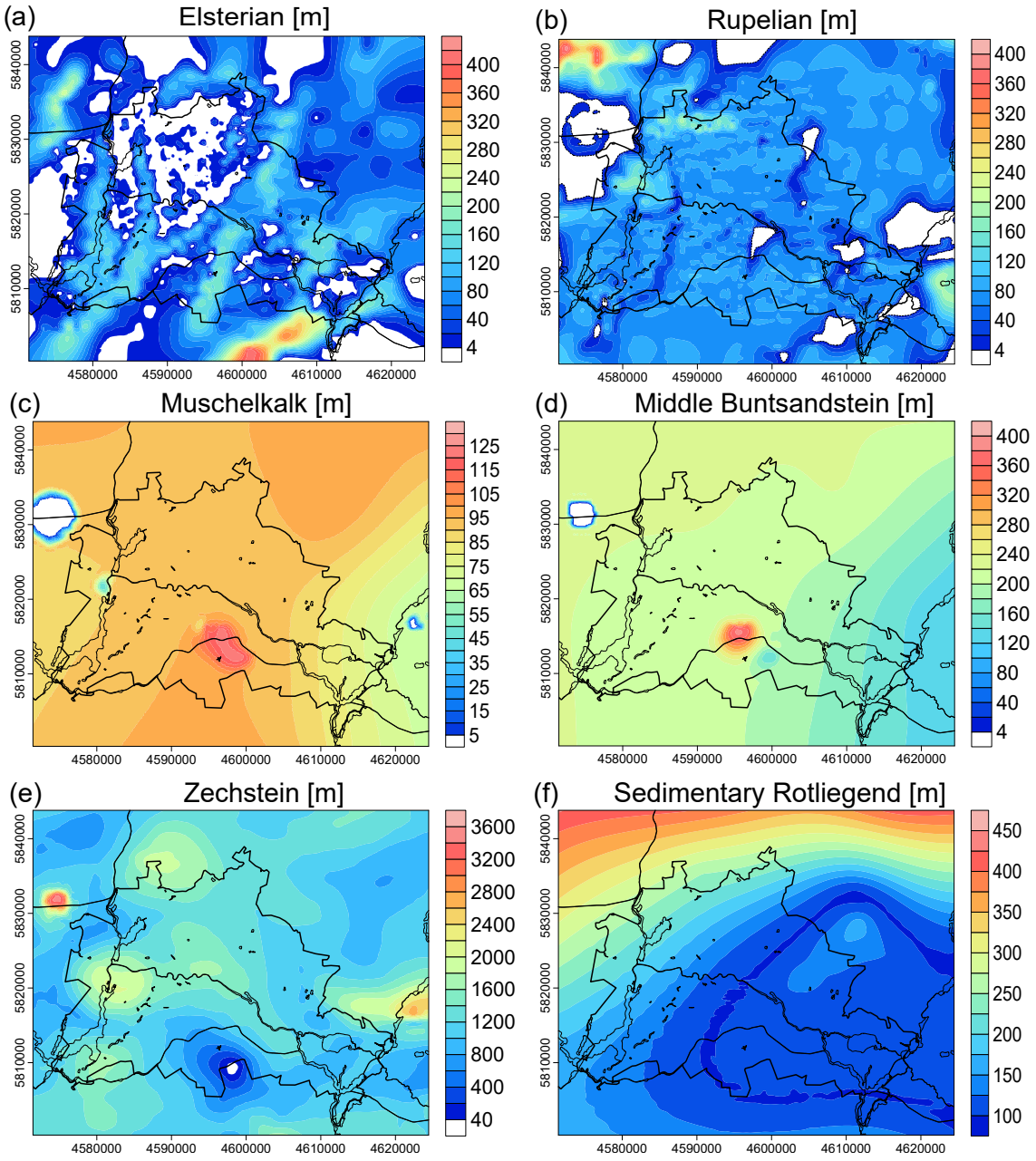

Figure 2.4.: Thickness distribution of important geological (model) units. Coordinates [m] in Gauß-Krüger DHDN Zone 4. (a) Neogene Elsterian, (b) Paleogene Rupelian, (c) Triassic Middle Muschelkalk, (d) Triassic Middle Buntsandstein, (e) Permian Zechstein, (f) Permian Sedimentary Rotliegend.

(Lüders et al., 2010), thus excluding dissolution of the overlying Zechstein as possible source. This compartment is locally connected to the intermediate compartment, where the Zechstein unit is missing due to its mobilization and complete withdrawal in the S of the model area (S of Tempelhof, Fig. 2.4e). The intermediate compartment is composed of Triassic sand-, silt-, clay- and limestones whereas the most important unit from a geothermal perspective is the Middle Buntsandstein. This unit is considered as an aquifer, while under- and overlying units show low permeabilities, thus classifying them as aquitard. This compartment is separated from the shallow aquifer system by the Middle Muschelkalk, again of evaporitic origin, thus being impermeable and considered an aquiclude. The pore water content is again highly saline but shows signatures related to the dissolution of the underlying evaporites, as opposed to the compartment below (Möller et al., 2007). Above the Middle Muschelkalk, a succession of Triassic to Paleogene clay-, lime- and sandstones comprises the lower part of the shallow compartment. Herein, the upper part (Jurassic-Paleogene) shows higher permeabilities, thus classified as aquifers, and the lower part (Triassic) low permeabilities, marking it an aquitard. Like the compartments below, the pore water content is mostly saline but the shallower parts already move towards brackish. This can be explained by exchanges with both the underlying as well as overlying aquifers, thus depicting a mixture of Permian evaporites from below and also meteoric water from above (Tesmer et al., 2007; Möller et al., 2007). This mixture might be related to regional flow components, where exchange between the compartments is possible, or a leakage provided by incomplete sealing of the aquicludes (Möller and Burgschweiger, 2008; Cai et al., 2015; Limberg et al., 2016).

The upper shallow groundwater compartment shows a high degree of complexity, as depicted in Fig. 2.5 wherein the uppermost units (Holocene to Cottbus) make up the drinking water aquifers which are all utilized to a higher or lesser degree, locally separated by the Holstein strata, which are classified as an intermediate aquitard (Hannappel and Asbrand, 2002). These are then separated from the brackish to saline aquifers below (Tesmer et al., 2007) by a local aquitard to aquiclude, namely the Paleogene Rupelian. Due to its role as a natural boundary between the fresh water compartments and the underlying brackish aquifers, several studies have attempted a characterization of this hydrostratigraphic unit. Despite all efforts, mainly due to the scarcity of available data, there is still no consensus on neither its regional thickness configuration nor its physical behavior. All previous studies agreed in depicting a heterogeneous configuration of the Rupelian clay unit, characterized by local discontinuities in its thickness (hereafter referred to as hydrogeological windows). However, their lateral extents and locations are still a matter of debate as the results derived from different recent studies indicate (Zech and Stoltmann (2012) and SenStadtUm (2013a) based on lithological log correlation analysis, Tesmer et al. (2007) based on isotopic measurements, Möller and Burgschweiger (2008) and Cai (2014) based on hydro chemical data, and Limberg et al. (2016) based on hydro-physical analysis of sampled waters). Despite some differences in the respective results, all these studies provide strong indications for the potential of leakage and mixing of water of different origin and salinity through the clay aquitard. The possibility of leakage was also identified in the work directly preceding this thesis in Frick et al. (2016b), where a new parameterization of the unit was proposed as derived from

its grain size distribution, marking it as lowly permeable. All of these observations show that evidence for a connection between the lower saline and the upper freshwater aquifers requires an in depth analysis of the controlling factors for groundwater circulation in this specific setting. Herein, the role of anthropogenic overprinting and the connected realization of the hydraulic boundary conditions is focused on in the first chapters of this thesis (Chapters 3 and 4). The visualization of the major flow patterns predicted by the models is carried out via the Stream Tracer Filter of Paraview (Squillacote et al., 2007) for the final simulation time step and color-mapped by the Z-component of the volumetric flux vector. In the resulting top-view, highest encountered volumetric fluxes integrated over depth discern the color which I deemed best to visualize major flow patterns. They are however not representative for the entire depth interval.

2.3. Geothermal Field

The geothermal field of the NEGB in general, and the subsurface of e.g. Berlin have been investigated in numerous studies (e.g. Hoth et al., 1997; Sanner et al., 2005; Cacace et al., 2010; Noack et al., 2010; Przybycin, 2011; Noack et al., 2012, 2013; Sippel et al., 2013; Cherubini et al., 2013; Kastner et al., 2013; Frick et al., 2015, 2016b). In detail, the deep geothermal field has been shown to be controlled mostly by conductive heat transport. Here, contrasts in the thermal conductivity of model units coupled with their complex geometry (Fig. 2.2) lead to a highly heterogeneous temperature distribution. This is illustrated exemplary by looking at the temperature distribution extracted along a slice of the 3D model at -6000 m a.s.l., where temperatures range between 197 °C and 221 °C (Fig. 2.6a). Here, a SE-NW decreasing trend results from the geometry of the Upper Crust (described before as depth to basement), a unit which has a higher radiogenic heat production than that of the overlying units, therefore showing a positive correlation between its thickness distribution and the temperature predicted above its top at this depth level (Sippel et al., 2013). This general trend of basal heat input into the sedimentary succession is heavily overprinted by the aforementioned complex geometry of contrasting thermally conductive units. Most importantly for the NEGB and for Berlin, the thickness distribution of the Permian Zechstein controls the intermediate geothermal field, i.e. at the -3000 m a.s.l. depth level, where local minima of 108 °C correlate spatially with thickness maxima of the unit and local maxima of up to 130 °C with thickness minima (Fig. 2.6b). These correlations derive from the composition of the unit, mainly rock salt, leading to higher thermal conductivities compared to the surrounding clastics. Consequently, temperature patterns at this depth derive from the more efficient heat transport within the conductive salt compared to the insulating clastic sediments. Where high overall thicknesses of the salt are encountered, negative thermal anomalies are predicted at depth (-3000 m a.s.l.) and positive ones in the shallow model domain (-500 m a.s.l., Fig. 2.6c). Consequently, where the unit is thin or missing, positive thermal anomalies are evident at -3000 m a.s.l. (Fig. 2.6b).

Recent studies focus on the shallower model domain, as economically and technically, these depths hold the most promising targets for geothermal utilization. Additionally, the dynamics at shallower depth are more complex, because convection is more dominantly shaping the

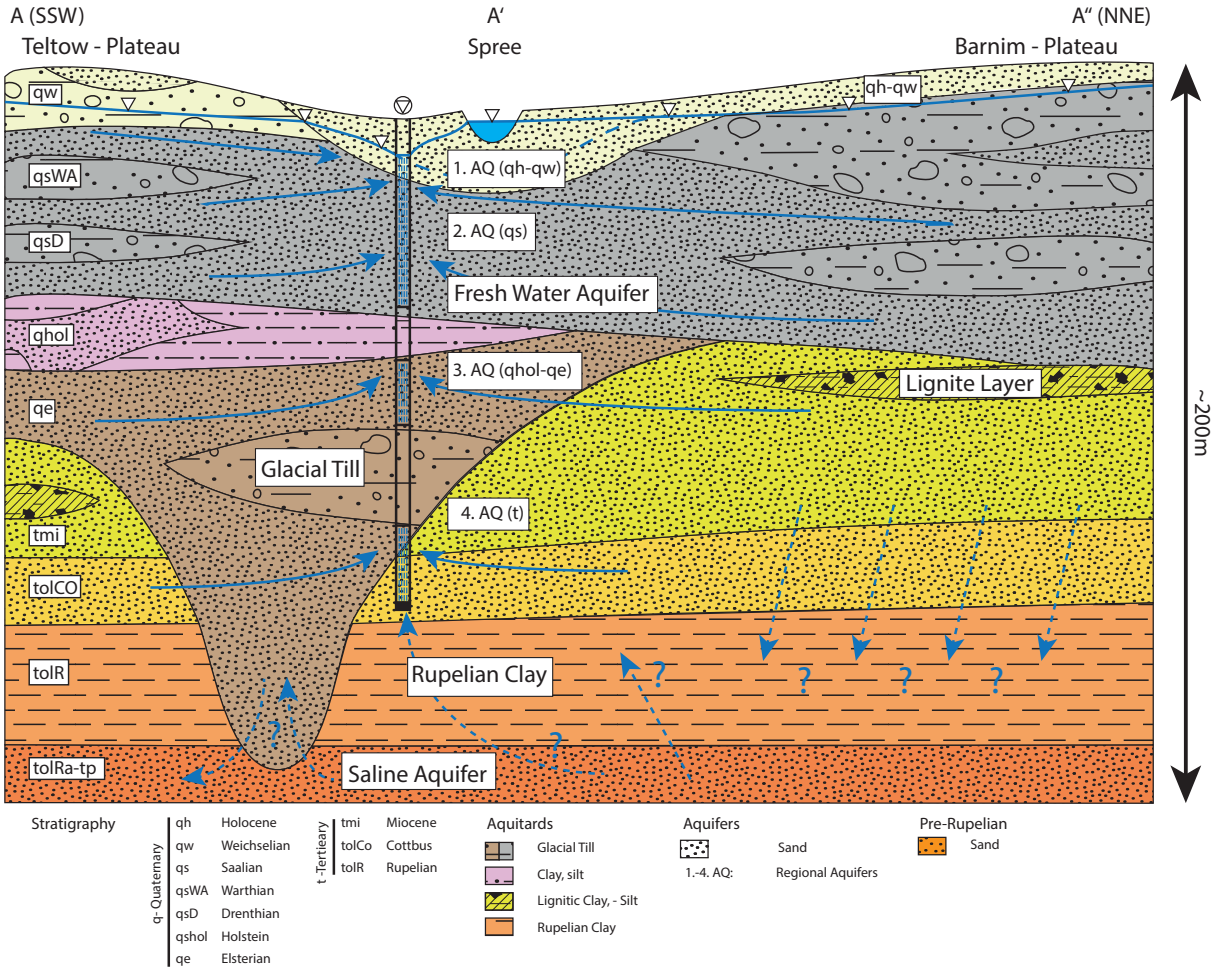

Figure 2.5.: Schematic hydrogeological cross-section through the model area (S-N) after Limberg and Thierbach (1997) and Frick et al. (2018a), Blue arrows represent expected fluid pathways, stippled = conceptual; Stippled blue line on top represents approximation of interpolated groundwater head when disregarding surface water bodies; White triangles = groundwater head monitoring wells; fresh water aquifer refers to main shallow aquifer; exemplified well, depicting screening in one or multiple of the shallow aquifers.

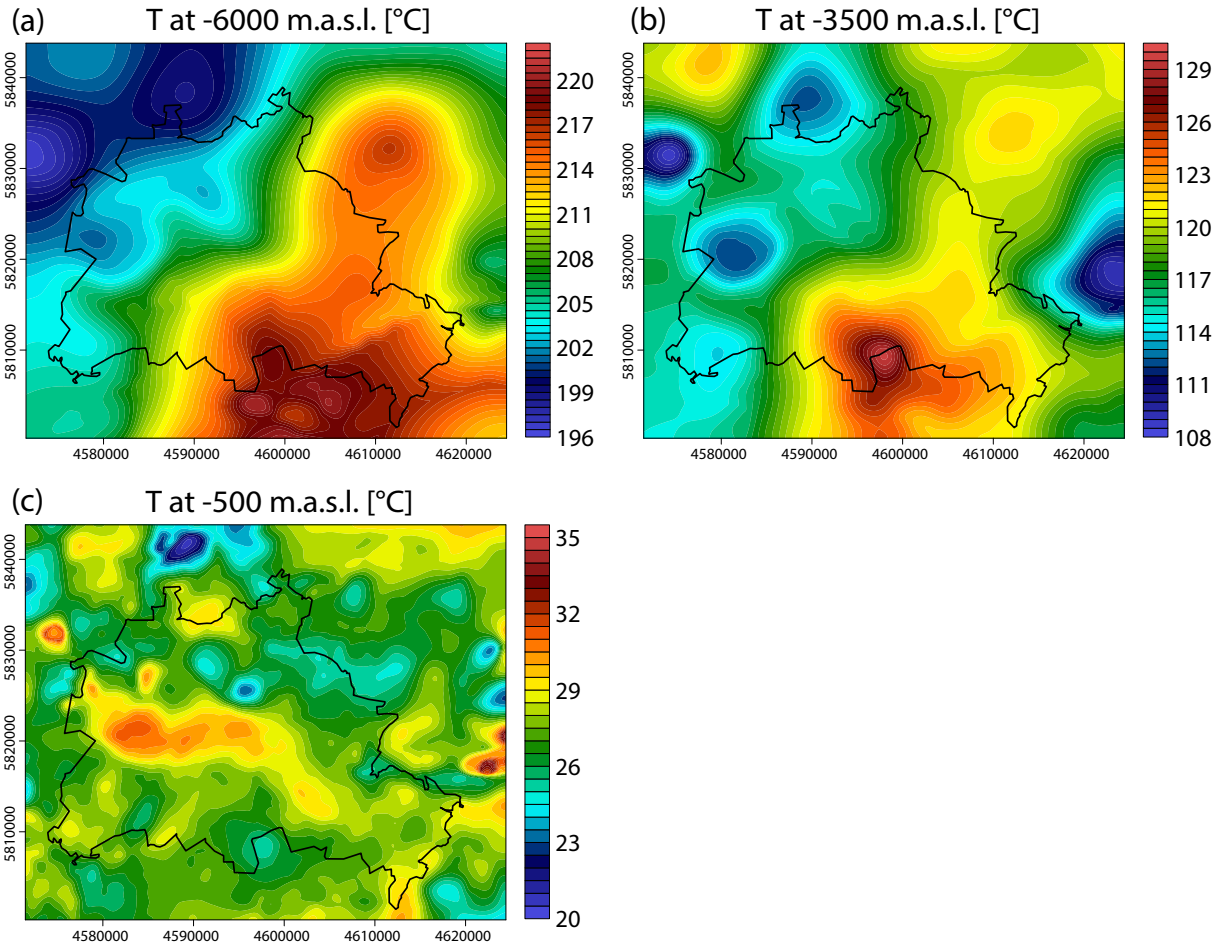

Figure 2.6.: Temperature distribution of selected depth levels as predicted by Model 3 by Frick et al. (2016b). Coordinates [m] in Gauß-Krüger DHDN Zone 4. (a) -6000 m a.s.l., (b) -3500 m a.s.l., (c) -500 m a.s.l.

thermal field and is in turn influenced by numerous parameters. These parameters include most importantly (1) the permeability of model units and (2) the hydraulic boundary condition(s). This is partly elucidated in the temperature distribution at -500 m a.s.l., where a complex pattern of high and low temperatures is predicted by the models preceding this thesis. These only partly correlate spatially with the conductive components of the geothermal field as described above. Here, a strong overprinting of the background conductive field is manifested in minima of 20 °C, where low surficial temperatures from the upper model boundary are carried on to higher depths by forced convection. The latter derives from high hydraulic gradients imposed by the upper hydraulic boundary condition, manifested in negative thermal anomalies at -500 m a.s.l. (Fig. 2.6c). Areas of low hydraulic gradients are defined by uprising of heated water from the deeper subsurface as can be seen by positive thermal anomalies in areas where no salt diapirs or pillows coincide spatially.

2.4. Numerical Modeling Method

The structural and physical information described above have been integrated into the commercial software FEFLOW© (Diersch, 2014). This software solves for (un)saturated groundwater flow and heat and mass transport in porous media, additionally taking conductive, advective and buoyant heat transport processes into account. All simulations are carried out in a finite element based computational framework. The formulation of the mathematical problem posed can then be expressed as a system of three coupled equations representing the conservation of fluid mass, momentum and energy which under the Boussinesq assumption (Holzbecher, 1998; Kolditz et al., 1998; Nield and Bejan, 2006) reads as follows:

$$S_{eff}\frac{\partial p^f}{\partial t} + \boldsymbol{\nabla}\cdot\left(\rho^f \boldsymbol{q^f}\right) = \phi Q_\rho \tag{2.1}$$

with S_{eff} = storage coefficient, p^f = pore pressure, t = time, ρ^f = density of the fluid, q^f = specific discharge (Darcy's velocity), ϕ = porosity, Q_ρ = sink–source mass term.

The specific discharge is given by:

$$\boldsymbol{q^f} = -\frac{\boldsymbol{k}\rho_0^f g}{\eta_0^f}\left(\boldsymbol{\nabla}h + \frac{\rho^f - \rho_0^f}{\rho_0^f}\frac{\boldsymbol{g}}{|\boldsymbol{g}|}\right) \tag{2.2}$$

with q^f = volumetric flux (Darcy flux), k = permeability tensor, η^f = fluid viscosity, h = hydraulic head, g = gravitational acceleration, ρ_0^f = reference mass density of the fluid ($999.793\frac{kg}{m^3}$).

The energy balance equation then reads as:

$$\left(\phi\rho^f c^f + (1-\phi)\rho^s c^s\right)\frac{\partial T}{\partial t} + \rho^f c^f \boldsymbol{\nabla}\cdot\left(\boldsymbol{q^f}T\right) - \boldsymbol{\nabla}\cdot\left(\left(\phi\lambda^f + (1-\phi)\lambda^s\right)\boldsymbol{\nabla}T\right) = Q_r \tag{2.3}$$

with $\phi\rho^f c^f + (1-\phi)\rho^s c^s = (\rho c)_{fs}$ = specific heat capacity of the system with a fluid and solid phase. T = temperature, $\rho^f c^f$ = specific heat capacity of the fluid, $\phi\lambda^f + (1-\phi)\lambda^s = \lambda^{fs}$ = thermal conductivity tensor for the solid and fluid phase, Q_r = heat source function. Bold symbols represent vectors, all other scalars.

The resulting system of partial differential equations (Eqs. (2.1) to (2.3)) is closed by setting an Equation Of State for the fluid density (as a function of the system variables) after Magri (2004) and Magri et al. (2005), thus introducing a non-linear coupling among the equations as follows:

$$\rho_f = \rho_{f_0}\left(1 - \beta(T,p)\,(T - T_0) + \gamma(T,p)\,(p - p_0) + \frac{\alpha(T,C,p)}{C_s - C_0}\,(C - C_o)\right) \tag{2.4}$$

With ρ_f= fluid density, ρ_0^f = reference mass density of the fluid ($999.793\frac{kg}{m^3}$), $\beta(T,p)$ = thermal expansion coefficient, $\gamma(T,p)$ = compressibility and $\alpha(T,C,p)$ = density ratio, T = temperature, T_0 = reference temperature ($=0°C$), p = pore pressure, p_0 = reference pressure ($=1E05Pa$), C_s = saturation concentration ($=0.35\frac{kg}{l}$), C_0 = reference concentration ($=0\frac{kg}{l}$). For the scenarios without mass transport, $\frac{\alpha(T,C,p)}{C_s - C_0}\,(C - C_o)$ equals 0.

The fluid viscosity is approximated by the built-in function of FEFLOW©(Diersch, 2014) after the empirical mathematical equation from (Mercer and Pinder, 1974):

$$\frac{\eta}{\eta_0} = \frac{1 + 0.7063 * \zeta_0 - 0.04832 * \zeta^3}{1 + 0.7063 * \zeta - 0.04832 * \zeta^3} * \frac{1 + 1.85 * \omega - 4.1 * \omega^2 + 44.5 * \omega^3}{1 + 1.85 * \omega_0 - 4.1 * \omega_0^2 + 44.5 * \omega_0^3} \tag{2.5}$$

with

$$\zeta = \frac{T - 150}{100} \quad \zeta_0 = \frac{T_0 - 150}{100} \quad \omega = \frac{C}{\rho} \quad \omega_0 = \frac{C_0}{\rho} \tag{2.6}$$

Where η = dynamic fluid viscosity, η_0 = reference viscosity ($0.0018 \frac{kg}{m*s}$), ζ = relative temperature coefficient, ζ_0 = reference relative temperature coefficient, ω = mass fraction and ω = reference mass fraction ($= 0 \frac{kg}{m^2 s^2}$). For the scenarios without mass transport, $\frac{1+1.85*\omega-4.1*\omega^2+44.5*\omega^3}{1+1.85*\omega_0-4.1*\omega_0^2+44.5*\omega_0^3}$ equals 1.

More details about the mathematical background and its numerical formulation can be found in Diersch (2014).

To add to the predictive capabilities of the models, we use the predicted temperatures in a twofold manner, (1) where we look at their absolute values for determining potential sites for geothermal utilization and (2) as a further means to better quantify and visualize the induced changes in the regional hydraulics (e.g. Saar, 2011; Racz et al., 2012). Salinity as another tracer was considered to be of secondary relevance for the specific goal of the present study. The paucity of available data which, at the current stage, will not permit an investigation of its impact on the city-wide groundwater and geothermal configuration, also influenced this decision.

The numerical models depict a similar or higher resolution compared to the structural model, focusing on local areas of interest, where the resolution has been further increased. The details of each mesh are explained in the related chapters of this thesis.

For all models different sets of boundary and initial conditions were applied. In detail, upper and lower thermal boundary conditions were realized as Dirichlet Boundary condition for the entire model run as outlined in Chapter 3. The hydraulic boundary condition was realized in two ways: (1) as Dirichlet boundary condition fixed at the top (Chapters 3 to 5) and (2) as well boundary condition at the position of the well screen middle (Chapter 4). The initial conditions for all models were derived from calculating the pressure and temperature field decoupled in steady state.

2.5. Previous Studies

In this section I want to briefly detail the relevant studies preceding this thesis. These studies focus on Berlin specifically or include Berlin as part of the models opting at confining the structural and physical state of the subsurface. The first work I want to mention in this respect is Scheck and Bayer (1999), which integrates geophysical and geological data, featuring a 3D structural model of the Northeast German Basin. This model was then used to built successively more detailed models, implementing more highly resolved data. These were firstly

focusing on the conductive thermal field, moving on to thermohydraulic 3D models of the state of Brandenburg (Bayer et al., 1997; Noack et al., 2010, 2012, 2013). These models outline the detailed structure of the sedimentary succession as well as dominating heat transport processes at the different depth levels. Additionally, some pioneering work concerning solute transport in this framework was presented by Kaiser et al. (2013b), whose study site is located northeast of the study area presented in this thesis. To detail the basic findings concerning heat transport in the subsurface of Berlin, the work by Sippel et al. (2013) laid the foundation. The authors of the latter found that there are, as mentioned above, two distinct domains where different heat transport mechanisms dominate, reflecting the complex structure of the subsurface and therefore physical properties. The deeper model domain is controlled by conductive heat transport, which is in turn mainly bound to the distribution of thermal conductivities (contrasts) and the structural configuration of geological units (most importantly Zechstein salt). The upper model domain is additionally overprinted by a component of forced convection which is controlled by the configuration of the upper hydraulic boundary condition and the geometrical configuration of major aquitards, that is the Rupelian clay and the Middle Muschelkalk.

In this study (Sippel et al., 2013) some limitations of the models were revealed, which concerned most of all the aforementioned parameters. In detail, the hydraulic head boundary condition being approximated by the topography results in overpressured infiltration of cold surficial water, leading to an overestimation of advective cooling of the deeper subsurface. This process is also aided by uncertainties in the structuration of the Rupelian aquitard, whose discontinuities enable intra-aquifer flow. Based on these limitations, Frick et al. (2015) and Frick et al. (2016b) presented models improving the representation of the upper hydraulic head boundary condition as well as the resolution of resolved shallow geological features based on newly available data. The new models show a hydraulic head distribution derived from gridded groundwater head data as well as a more continuous Rupelian which was additionally proposed to be lowly permeable. The results of these studies show, that the drop in hydraulic gradients prescribed by the boundary conditions combined with a more continuous Rupelian lead to a less vigorous cooling of the subsurface which shows a better fit with observed deep temperature measurements. Additionally, the consideration of the Rupelian as lowly permeable aquitard permitted slow exchange between the groundwater compartments also at locations where the Rupelian is continuous. The studies also outlined the sensitivity of the shallow groundwater compartment to any changes in the models setup. Concerning the geothermal potentials of the subsurface, Kastner et al. (2013) and Kastner et al. (2015) did some pioneering work, predicting extractable heat from two deep reservoirs, relying on temperature results from early models of the geothermal field (Sippel et al., 2012; Sippel et al., 2013). The results from these studies show that a provision of heat from the subsurface is possible and therein highly heterogeneously distributed.

All of these predecessor studies open specific research topics and enable targeting associated research questions as well. In detail, the studies preceding this thesis targeted most of all the deep geothermal and hydraulic configuration in general. Therefore, the studies presented in the following focus more on the interaction of the deep and shallow compartments of the subsurface

and resulting sensitivities to changes in boundary condition set-up. This is of particular importance since the subsurface in urban areas is overprinted by human activities to a high degree, the effect of which is focused on qualitatively and quantitatively. This links back to the objectives of this thesis (Section 1.2) where we opt for understanding the influence of major surface water bodies on the resulting hydraulic and thermal configuration of the subsurface in an anthropogenically overprinted setting. Additionally, the respective reconstruction of the natural hydraulic configuration was targeted, and building on this, an analysis of the impact of groundwater pumping on temperature, pressure and mass transport was carried out. Overarching these components, one of the main questions that was focused on for the last years, was investigated: what is the geothermal potential of the subsurface of Berlin? This question is answered in new detail given the newly built models of this thesis.

3. Surface to groundwater interactions beneath the city of Berlin - Results from 3D models

Frick, M., Scheck-Wenderoth, M., Schneider, M., and Cacace, M. (2018a). "Surface to Groundwater Interactions beneath the City of Berlin - Results from 3D Models." In: *Geofluids* In Press

Abstract

Knowing the thermal and hydraulic conditions below major urban centers is of increasing importance in the context of energy and water supply. With this study, focusing on the major urban center of Berlin, Germany, we aim to gain insights on the coupling of surface water bodies to the subsurface thermal and hydraulic field, investigating shallow water to deep groundwater interactions. Therefore, we use a 3D structural model of the subsurface, constrained by all available data and observations, as a base for simulations of coupled transport of fluid and heat. This model resolves the 3D configuration of the main geological units and thus enables to account for related heterogeneities in physical properties. Additionally, we resolve surface water body geometries with newly available data.

To assess how surface water bodies interact with the deeper groundwater at different depths in the model domain, the influence of different hydraulic boundary conditions is quantified, which indicates that the coupling of surface water bodies and groundwater strongly modifies predicted groundwater circulation. Consequently, changes in subsurface temperatures are also predicted, where lakes may account for temperature differences up to ±5 °C and rivers could account for up to ±1 °C visible at depths ≤ -500 m a.s.l.. These differences are mainly connected to changes in the advective component of heat transport caused by the modifications of the hydraulic boundary condition. Pressure driven heat transport is most efficient where differences between hydraulic heads of aquifers and surface water bodies are highest. This study therefore illustrates the impact of surface to subsurface water interactions in an urban context.

3.1. Introduction

In the last decade, the need for big cities to make efficient, environmentally friendly use of the subsurface on which they stand is increasingly getting attention (Huenges et al., 2013b). In order to properly engage in this endeavor, a systematic understanding of the distribution of available natural resources, like groundwater and geothermal energy in the subsurface, is a prerequisite. One of the major limiting factors preventing both an efficient and economically viable planning of georesource utilization derives from a poor understanding of the hydrogeological conditions, including the geological configuration and hydrodynamics below urban areas. This study presents a 3D workflow integrating geological and hydrogeological

data, numerical modeling and available data from monitoring activities into physically based 3D models as a tool to assist in the development of good practices with respect to usage and maintenance of groundwater and geothermal resources. Herein, especially the configuration of groundwater and surface water as boundary conditions (BCs) in these models are the focus of the study, since their realization is often simplified in modeling studies of this type as outlined in the following chapters. We take the example of the city of Berlin (Fig. 3.1a), capital of Germany, as a natural laboratory where to develop and test our approach. The model area therefore stands representative of a major urban center with more than four million inhabitants, which largely reshaped surface morphology and shallow hydraulics, also depicting a complex hydrogeological setting.

The study area is located in the Northeast German Basin (NEGB), a sub-basin of the larger Central European Basin System (Bayer et al., 1997). Previous 2D and 3D studies focusing on the basin wide hydrothermal configuration of the NEGB have revealed the presence of a regional hydrothermal regime driven by different physical processes. Those processes include heat diffusion, which is active especially at great depths (below the Zechstein salt), and its coupling to a regional component of pressure driven groundwater flow within the Mesozoic to Cenozoic aquifers (i.e. Kaiser et al., 2013b,a; Noack et al., 2013). This component of fluid related heat transport has been shown to be mainly controlled by the (1) subsurface porosity and permeability distribution, and, of special relevance for this study, (2) the surface hydraulic configuration, imposed in the models as an upper hydraulic BC. In this regard, the major limitation common to previous studies was to make use of a constant hydraulic head at topographic level, which arguably imposes unrealistically high hydraulic gradients supposedly leading to an overestimation of advective cooling (Kaiser et al., 2011; Noack et al., 2013; Freymark et al., 2017). This in turn has a crucial impact on the resulting shallow to deep groundwater circulation, detailed in deeper infiltration of meteoric water into, and uprising of deep seated water out of the model domain. Therefore, a proper quantification of the urban wide hydraulic and thermal configuration requires a better, more realistic approximation of the hydraulic BC. In the context of the model area, this is also of crucial interest since most of the fresh water resources for the city of Berlin are produced from shallow aquifers (Limberg and Thierbach, 1997) and might be subject to mixing of waters of different ages and salinity content, which might impact water quality (Fig. 3.1b). Hence, the investigation of the controlling mechanisms of subsurface hydrodynamics is crucial to first of all reproduce the observed hydraulic and thermal regimes (present day status) and to make reliable predictions of the dynamic response of the system to further anthropogenic forcing (subsurface utilization).

Recent studies (Frick, 2015; Frick et al., 2016b; Sippel et al., 2013) have demonstrated that the hydraulic and thermal configuration at shallow and intermediate levels ($\geq$-1000 m a.s.l.) of the study area is controlled to a large degree by the elevation (top and base, Fig. 3.2a) and thickness distribution (hereafter called structural configuration, Fig. 3.2b) of the Rupelian aquitard. This unit separates fresh water (above) from saline water (below) but it also experienced glacial erosion, resulting in holes through the root of its base, hereafter referred to as hydrogeological windows (Fig. 3.1b, Fig. 3.2b). Because of its discontinuous nature, former studies focused on

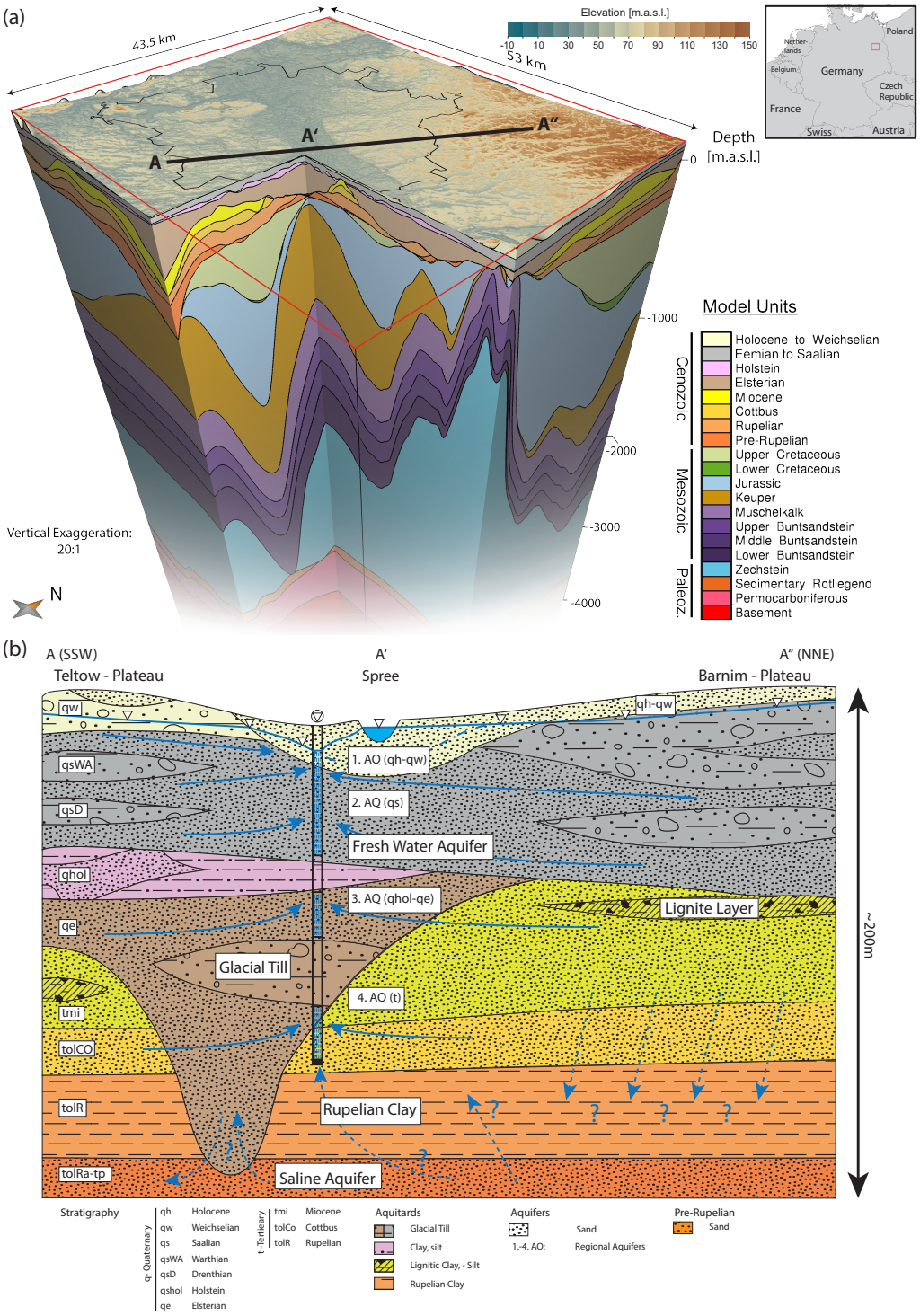

Figure 3.1.: Structural model and schematic hydrogeological cross-section. (a) 3D structural model as used for all thermal simulations. Depicted on top is the elevation distribution of the uppermost layer. Thin black line indicates political border of Berlin. Modified after Frick et al. (2016b), (b) Schematic hydrogeological cross-section through the model area (S-N) after Limberg and Thierbach (1997), Blue arrows represent expected fluid pathways, stippled = conceptual; Stippled blue line on top represents approximation of interpolated groundwater head when disregarding surface water bodies; White triangles = groundwater head monitoring wells; fresh water aquifer refers to main shallow aquifer; exemplified well, depicting screening in one or multiple of the shallow aquifers.

quantifying the degree of hydraulic connectivity between the supra- and sub-Rupelian aquifers in the vicinity of these hydraulic windows (i.e. Kaiser et al., 2013b; Magri et al., 2008). These studies showed that hydrogeological windows likely act as preferential pathways for deeper groundwater to upcone to the surface and for shallow (meteoric) water to penetrate deeper into the lower aquifers. The depth extent of this mixing zone, as well as the vigor of this process, have been shown to be controlled by the hydraulic configuration at the surface and by the hydromechanic characteristics of the relevant aquifers and aquitards (Frick et al., 2016b; Frick, 2015). These studies have highlighted a causal relationship between the vigor and depth extent of the mixing zone and (1) the pressure hydraulic surface forcing (i.e. groundwater heads) and (2) the hydrogeological configuration and spatial configuration of the Rupelian aquitard. For (1) a careful representation of the hydraulic BC is key and the progress in this regard is explained in more detail in Sections 3.3 and 3.4.4.1. For (2) a possible leakage through the clay layer in areas where no hydrogeological windows are present is predicted, which stands in contrast to earlier models findings (Sippel et al., 2013; Noack et al., 2013). Another recently published study (Scheck-Wenderoth et al., 2017) showcases, how an in-depth knowledge of shallow subsurface hydraulic and thermal conditions is of utmost importance for any planned geothermal utilization, thus outlining the importance of the work presented in this paper. Scheck-Wenderoth et al. (2017) show, that predictions highly rely on the spatial scales considered, stressing that local, highly refined models (like the one presented here) are necessary for robust results.

With this study, we want to investigate deep to shallow interactions as represented in different model scenarios, focusing on the changes in local hydrodynamics resulting from different, increasingly more realistic representations of the upper hydraulic BC. We opt for a most accurate implementation of the hydraulic BC by utilizing a wider database for the groundwater heads compared to previous studies (Frick et al., 2016b) as well as lakes and rivers as new elements, based on newly available data. Hereby, we are able to make qualitative and quantitative predictions of changes in hydrodynamics induced by each of these elements. We make use of modeled temperature as a passive tracer which serves as an indicator for the depth and lateral extent of modifications in advective heat transport. Predicted temperatures and respective changes are also used to determine shallow geothermal potentials.

3.2. Geological Setting

The sedimentary succession in the model area ranges from Permian (Sedimentary Rotliegend) to Neogene (Holocene) in age and consists predominantly of clastics, carbonates and rock salt (Bayer et al., 1997). This sedimentary succession is underlain by variably thick volcanics which are Permocarboniferous in age (Scheck and Bayer, 1999). The Mesozoic evolution of the basin has been largely controlled by halokinetic mobilization of the Permian (Zechstein) salt rock layer, which occurred during several stages starting from late Middle Triassic onward (Scheck et al., 2003). This process largely influences the geometry of all overlying units, as illustrated in Fig. 3.1a. Within the study area, the Zechstein salt layer shows a heterogeneous thickness distribution, with local maxima exceeding 3,500 m, envisaged in the NW and E of the model

area, and domains of reduced thickness or complete withdrawal, as visible along the southern boundary of the model near Tempelhof area in the S (Fig. 3.2e,f, Scheck et al., 2003).

The Mesozoic sedimentary sequences consist predominantly of consolidated clastics or carbonates (Noack et al., 2010). The succession also includes the Middle Triassic (Middle Buntsandstein) and Permian Sedimentary Rotliegend, which consist of sandstones consolidated to varying degrees, displaying sufficiently high porosity and permeability distributions, to be considered as target horizons for deep geothermal energy extraction (Table 3.1, Huenges and Ledru, 2011).

The Cenozoic sedimentary succession is predominantly composed of unconsolidated clastics (Fig. 3.1b) overlying older strata in a discordant pattern (Fig. 3.1a). The basal unconformity is expressed by Cretaceous, Jurassic or Keuper sediments directly underlying Upper Paleogene or Neogene strata. Moreover, Paleogene sediments display inhomogeneous thickness distributions, as envisioned by the Oligocene Rupelian clay. The initial thickness distribution of this unit was approximately 80 m, but has been altered significantly, as manifested in numerous glacial erosional channels and discontinuities (Fig. 3.1b, Fig. 3.2b).

3.3. Hydrogeological Setting

The hydrogeology of Berlin has been studied intensively for several decades now, yet a number of open questions remains, owing to the fact, that information about structure and hydraulic parameters is sparse, especially considering the deeper subsurface (i.e. Krems, 1975; Brühl, 1975; Brühl and Trapp, 1983; Limberg and Thierbach, 1997; Sippel et al., 2013; Frick et al., 2017).

In this respect, the lower constraint is the crystalline basement which is considered impermeable (Noack et al., 2013). The overlying Permian strata are low permeability volcanics (Permocarboniferous), considered as aquitard, and strongly compacted sediments with comparatively high permeability (Rotliegend), considered as aquifer, making up the very deep groundwater compartment (Table 3.1). These are overlain by impermeable evaporites (Zechstein), separating them from the shallower groundwater compartments.

The intermediate groundwater compartment is described by mostly clastic Triassic sediments of varying degrees of sand-, silt-, clay-, and limestone separating them into one lowly permeable unit at the bottom (Lower Buntsandstein), one highly permeable unit in the middle (Middle Buntsandstein) and two lowly permeable units on top (Upper Buntsandstein and Lower Muschelkalk, Table 3.1). This compartment is separated from above by a layer of tight evaporites (Middle Muschelkalk), considered as a regional aquitard located in depths between 0 to -2400 m a.s.l. with an average thickness of 90 m (Pöppelreiter et al., 2005, Table 3.1 and Fig. 3.2c, d). The remaining Mesozoic units show increasing permeabilities from bottom to top, as younger units have experienced less compaction and show increasingly larger proportions of sand and silt in comparison to marl and clay (Table 3.1).

The hydrogeological configuration of the Cenozoic sedimentary succession is depicted schematically in detail in Fig. 3.1b. The base is described by a medium permeability unit (Pre-Rupelian) with a brackish to saline pore fluid (Tesmer et al., 2007). This characteristic

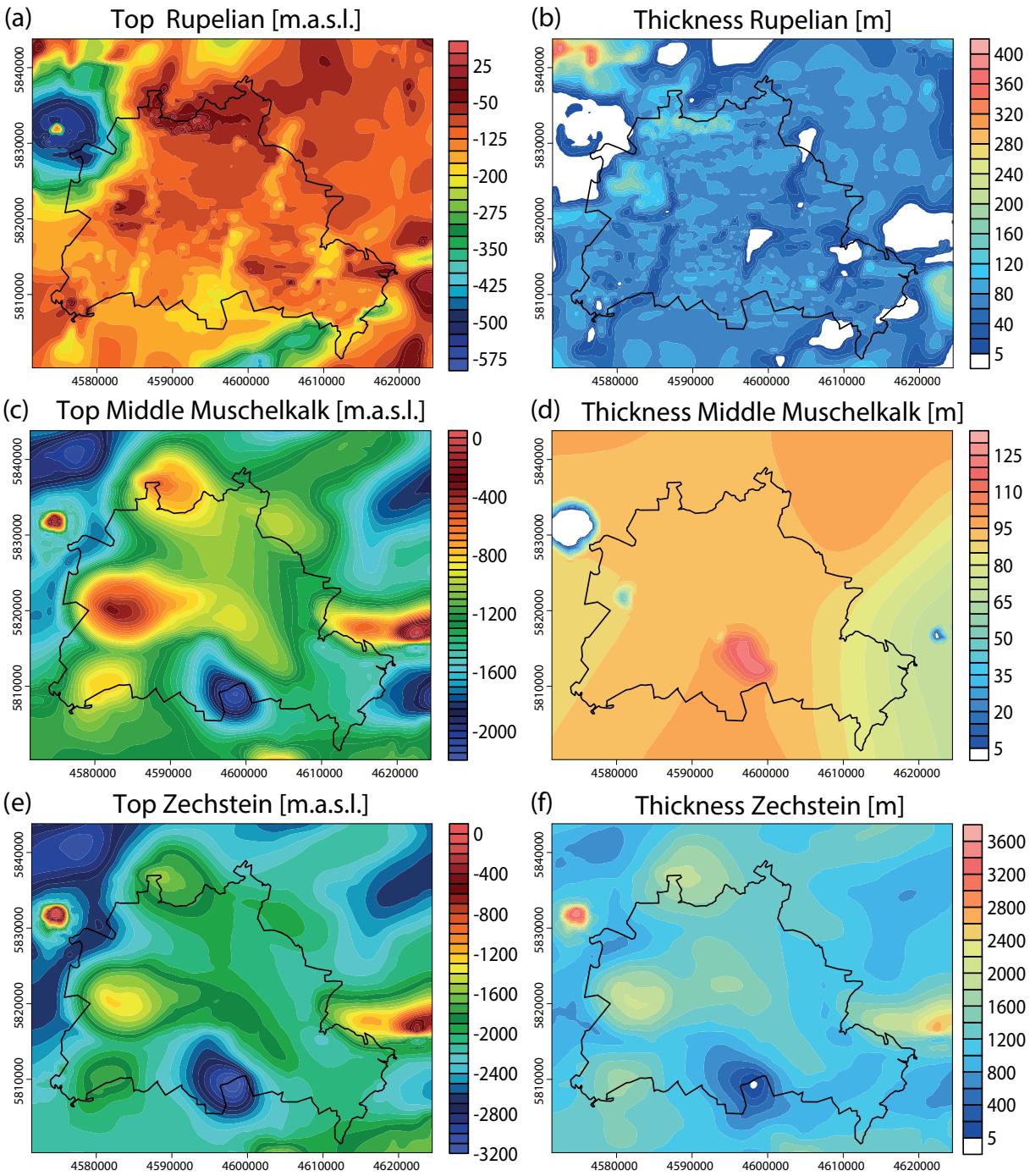

Figure 3.2.: Geometric configuration of important stratigraphic units after Frick et al. (2016b). (a) Top Rupelian, (b) Thickness Rupelian, (c) Top Middle Muschelkalk, (d) Thickness Middle Muschelkalk, (e) Top Zechstein, (f) Thickness Zechstein. (b,d,f) White areas represent discontinuities, Coordinates [m] in Gauß-Krüger DHDN Zone 4. For database, please refer to Frick et al. (2016b) as well as the supplementary material of this article.

Table 3.1.: Physical properties of the model units as used for the numerical simulations. $\lambda^{(b)}$ = bulk thermal conductivity, Q_r = radiogenic heat production, $c^{(s)}$ = volumetric heat capacity of solid, ϕ = porosity, κ_{xyz} = hydraulic conductivity; impermeable refers to κ_{xyz} = 1E-40 m/s. Values were derived from (Otto, 2012; VDI, 2010; Norden and Förster, 2006; Norden et al., 2012; Das, 2013; Devlin, 2015; Sippel et al., 2013) more details about Cenozoic in Frick et al. (2016b) and pre-Cenozoic in Sippel et al. (2013).

	Geological unit (Predominant Lithology)[1]	$\boldsymbol{\lambda^{(b)}}$ $[W/(m*K)]$	$\boldsymbol{Q_r}$ $[W/m^3]$	$\boldsymbol{c^{(s)}}$ $[MJ/(m^3*K)]$	$\boldsymbol{\phi}$ $[-]$	$\boldsymbol{\kappa_{kyx}}$ $[m/s]$
Neogene	Holocene to Weichselian (Slightly gravelly sand)	2.71	0.9E-06	1.57	0.32	1.42E-05
	Eemian to Saalian (Gravelly muddy sand)	2.59	0.9E-06	1.58	0.314	4.04E-06
	Holstein (Gravelly mud)	2.17	0.9E-06	1.67	0.296	1.91E-08
	Elsterian (Gravelly muddy sand)	2.35	0.9E-06	1.61	0.304	8.98E-07
	Miocene (Slightly gravelly muddy sand)	2.47	1.0E-06	1.56	0.301	6.88E-07
Paleogene	Cottbus (Slightly gravelly muddy sand)	2.62	1.3E-06	1.7	0.305	1.15E-06
	Rupelian (Slightly sandy mud)	1.64	1.3E-06	1.81	0.237	3.23E-08
	Pre-Rupelian (Slightly gravelly muddy sand)	2.48	1.3E-06	1.7	0.297	6.56E-07
	Upper Cretaceous (Limestone with marl)	2.82	0.6E-06	2.29	0.11	4.81E-07
	Lower Cretaceous (Marl with claystone)	2.36	1.5E-06	2.29	0.11	4.81E-07
	Jurassic (Claystone with silt- and sandstone)	2.71	1.5E-06	2.25	0.189	4.81E-07
Triassic	Keuper (Claystone with marl and gypsum)	2.35	1.6E-06	2.32	0.128	9.62E-09
	Upper Muschelkalk (Limestone with marl)	2.3	1.0E-06	2.25	0.15	9.62E-09
	Middle Muschelkalk (Evaporites)	2.3	1.0E-06	2.25	0.036	impermeable
	Lower Muschelkalk (Limestone with mudstone)	2.3	1.0E-06	2.25	0.12	5.77E-10
	Upper Buntsandstein (Silt- and sandstone with rock salt and carbonates)	3.0	1.8E-06	2.19	0.025	6.44E-09
	Middle Buntsandstein (Sandstone with silt- and claystone)	2.0	1.8E-06	2.39	0.135	5.84E-07
	Lower Buntsandstein (Silt- and claystone)	1.84	1.8E-06	2.39	0.049	1.25E-09
Permian	Zechstein (Rock salt with gypsum and carbonate)	4.5	0.4E-06	1.94	0.005	impermeable
	Sedimentary Rotliegend (Claystone with silt- and sandstone)	3.0	1.4E-06	2.18	0.078	5.06E-08
	Permo-Carboniferous (Rhyolite and andesite)	2.5	2.9E-06	2.6	0.032	8.66E-10
	Basement (Strongly compacted clastics)	2.2	2.8E-06	2.3	0.01	impermeable

is also common for all older strata, supposedly connected to the dissolution of rock salt from the Zechstein unit (Tesmer et al., 2007; Möller et al., 2007; Kloppmann et al., 2001). The only exception to this rule are the formation waters of the Rotliegend which are mainly preserved with their original signature of seawater evaporation as main source (Lüders et al., 2010). The saline formation waters of the Post-Rupelian are then separated from above to a certain degree by the lowly permeable Rupelian clay, a local aquitard of discontinuous nature, depicting hydrogeological windows (Fig. 3.2a,b, Fig. 3.1b, Tesmer et al. (2007)). Overlying this strata, five geological units in total are classified as aquifers (Cottbus, Miocene, Elsterian, Saalian, Holocene), only interrupted locally by the Holstein strata (Fig. 3.1b) which are classified as an aquitard (Table 3.1, Hannappel and Asbrand (2002)). Fig. 3.1 clearly shows, that these aquifers depict a high level of heterogeneity, deriving mainly from the depositional or erosional character of the glacial and interglacial periods. Here, especially the glacial erosional channels from the Elsterian period are worth mentioning since they locally cut through the base of the Rupelian aquitard (Fig. 3.2b). These channels are mainly filled by sand dominated deposits, thus presenting possible pathways for fluid exchange between the different compartments. We differentiated the Cenozoic strata according to their geometrical relevance, which means, that only strata of a certain thickness and spatial extent were resolved in the structural model (Fig. 3.1a). However, for each of these strata, lithological distributions derived from the available $\sim$ 630 well logs were analyzed and taken into account (more details in Frick et al. (2016b)), classifying the units as outlined above and in Table 3.1, therefore resolving the heterogeneity of the units and the main aquifer to a certain extent.

The Cenozoic succession also includes the main aquifers (Cottbus, Miocene, Elsterian, Saalian, Holocene) for drinking water production (Fig. 3.1b). Therefore, the realization of aquifer groundwater levels and surface water body levels is of especial interest for this study. For the model area, earlier studies and newly available datasets suggest a natural direct connection between these two (Fig. 3.1b, Jarmersted, 1992; Limberg and Thierbach, 2002). Here, depending on the locality, either effluent or influent conditions are observed, depending in turn on local geology as well as anthropogenic overprinting due to groundwater pumping activities. Concerning this specific configuration, predecessor studies focusing on different aspects of the subsurface derived the hydraulic potential solely from measured groundwater data (Frick et al., 2015, 2016b) or topographic levels (Sippel et al., 2013). However, the data provided for this study show that there is a significant difference between interpolated groundwater levels used as a hydraulic BC in the studies mentioned above, and surface water levels. In detail, interpolated values over- or undershoot hydraulic potentials in areas where data coverage is sparse, high gradients emerge between two groundwater head measurements, or anthropogenic overprinting lead to a drop in observed heads. As outlined in Section 3.4.4.1, the scenarios investigated here opt for a more realistic representation taking into account measured surface water heads.

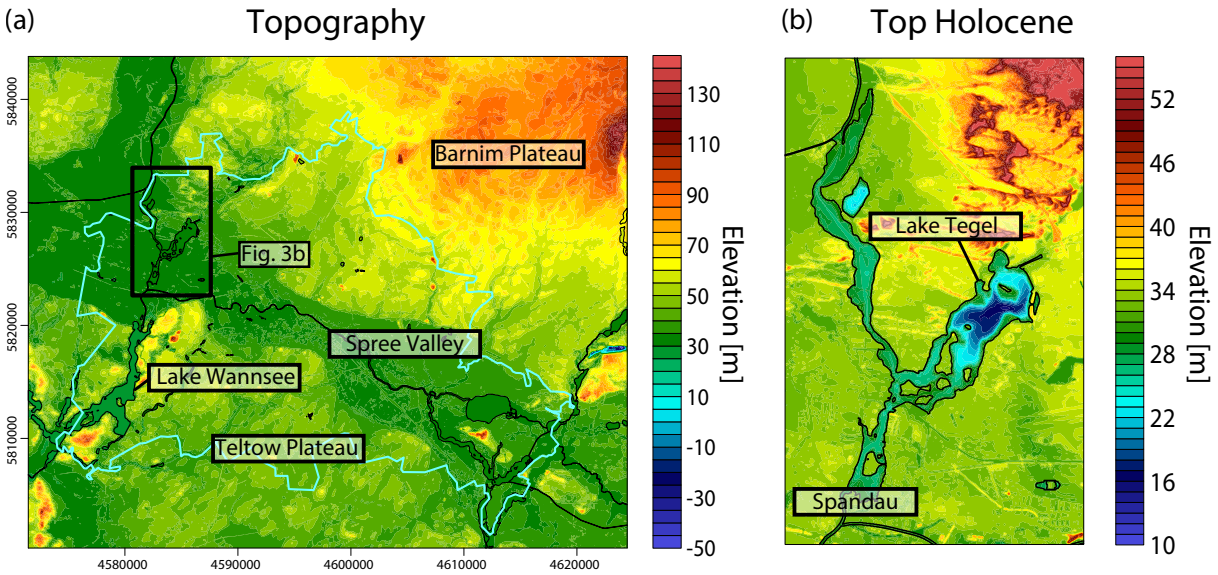

Figure 3.3.: Elevation distribution of topography and geological top surface. Thin black lines represent surface water body outlines. (a) Topographical distribution of the model area as derived from a high resolution digital elevation model (DEM) (Geodäsie, 2012), represents top of surface water bodies. Light blue line represents political border of Berlin. (b) Elevation distribution of topmost geological surface (Holocene) for exemplary site Lake Tegel as derived from combining the elevation data from Fig. 3.3a and water depth data (Fig. 3.4); Top Holocene represents bottom of surface water bodies. Coordinates [m] in Gauß-Krüger DHDN Zone 4.

3.4. Model Development and Scenarios

3.4.1. Refinement of the Model Surface

To understand the coupling between surface and subsurface water in the presence of major water bearing bodies (i.e. lake and rivers), new data have been integrated into the structural model as described in the previous section (Frick et al., 2016b). In a first step we derived a new top structural surface (i.e. Top Holocene) as based on a high resolution digital elevation model (DEM, grid resolution = $10x10$ m, Geodäsie (2012), Fig. 3.3a). It represents the water table of all surface water bodies, where present, or the surface of the solid earth.

The topography of the model area is typical of a post-glacial landscape, which has been formed during the latest glacial and interglacial periods as evidenced by extensive glacial spillways with meltwater valleys, low fluvial terraces and periglacial basins (i.e. greater Spree valley in the center of the model area, see Fig. 3.3a). The areas of higher elevation in the NE and S consist of ground and terminal moraines as well as young and old drift plateaus. Overall, erosional and depositional processes have shaped the area in a cyclic pattern associated with the different glacial and interglacial periods (Sonntag, 2005). These processes are also well represented in the lithological distribution (Fig. 3.1b) and structural configuration (Fig. 3.2b) of model units.

To derive the geological surface of the model area, the volume of the water bodies was subtracted from the DEM. This was done by compiling long term average data for lake water depth and river depth (data provided by MRDEA, SenStadtUm and WSA, see Acknowledgments). To derive the absolute depth values of the lakes, available contour maps of water depths were interpolated to regularly gridded surfaces within the supplied bounds

(Fig. 3.4b). These depths were then subtracted from the absolute elevation values of the DEM, thus resulting in the surface horizon (Fig. 3.4a). In areas where rivers are present, we derived this surface by combining the newly created lake bottom data (outlet of lakes) with river water depth measurements. Since all investigated rivers are connected to at least one of the lakes, in- and outlet geometries (Fig. 3.4c) were used as starting or endpoints for the rivers. To derive the bottom surface of the rivers, an average width buffer was applied to the available centerlines while respective widths have been derived from satellite data (Fig. 3.4c). The created outlines of the rivers were then assigned interpolated elevation values between the starting and end point, keeping true to an elevation drop of the top surface downriver. The elevation data for the center line were derived by subtracting measured or interpolated water depth data from the absolute elevations of the outline. Finally, the geological surface was constructed by interpolating between the outlines and the centerline (Fig. 3.4c).

The resulting geological surface (Fig. 3.3b) was then integrated into the structural model (Fig. 3.1a) modifying the underlying interfaces accordingly.

3.4.2. Assignment of Physical Properties

For the numerical simulations carried out in this study, each of the geological layers has been assigned constant values for thermal and hydraulic properties according to Table 3.1. These physical properties were either derived from measured values or based on literature data according to the dominant lithology. Special attention was given while parameterizing the partly discontinuous Rupelian clay. Assuming all unconformities to be the results of glacial erosion, we have parameterized these areas by giving the same set of parameters as to the unit locally overlying the Rupelian. All Cenozoic units were parameterized according to the petrological information supplied in the well database (Frick et al., 2016b). These lithologies were combined with literature data in order to derive values for the physical properties (Table 3.1), the exact procedure of which is explained in detail in Frick et al. (2016b). Heterogeneities in lithological distributions of the different geological units have therefore been taken into account as part of the parameterization. This approach was chosen since resolving those heterogeneities geometrically would have led to a drastic increase in model elements and therefore simulation time, with little influence on the model result. We chose not to integrate any hydraulic conductivity anisotropies for the study area ($\kappa_x = \kappa_y = \kappa_z$), since no data on this property are available and a general analysis of the influence of this parameter is not scope of this study. However, fundamental work on the topic of geological entropy and the associated κ field have been published recently and should be considered in future studies of the region, especially in studies opting for solute transport (Bianchi and Pedretti, 2017). Since no measured data about the storage coefficient are at our disposal, we used the FEFLOW© default value of $0.0001\frac{1}{m}$.

3.4.3. Modeling Method

The structural information described above has been integrated into a 3D structural model after Frick et al. (2016b). This model differentiates 18 sedimentary basin fill units (eight of which are Cenozoic in age, Fig. 3.1a) and two units for the underlying non-sedimentary units, namely

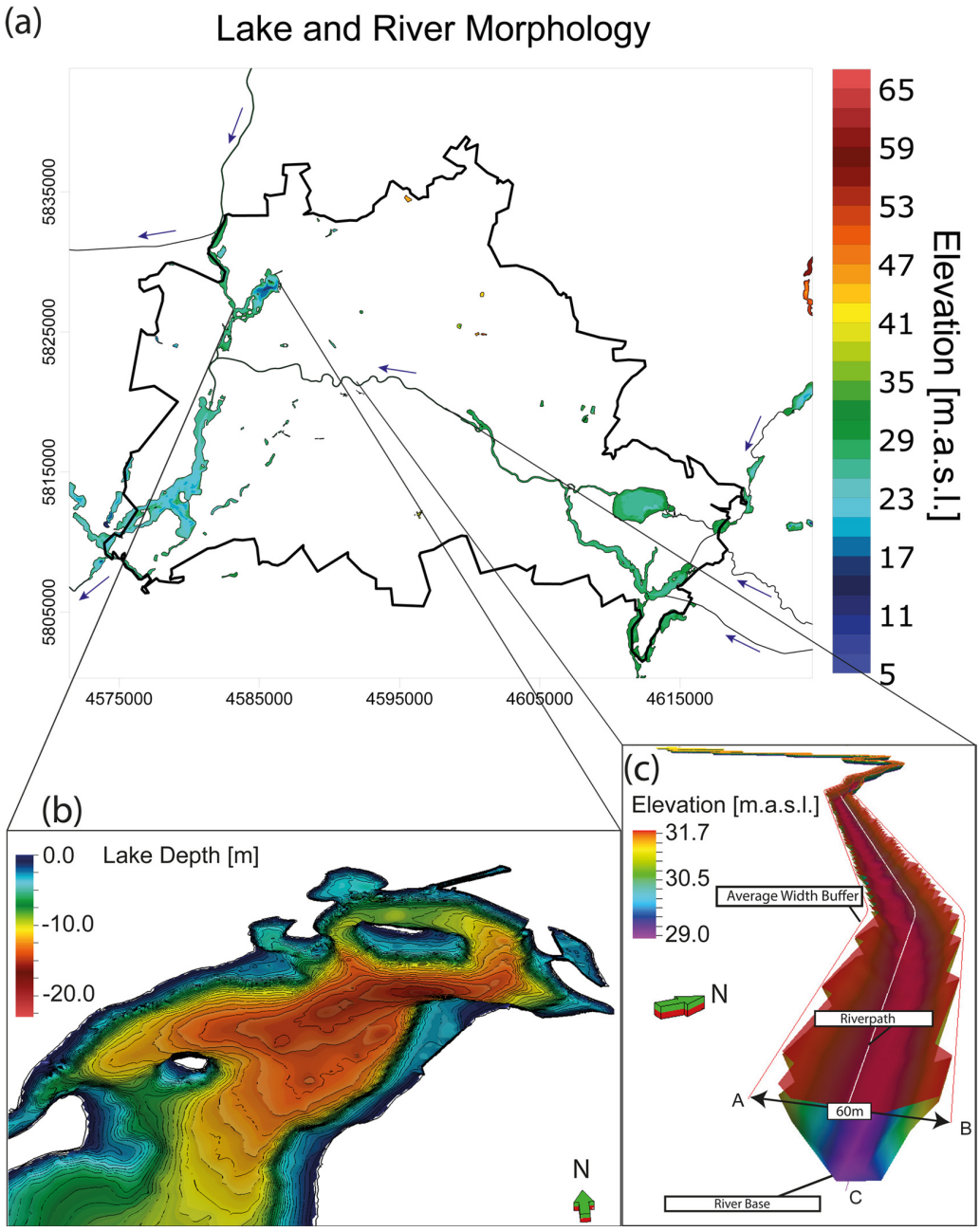

Figure 3.4.: Lake and river morphology. (a) Elevation distribution of the base of all rivers and lakes in the model area. Blue arrows indicate flow direction of rivers. (b) Zoom into lake base morphology for the example site of Lake Tegel. Black lines represent input data. (c) 3D river realization for the River Spree. Location in (a) indicated by lines. A,B,C indicate outlet geometry data used for the construction. Coordinates [m] in Gauß-Krüger DHDN Zone 4.

Permocarboniferous Volcanics and Basement (comprised of Pre-Permian and Upper Crust). The model is part of a series of studies, investigating different aspects of the geological subsurface. In this, models are becoming increasingly more local, thus increasing in resolution and physical processes considered. These models rely on an extensive database, both in geological information as well as physical parameters. The study presented here, therefore makes use of these 3D gravity constrained, calibrated models and builds on them (i.e. Scheck and Bayer, 1999; Maystrenko et al., 2008; Kaiser et al., 2013a; Noack et al., 2013; Sippel et al., 2013, also refer to the supplementary material). The vertical extent of the model is limited to an elevation of -6000 m a.s.l., thus integrating all 18 sedimentary units overlying the two non-sedimentary layers, the lowermost one of which has been clipped at -6000 m a.s.l..

In order to investigate the effects of different set-ups of the surface hydraulic conditions, we use coupled heat and fluid transport simulations. While the main subject of this study is a quantification of the groundwater dynamics, we also use modeled temperatures as a passive tracer to analyze predicted variations in the hydraulic setting as induced by the model modifications. For this purpose, the 3D geological model was imported into the commercial software package FEFLOW©(Diersch, 2014). The latter solves for (un)saturated groundwater flow in porous media taking into account conductive, advective and buoyant (fluid-density related) heat transport processes within a finite element based computational framework. The mathematical formulation to solve for those processes is based on a system of three coupled equations, expressing conservation of fluid mass, momentum and energy, which under the Boussinesq assumption reads as:

$$S_{eff}\frac{\partial p^f}{\partial t} + \boldsymbol{\nabla}\cdot\left(\rho^f \boldsymbol{q^f}\right) = \phi Q_\rho \tag{3.1}$$

where S_{eff} is the storage coefficient, p^f is the pore pressure, t is time, ρ^f the mass density of the fluid, q^f the specific discharge (Darcy's velocity), ϕ is the porosity, and Q_ρ the sink–source mass term.

The specific discharge is given by:

$$\boldsymbol{q^f} = -\frac{\boldsymbol{k}}{\eta^f}\left(\boldsymbol{\nabla} h + \frac{\rho^f - \rho_0^f}{\rho_0^f}\frac{\boldsymbol{g}}{|\boldsymbol{g}|}\right) \tag{3.2}$$

where q^f is the volumetric flux (Darcy flux), k is the permeability tensor, η^f the fluid viscosity, h the hydraulic head, g the gravitational acceleration and ρ_0^f the reference mass density of the fluid ($999.793\frac{kg}{m^3}$).

We also use temperatures predicted by the models as a further means to better quantify and visualize the induced changes in the regional hydraulics (e.g. Saar, 2011; Racz et al., 2012). In this respect, salinity as another tracer was considered to be of secondary relevance for the specific goal of the present study. The paucity of available data which, at the current stage, will not permit an investigation of its impact on the city-wide groundwater and geothermal configuration

also influenced this decision. The energy balance equation then reads as:

$$\left(\phi\rho^f c^f + (1-\phi)\rho^s c^s\right)\frac{\partial T}{\partial t} + \rho^f c^f \boldsymbol{\nabla}\cdot\left(\boldsymbol{q^f} T\right) - \boldsymbol{\nabla}\cdot\left(\left(\phi\lambda^f + (1-\phi)\lambda^s\right)\boldsymbol{\nabla} T\right) = Q_r \qquad (3.3)$$

where $\phi\rho^f c^f + (1-\phi)\rho^s c^s = (\rho c)_{fs}$ is the specific heat capacity of the system with a fluid and solid phase. T is the temperature, $\rho^f c^f$ is the specific heat capacity of the fluid, $\phi\lambda^f + (1-\phi)\lambda^s = \lambda^{fs}$ the thermal conductivity tensor for the solid and fluid phase and Q_r the heat source function. Bold symbols represent vectors, all other scalars.

The resulting system of partial differential equations (Eqs. (3.1) to (3.3)) is closed by setting an Equation Of State for the fluid density (as a function of the system variables) after Blöcher et al. (2010), thus introducing a non-linear coupling among the equations. More details about the mathematical background and its numerical formulation can be found in Diersch (2014).

The horizontal resolution of the model is $100x100$ m (derived from average mesh triangle area). In detail, the mesh consists of 175856 triangular elements, wherein the refinement of locations where rivers, lakes and also Rupelian windows are encountered is four times higher compared to the surroundings. The refinement in areas where rivers and lakes are encountered depicts an increase in resolution compared to (Frick et al., 2016b), where rivers and lakes are not yet resolved. To guarantee a good vertical to horizontal element shape ratio, the original model configuration, consisting of 20 geological units (Fig. 3.1a) with distinct physical properties, was further refined, so that the final structural model is composed of 56 computational layers. Here, a minimum of two slices per geological unit was realized, whereas new slices were integrated in an equidistant manner between the geological surfaces from the structural model. The resulting numerical model consists of 9847986 elements. Due to the high non-linearity of the coupled problem, models were run in transient state for both, fluid and heat transport, until reaching quasi-steady-state conditions. The latter were reached after approximately 250k yr simulation time. The initial time step length was set to 10^{-3} d and the maximum time step length was $5x10^4$ d.

3.4.4. Boundary and Initial Conditions

Equations (3.1) to (3.3) represent an initial and boundary value problem. Therefore, in order for the problem to be well posed, a proper set of initial and boundary conditions must be assigned. We consider all lateral boundaries closed to both, fluid and heat transfer. This approach allows for a stable solution but also requires all sources and sinks of heat and fluid to be located within the model boundaries and that no heat or fluid is transferred to neighboring areas beyond the boundaries of the models, the shortcomings of which have already been discussed in Bayer et al. (1997). However, the region under study is located in the middle of the North German plain within an intracratonic area undergoing slow deformation without being surrounded by mountainous regions at its borders. Therefore cross-boundary flow is likely to be very small and was neglected in this study. Given these conditions, the prescription of the hydraulic load (with prescribed preferential flow areas at the lakes and rivers) as varying across the study area provides enough constraints to capture the groundwater dynamics at the scale of interest. Additionally,

the model scenarios described in the following depict fluid and heat budgets within reasonable bounds ($imbalance_{max} \leq 0.00001 * flux_{tot}$).

3.4.4.1. Hydraulic Boundary Conditions

In order to understand the hydraulic forcing due to rivers and lakes and related changes in the thermal and hydraulic budgets, we set up three different model scenarios. The first of these scenarios (reference model, M1) implements a set of BCs which were parameterized as first order, Dirichlet-type across the top surface of the model domain. We impose fixed hydraulic head values as derived from measured groundwater levels only (Fig. 3.5a) for all respective nodes of the uppermost slice of the model. With respect to previous studies (Frick, 2015; Frick et al., 2016b), we make use of a larger and denser database consisting of more than 2000 wells (Data provided by Department for Urban Development and the Environment of Berlin (SenStadtUm) and Ministry of Rural Development, Environment and Agriculture of the Federal State of Brandenburg (MRDEA), Fig. 3.5a). These data represent the recent measured groundwater heads for the main shallow aquifer in the model area (Fig. 3.1b). In comparison to the predecessor studies, a more accurate representation of this surface is achieved, whereas differences in elevation are as large as +16.2 m (-12.5 m).

For this scenario, the hydraulic head BC implemented derives solely from interpolated (Convergent interpolation) measured groundwater heads which differ substantially from surface water heads, deriving partly from an over-exaggeration of depressions in areas overprinted by anthropogenic effects (e.g. Lake Tegel area, groundwater pumping, Fig. 3.5a,b). Groundwater heads for this scenario range between 24.5 m and 77.2 m, whereas large heads are observed at topographic highs and small heads are observed in the valleys (Fig. 3.3). Comparatively low hydraulic heads are found in the W model domain, where groundwater pumping activities have led to a reduction in groundwater heads (Fig. 3.5a). The distribution of the hydraulic gradient displays clear domains of maxima located preferentially in the center of the study area, between the Barnim-Plateau and the Greater Spree Valley, consistent with the presence of major gradients in the surface elevation in these areas (Fig. 3.3a). This model is used as the reference model for this study and stands representative for a model scenario, where only measured groundwater heads are available since we want to investigate whether such a setup is sufficient to reproduce local flow regimes or if additional data are needed.

The second model scenario aims at quantifying the impact of lakes, represented by the related hydraulic BC, on the resulting subsurface hydraulics and temperature distribution (M2 hereafter). In order to include this additional surface component, the absolute elevations of the water levels of all lakes (derived from the high resolution DEM, Fig. 3.3a) have been implemented as fixed hydraulic heads, which results in the introduction of local gradients in hydraulic potential across the interface of lakes and bounding aquifers (Fig. 3.5b). We assume a direct connection between the aquifer and the lakes, depicting either influent or effluent conditions, depending on whether the surface water level is higher or lower than the surrounding groundwater level. The resulting heads range between 24.5 m and 77.2 m again, however, locally changes of up to +12.2 m (-7.4 m) can be observed, which correlate spatially with the location of the implemented water

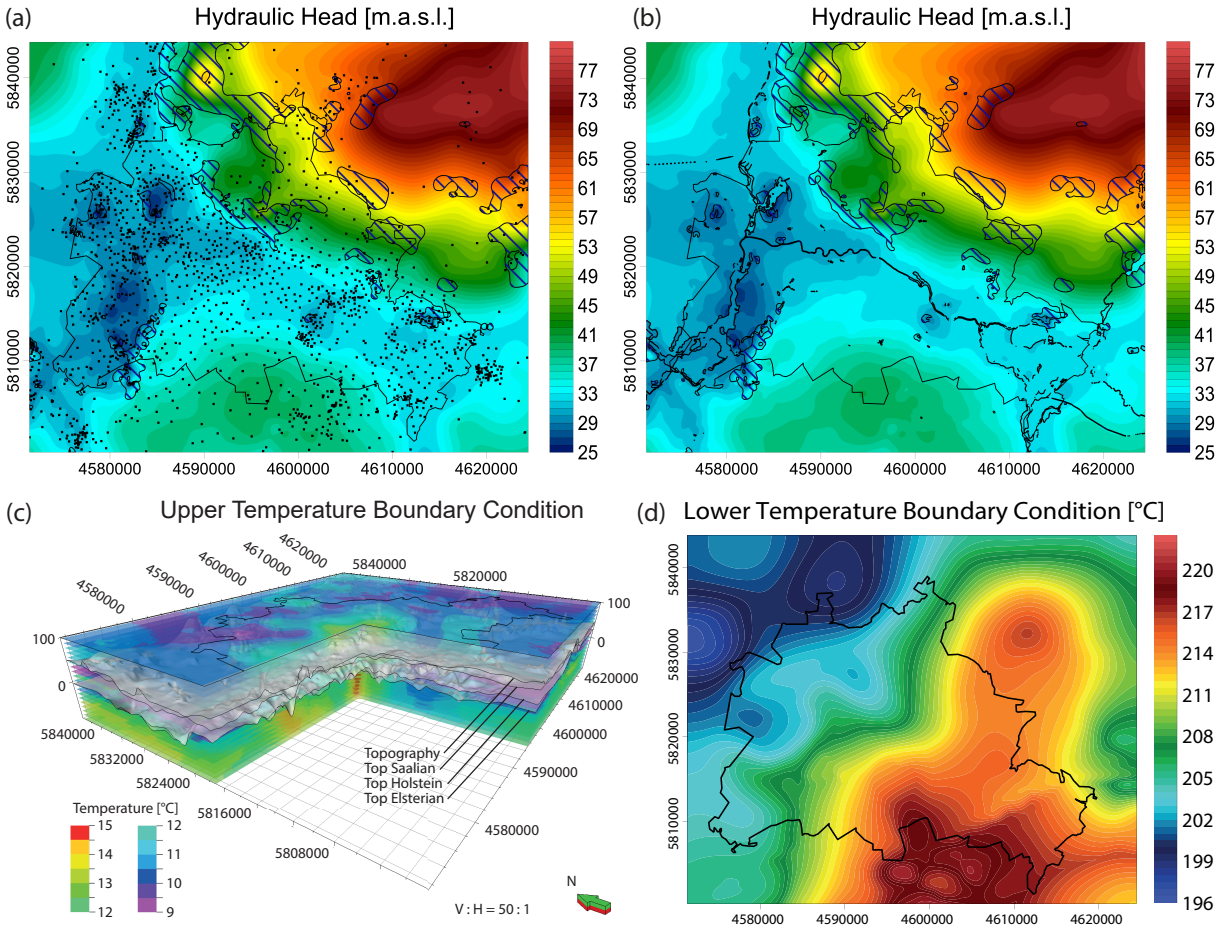

Figure 3.5.: Upper and lower hydraulic and thermal boundary conditions (BC). (a) Upper hydraulic BC as derived solely from measured groundwater levels (GWLs, location of input data indicated by black dots), utilized for Model 1; (b) Upper hydraulic BC as derived from measured GWL and DEM topographical data along with river level measurements, utilized for Model 2 (GWLs+Lake surfaces) and Model 3 (GWLs+Lake surfaces+river surface), major differences are found where surface water bodies are located; (a,b) shaded areas represent above average hydraulic gradient ($\nabla h \geq 0.16°$).(c) Upper thermal BC viewed in 3D, derived from temperature measurements reaching from +90 m a.s.l. to -100 m a.s.l., interpolated in 3D after the inverse distance weighted method; after Frick et al. (2016b); (d) Lower thermal BC as extracted from a purely conductive lithosphere scale model of the area at -6000 m a.s.l. (Frick et al., 2016b); Coordinates [m] in Gauß-Krüger DHDN Zone 4.

bodies.

The last model of this study (M3 hereafter) integrates rivers as connecting elements between the lakes (Fig. 3.4c). Therefore, assigned hydraulic heads (Dirichlet BC) display a gradient along the course of the river and more prominently to the surrounding aquifer (Fig. 3.5b). Again, differences in head between the different model scenarios are substantial, standing representative for differences to overrepresented depressions deriving from anthropogenic overprinting. The resulting heads range between 24.5 m and 77.2 m again, however, locally changes of up to +2.0 m (-8.3 m) can be observed, which correlate spatially with the location of the implemented water bodies.

With these distinct model scenarios, we are able to quantify the impact of surface water bodies (M2 = lakes, M3 = rivers) on the resulting hydraulic and thermal field.

The pressure and temperature initial conditions for the transient simulations were derived by solving for pressure and temperature separately under steady state conditions.

3.4.4.2. Thermal Boundary Conditions

The upper thermal BC was defined by imposing fixed values (1st kind Dirichlet BC) for the temperature across the uppermost four geological surfaces (Holocene, Saalian, Holstein and Elsterian), the value of which has been derived from interpolated grids based on measured (groundwater) temperatures distributed across the model area (Fig. 3.5c, SenStadtUm, 2014; Frick et al., 2016b). The top Holocene depicts fixed temperatures of 10.8°C derived from long term average air temperature data (DWD, 2015). The distribution of the temperatures of the following three geological surfaces shows that the hottest regions are located below the city centers of Berlin and Potsdam, correlating spatially with the amount of surface sealing (up to 15 °C, Henning and Limberg, 2012). In comparison, the lowest temperatures are found below least urbanized regions and in proximity to surface water bodies (7.8 °C). This BC was chosen in order to represent the anthropogenic overprinting produced by surface sealing (Henning and Limberg, 2012) and heat input from industrial activities on the present day thermal field. By assuming stable temperature conditions at the surface, we were able to investigate the impact of the surface to groundwater dynamics on the thermal configuration of the subsurface. Here, depth and lateral variations of the thermal configuration as induced by predicted changes in fluid dynamics due to each modification of the reference model were systematically investigated.

The lower temperature BC, representing heterogeneously distributed temperatures at -6000 m a.s.l., was derived from a lithosphere-scale 3D conductive model (Frick et al., 2016b) in order to have a quantifiable heat input coming from the deeper parts (crustal and mantle) into the study domain. Figure 3.5d illustrates the distribution of the imposed temperature, showing a gradual increase from 196.6 °C to 220.5 °C while moving NW to SE.

3.5. Model Results

The model results will be presented in terms of pressure, fluid flow and temperature distribution, predicted by each of the three different model scenarios and their respective comparison. They

are shown either as absolute values or relative differences between the model realizations.

3.5.1. Pressure and Fluid Flow Field Distribution

3.5.1.1. Reference Model (M1)

The pressure distribution at the uppermost slice of the first model (topography) shows distinct areas of negative (unsaturated conditions) and positive (saturated conditions) pressure (Fig. 3.6). Areas with negative pressure make up most of the model area and reach values of up to -8.11 bar. These areas are located beneath topographical highs (Fig. 3.3a). Likewise, a general correlation between the topology of the topography and the pressure is evident (Figs. 3.3 and 3.6a). Areas of high topography display highest negative pressures and vice versa. Accordingly, areas of positive pressure are found in the valleys and lowlands, as particularly visible at Lake Wannsee (Fig. 3.3a, Fig. 3.6a). Highest positive pressure values are located in the very eastern portions of the model area (8.09 bar, Fig. 3.6) and correlate with the topographical low of the limestone mine in Rüdersdorf. These high pressures also correlate with the location and extent of surface water bodies located in the model area (Fig. 3.5b). However, the absolute values display high differences to the present day situation. This can be seen in water depths at e.g. Lake Tegel $\geq$ 16 m, standing representative for a hydrostatic pressure of 1.6 bar, clearly indicating how the hydraulic potential of these water bodies is only approximated in a very crude manner by such a hydraulic boundary setting (p_{max} at site = 1.1 bar).

The pressure distribution at -50 m a.s.l. (chosen as first continuous surface) shows a similar trend as the one described above. Areas of high pressure are located in the NE, S and NW, correlating well with the topographic highs as well as areas of high hydraulic potential (Fig. 3.3a, Fig. 3.5a). Lower pressures are predicted for the central model domain, correlating with areas of low topography, most prominently the greater Spree valley (Fig. 3.3). These areas also display a low hydraulic potential (Fig. 3.5a). This pressure distribution continues at greater depths, reaching the first regional impermeable layer in the model (Middle Muschelkalk, Fig. 3.2c,d). Predicted fluid flow patterns (Fig. 3.7a) follow the general hydraulic gradients as imposed by the upper hydraulic potential. Infiltration mainly occurs beneath areas of high hydraulic potential in the NE, NW and S almost independently of the geological structure underneath. In comparison, exfiltration is strongly linked to areas of low hydraulic potential, mainly located in the central model domain (Greater Spree Valley) prominently visible at lake sites, the latter not yet resolved in terms of their hydraulic behavior in this model (Fig. 3.7a). The example site of Lake Tegel in the east-southeast domain of the study area additionally displays two major domains: (a) influent conditions in the E and (b) effluent conditions in the W (Fig. 3.7b).

3.5.1.2. Lake Model (M2)

The pressure distribution defined by the second model scenario shows some similarities both in trends and magnitude compared to the ones described above for the reference model (M1). Pressure changes between the two model realizations are mainly limited to areas of small lateral extent, directly below or nearby the extent of the surface water bodies implemented (Fig. 3.6c).

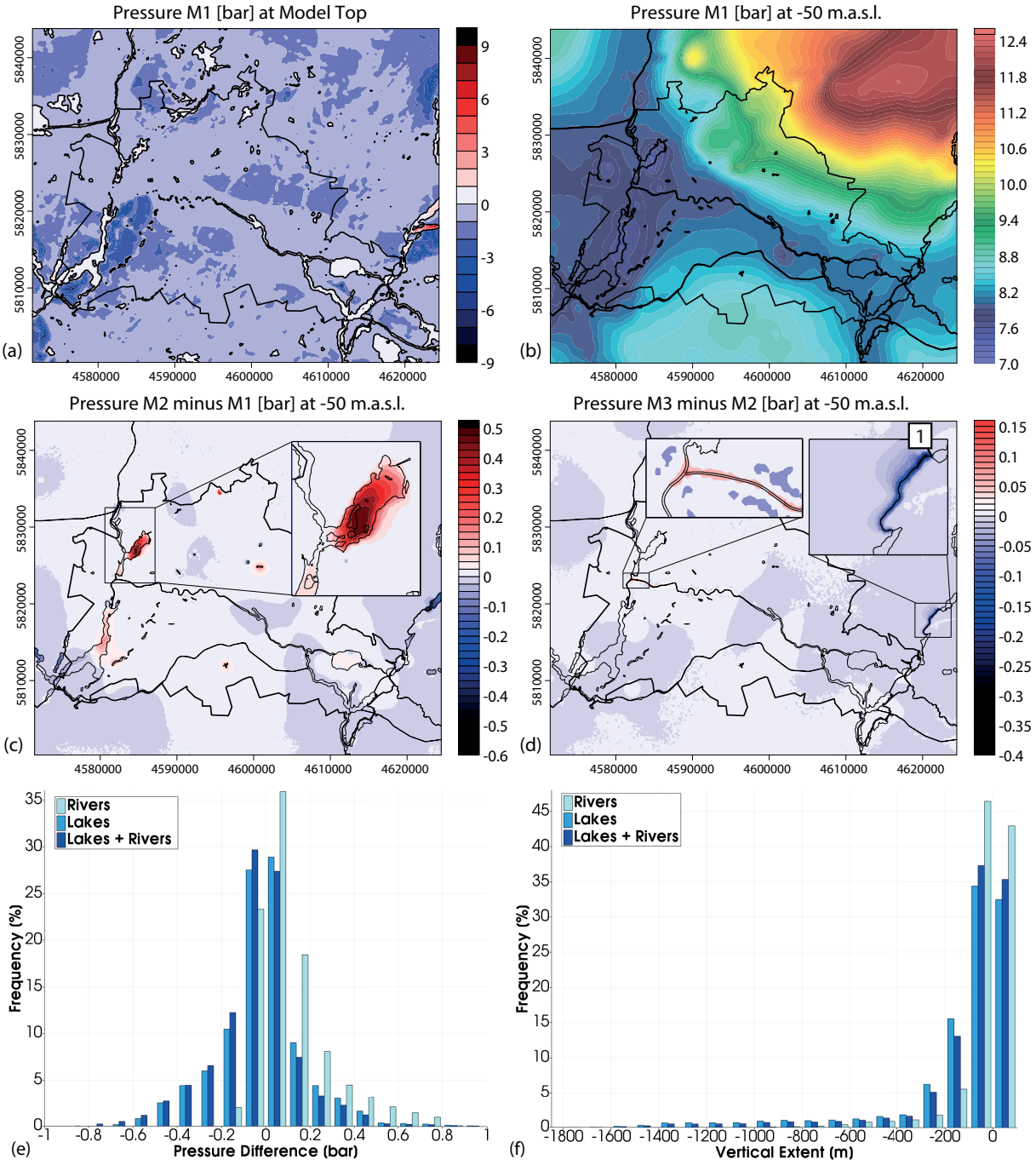

Figure 3.6.: Model results pressure. (a) Pressure distribution at model top for the Reference Model (M1). Change from positive to negative pressure indicated by the black contour line. (b) Pressure distribution for M1 at -50 m a.s.l. (c) Pressure difference between M2 and M1 at -50 m a.s.l.; Zoom in shows Pressure differences at Lake Tegel site. (d) Pressure differences between M3 and M2 at -50 m a.s.l., Zoom ins: (left) River Spree and Havel site, (right) Mühlenfließ, 1 - Outlet of Lake Stienitz; (e) Distribution of Pressure differences between the different model scenarios depicting the relative influence of Rivers, Lakes and Rivers + Lakes combined (Minimum difference of ±0.01 bar). (f) Distribution of significant pressure differences over depth between the different model scenarios (chosen threshold is ±0.01 bar). Coordinates [m] in Gauß-Krüger DHDN Zone 4.

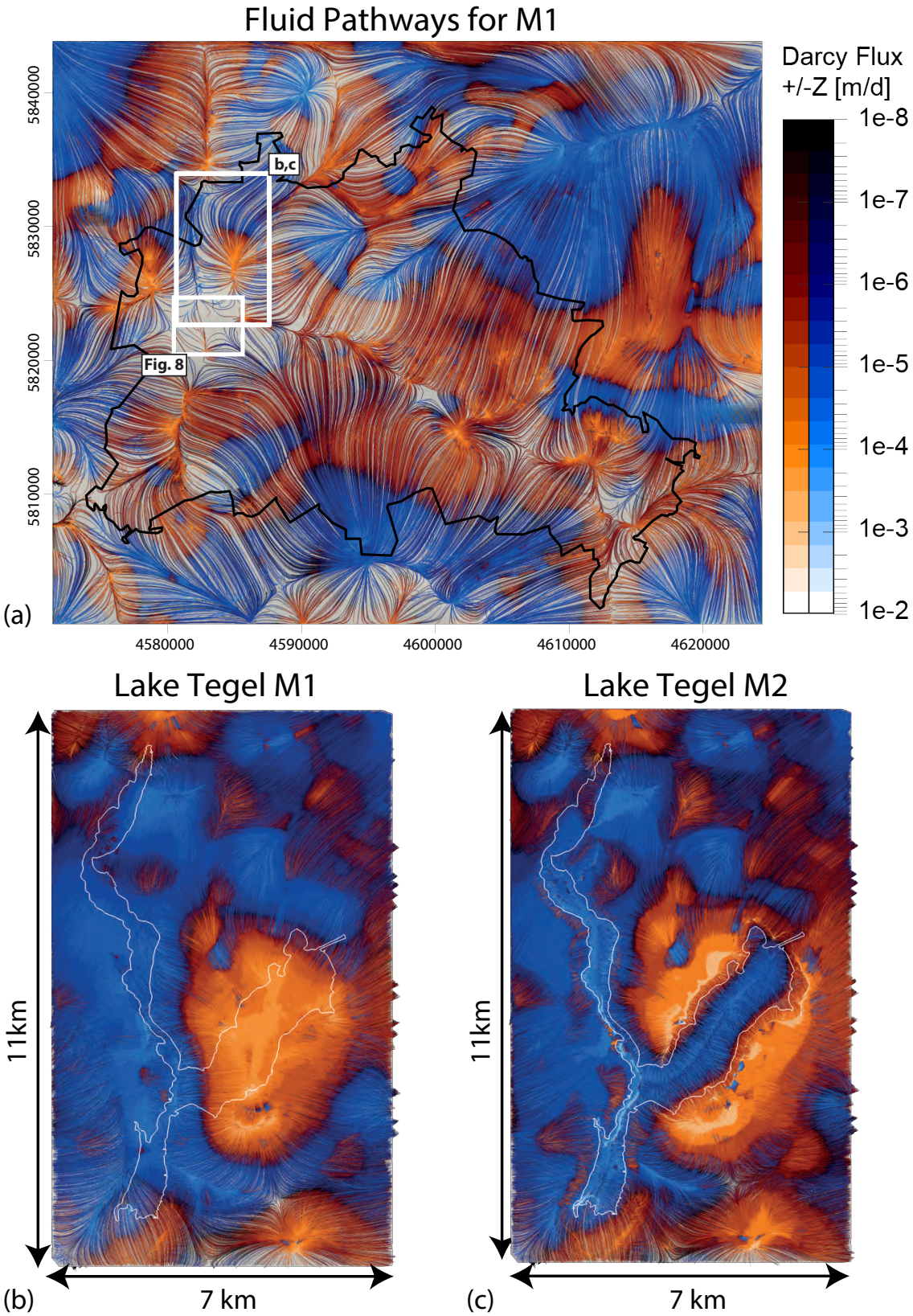

Figure 3.7.: Predicted fluid flow fields. (a) Fluid pathways for Model scenario 1 projected on the surface of the Triassic Muschelkalk. Pathways were derived from the modeled nodal volumetric flux through the Streamtracer filter of Paraview (Squillacote et al., 2007) for the final solution time step (quasi steady state). The color-coding represents the Darcy flux in vertically positive (uprising in orange) or negative (infiltrating in blue) direction. Termination points of lines correlate with either sites of recharge (light blue) or discharge (bright orange). White outlines indicate extent of (b,c) showing fluid pathways at example site Lake Tegel (b=M1, c=M2) and Fig. 3.8 showing fluid pathways at example site Spree-Havel. Coordinates [m] in Gauß-Krüger DHDN Zone 4.

Maximum predicted differences are of the order of ±1.0 bar (Fig. 3.6e). Areas of pressure increase mainly relate to lake sites where the hydraulic potential was formerly underestimated (losing lake, influent conditions) and pressure decrease commonly correlates with lake sites where the hydraulic potential was overestimated in M1 (gaining lake, effluent conditions). This hydraulic reversal can be best illustrated beneath the site of Lake Tegel (Fig. 3.6c), where pressure differences of +0.5 bar are predicted. This leads to a higher hydraulic potential than that of the surrounding aquifer. In contrast, Lake Stienitz to the very E of the model area displays a drop in pressure of up to -0.6 bar, thereby resulting in a comparatively low hydraulic potential area. The depth extent of these changes reaches as far as the top of the middle Muschelkalk, considered in all models presented as an aquitard of regional extent, with maximum values of -1920 m a.s.l. though they are mainly restricted to the shallow model domain down to -300 m a.s.l. (Fig. 3.6f).

The fluid flow field resulting from this pressure distribution is similar to the one described for M1. Major areas of recharge are located in the NE, NW and S and major discharge areas are located in the central model domain, namely the Greater Spree Valley, as well as localized areas of limited lateral extent in the SW and NW. The implementation of the additional hydraulic forcing due to the presence of major lakes leads to complete fluid flow reversal beneath areas that are hydraulically connected to the surface bodies. This is illustrated in the following for the specific Lake Tegel site in the east-southeast domain. While the western part remains a recharge area (Fig. 3.7c), though also increasing the vigor of flow ($q_{diff_{max}} = 1.7E07\%$), the eastern part displays a reversal in predicted flow directions. These changes in the hydraulic potential also lead to uprising of groundwater predicted in the direct vicinity of the lake. Here, pressure driven flow caused by the generally low hydraulic potential of these areas is supported by the buoyant upcoming of heated water which infiltrated at the lake site (see also thermal results described below). This behavior is observed across the whole model area and results in modifications of groundwater circulation mainly located where the hydraulic potential of lakes is significantly higher than that of the surrounding aquifers.

3.5.1.3. River Model (M3)

The last model scenario predicts pressures which are in the same order of magnitudes as those predicted by M1 and M2 when averaged on a regional scale. Hence, major areas of recharge and discharge show similar distributions. Similarly to M2, pressure changes have a limited spatial extent, located directly below or in vicinity to the implemented river bodies (Fig. 3.6d), reaching maximum values of ±0.80 bar (Fig. 3.6e). A distinct area of pressure increase is predicted where River Spree and Havel merge (to the S of Lake Tegel) with maximum values of +0.15 bar. This result is likely caused by the fact that the set-up of the previous models (M1, M2) resulted in effluent conditions (gaining stream) at this site, therefore likely underestimating the hydraulic potential carried by these two river bodies (Fig. 3.6d). In the very E of the model area, a local drop in pressure can be observed. Here, the hydraulic potential beneath the Mühlenfließ was overestimated in M1 and M2, consequently displaying a maximum drop of -0.4 bar leading to effluent conditions at this location. Pressure differences are observable down to depths of up to

-1030 m a.s.l. (Fig. 3.6f) which is approximately half as deep as the changes induced by the lakes and is likely connected to the smaller general volume of water represented by these water bodies. This is also reflected in the majority of changes displaying a vertical extent of $\geq$ -100 m a.s.l..

According to the results described above, the hydraulic field as predicted by M3 displays few modifications when compared to the previous model scenarios. These are mainly limited to domains in the direct vicinity of the major river bodies. This is shown clearly in the area where Spree and Havel merge. At this site, M2 predicts mainly discharge due to a low in hydraulic potential (Fig. 3.8a). In comparison, a complete reversal in flow directions is predicted by M3, changing from an area of discharge to an area where recharge is prevailing due to a local increase in the hydraulic potential (Fig. 3.8b). Through this change in local hydrodynamics, discharge is also predicted to the W of River Havel and S and N of River Spree. Accordingly, all sites where the pressure dropped in this model scenario, show an increase in the vigor of exfiltration (i.e. Mühlenfließ, $q_{diff-max} = 2.8E08\%$).

The results presented above show that with implementation of surface water bodies changes in fluid dynamics lead to a configuration where the gradients between the latter and surrounding aquifers cause the process of bank filtration. Here, infiltration from lake and river sites towards depressions in the hydraulic head is in accordance with fluid dynamics observed in other studies (Massmann et al., 2007; Massmann et al., 2008; Möller and Burgschweiger, 2008). This fit in circulatory patterns increases between the different model scenarios of this study, whereas M3 presents the best fit scenario of this study.

3.5.2. Temperature

The temperature distributions predicted by the different models are used as a passive marker in order to quantify both the lateral as well as the depth extent of the hydrodynamics caused by the changes in the surface hydraulic configuration. This approach is feasible since the upper model domain is dominated by pressure driven fluid flow. Thus, any modifications in the pressure configuration and resulting hydrodynamics also lead to changes in advective heat transport and consequently predicted temperatures.

3.5.2.1. Reference Model (M1)

Shallow temperatures predicted by M1 show a complex distribution of minima and maxima, ranging from 20.8 °C to 34.2 °C (Fig. 3.9a) at -500 m a.s.l. Highest temperatures are predicted in the center of the model area, and also locally in the E and NW. Negative thermal anomalies at this elevation are mostly confined to the N, E and NW areas of the model domain. Their locations correlate spatially with areas of high hydraulic potential (Fig. 3.5a, Fig. 3.6b) driving water to infiltrate from the surface into the deeper model domains (Fig. 3.7a). Areas of low hydraulic potential (Fig. 3.5a) are characterized by higher temperatures, mainly resulting from upconing of deeper and warmer water to shallow levels (Fig. 3.9a, Fig. 3.7a). The temperature distribution at this depth is additionally defined by the background conductive heat flow. Hence, the poorly thermally conductive Rupelian leads to high temperature gradients where maximum thicknesses of the unit are encountered (e.g. NW and SE Fig. 3.9a, Fig. 3.2b). The highly

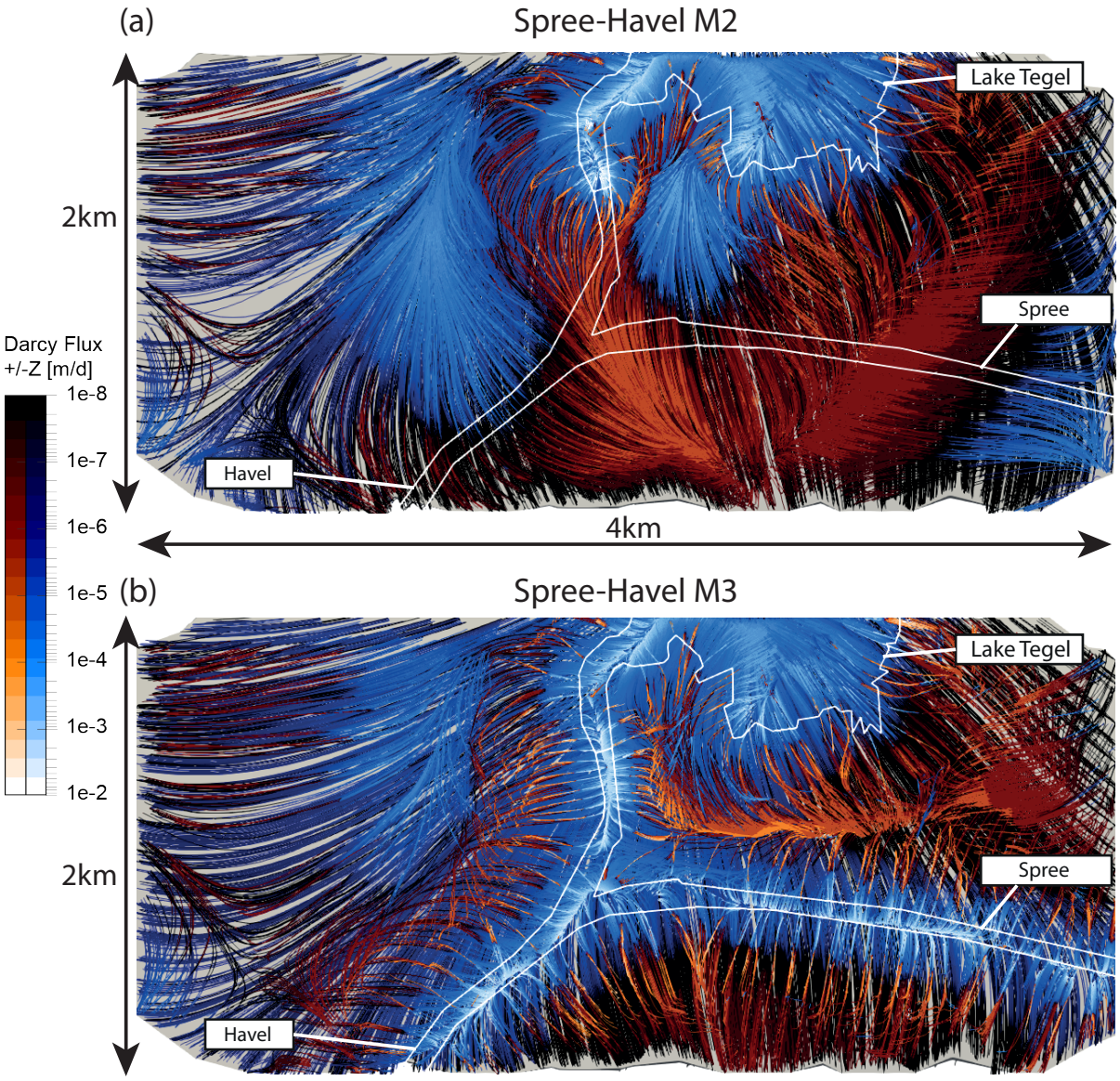

Figure 3.8.: Predicted fluid flow fields at example site Spree-Havel. (a) Fluid pathways for Model scenario 2, (b) Fluid pathways for Model scenario 3. Location of (a,b) in Fig. 3.7a. North is up. Pathways were derived from the modeled nodal volumetric flux through the Streamtracer filter of Paraview (Squillacote et al., 2007) for the final solution time step (quasi steady state). The color-coding represents the darcy flux in vertically positive (uprising in orange) or negative (infiltrating in blue) direction. Termination points of lines correlate with either sites of recharge (light blue) or discharge (bright orange).

thermally conductive Zechstein also displays a positive correlation of its thickness maxima to predicted temperatures at this depth (E, W and NE, Fig. 3.9a, Fig. 3.2f).

The temperatures predicted by M1 at -3500 m a.s.l. range from 108.8 °C to 129.6 °C (Fig. 3.9b). At this elevation, the thermal field is no longer influenced by any active component due to groundwater flow, being only controlled by diffusive processes. The temperature distribution reflects the distribution of the differently conductive layers, with the Zechstein salt playing the most prominent role (Bayer et al., 1997; Kaiser et al., 2011; Sippel et al., 2013). Indeed, highest temperatures are found in domains of minima in the salt thickness (Fig. 3.2f) where heat withdrawal and channeling is less effective compared to below salt structures (diapirs). Therefore,

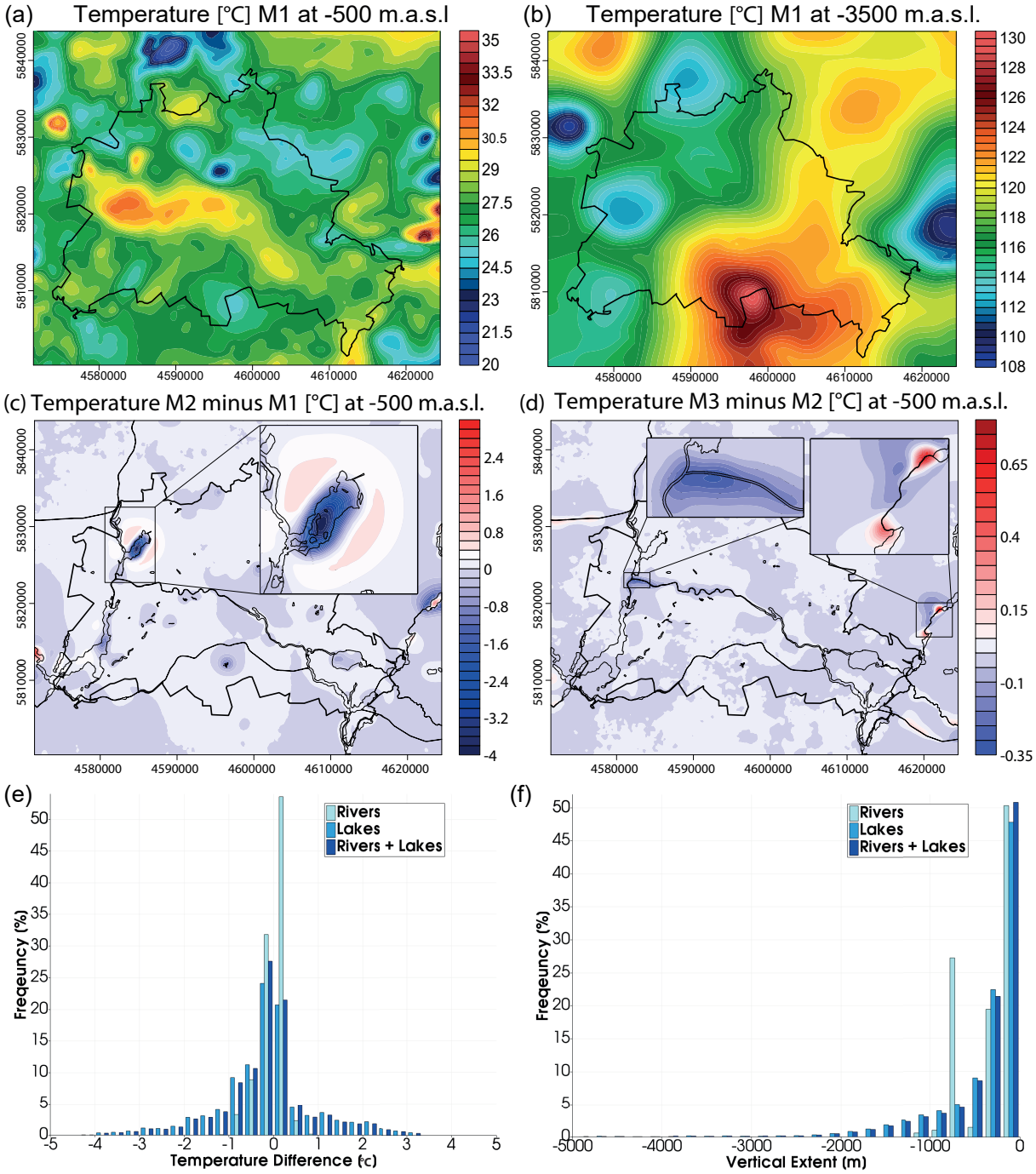

Figure 3.9.: Model results temperature. (a) Temperature distribution at -500 m a.s.l. for Model scenario 1. (b) Temperature distribution for M1 at -3500 m a.s.l. (c) Temperature difference between M2 and M1 at -500 m a.s.l.; Zoom in shows temperature differences at Lake Tegel site. (d) Temperature differences between M3 and M2 at -500 m a.s.l., Zoom ins: (left) River Spree and Havel site, (right) Mühlenfließ. (e) Distribution of temperature differences between the different model scenarios depicting the relative influence of rivers, lakes and rivers + lakes combined (Minimum difference of ±0.1 °C). (f) Distribution of significant pressure differences over depth between the different model scenarios (chosen threshold is ±0.1 °C). Coordinates [m] in Gauß-Krüger DHDN Zone 4.

lowest temperatures are predicted, where the highest thicknesses of the Permian unit is present. There is also a minor component of the lower thermal BC present, standing representative for the heat input from the deeper subsurface.

3.5.2.2. Lake Model (M2)

Despite a similar range in trend and magnitude of modeled temperatures, differences between predicted temperature distributions from M1 and M2 with depth are also found and lie within the range of ±5 °C, wherein most are located between -2 °C and +1 °C with a mean value of -0.2 °C(Fig. 3.9e). Highest differences at the investigated elevation level (±4.0 °C, Fig. 3.9c) are located in direct vicinity to the implemented surface water bodies and have a lateral extent as large as 4km (e.g. Lake Tegel, $T_{diff-min}$ = 0.1 °C = smallest value where a spatial correlation to surface water bodies is still observable). This is a strong indicator for the changes in fluid dynamics induced by either the modeled increase or decrease in hydraulic loading due to the implementation of lakes as surface hydraulic parameter. In detail, colder temperatures in M2 are found below surface water bodies, reflecting an increase in the hydraulic load above these areas (Fig. 3.6c). This increase in infiltration also leads to higher predicted temperatures surrounding Lake Tegel (Fig. 3.9c). This result derives from an increase in uprising of deep groundwater induced by changes of the upper hydraulic head BC in this region (Fig. 3.5a,b). The temperature differences also indicate changes in fluid dynamics with depth, with significant modifications (±1 °C) down to depths of more than -1500 m a.s.l. and differences greater than ±0.1 °C are displayed even at elevations up to -4800 m a.s.l., spatially correlating with pressure changes, thus likely linked to convective processes (Fig. 3.9f). In comparison, pressure differences can only be followed down to -1600 m a.s.l., indicating, that induced changes in fluid dynamics have a more wide-spread effect than indicated by the pressure change alone.

3.5.2.3. River Model (M3)

Temperature differences between M3 and M1 amount to ±5 °C, approximately at the same domains of maximum difference and lateral extent as described in the previous paragraph. However, comparing M3 and M2, local variations are also visible, though limited in magnitudes of up to ±1.3 °C (Fig. 3.9d) with most lying within a range of -1 °C to +0.5 °C (mean: -0.03 °C, Fig. 3.9e). The distribution of these differences is limited to areas directly beneath or adjacent to the implemented surface water bodies, that is beneath locations where the hydraulic gradients between rivers and adjacent aquifers reach their maximum values. Accordingly, local changes in modeled fluid dynamics result in lower temperatures where the hydraulic potential has been increased (i.e. Fig. 3.9d, Fig. 3.2a,b) and higher temperatures are calculated where it has been decreased (Fig. 3.9d). These induced changes in fluid dynamics display a small depth range, which is indicated by a maximum elevation of temperature differences of ±0.1 °C at -1200 m a.s.l. (Fig. 3.9f). Moreover, these elevations are far greater than the modifications in pressure indicate (-600 m a.s.l.), thus showing that this tracer has a significantly higher level of sensitivity to capture even small changes more accurately. The horizontal extent of these modifications is also

limited compared to M2, reaching its maximum value ($\sim$ 2200 m) at the outlet of Lake Stienitz (Fig. 3.6d,Fig. 3.9d) and up to 1000 m at the intersection of Havel and Spree (Fig. 3.9d).

3.6. Discussion

The results of the models presented in this study have demonstrated that the shallow hydraulic field below the city of Berlin is mainly controlled by the configuration of the imposed upper hydraulic BCs, specified by the groundwater level distribution and water levels of major surface water bodies. Resulting hydraulic potentials and gradients lead to a fluid flow pattern where infiltration into the deeper parts of the model domain is dominant in areas of high hydraulic heads or hydraulic gradients. Accordingly, exfiltration occurs at sites with low hydraulic potentials (Fig. 3.5a, Fig. 3.7a).

The first model scenario clearly shows that predicted groundwater circulation is controlled by two factors: (1) the hydraulic head BC and (2) the structure and hydraulic conductivity of model units. To discuss (2) shortly, the results from a previous study (Frick, 2015) are compared with the results derived in this study concerning the feasibility of the parameterization of the Rupelian aquitard. In our previous study, we considered the Rupelian to be completely impermeable, thus only allowing exchange between the different aquifer compartments at local discontinuities (hydrogeological windows). In contrast, a different parameterization of the clay unit has been performed in this study, wherein the Rupelian aquitard still shows a low permeability, though of higher magnitudes than previously done (κ_f = 3.23E-8 $\frac{m}{s}$, Table 3.1). To compare the two model realizations, fluid pathways and for travel times equivalent to Pleistocene ages were computed, utilizing the base of the Pleistocene as starting surface. This analysis was carried out, since previous fluid chemistry interpretations indicate mixing between infiltrating Pleistocene and recent waters of different salinity content at depths $\geq$800 m (Tesmer et al., 2007; Möller et al., 2007). These studies indicated a leakage through the Rupelian to depths well beneath its base independent of the location of the windows throughout the model domains lateral extent. Thus, predicted fluid pathways with the time-framing described above should cover the entire lateral model extent. Comparing the different studies then shows that for travel times of Pleistocene origin an impermeable Rupelian only produces a sparse distribution of lateral mixing of infiltrating water ($\sim$ 40% of model area). In comparison, even a comparatively lowly permeable Rupelian allows for faster infiltration and higher lateral mixing, as indicated by the large extent of infiltration below the Rupelian base ($\sim$ 90% of model area). Therefore, the hydrodynamics predicted by M1 of this study should be considered as more realistically representing real subsurface hydrology compared to the results from Frick (2015). Additionally, isotope ratios point towards an incomplete sealing of Permian and Triassic evaporites towards the overlying sediments (Möller et al., 2007), which questions the role of the Triassic Middle Muschelkalk as a tight aquitard (Pöppelreiter et al., 2005), but was not studied here due to the paucity of data to properly parameterize this unit. It has also be shown by Bianchi and Pedretti (2017) that solute transport specifically, and fluid pathways in general, are influenced strongly by the implementation of heterogeneities in the κ-field, which should be investigated further in

future studies.

Even more intensively than the hydraulic conductivity, the results of this study demonstrate how the configuration of the upper hydraulic head BC (1) and any changes to the latter likely lead to strong modifications of the pressure field and the resulting distribution of fluid pathways as outlined in Section 3.5. In this context, the sensitivity of the model to the implementation of surface water bodies along with the integration of high resolution topographical data has resulted in significant changes in the predicted hydraulic and the thermal field (Figs. 3.6 to 3.9). This is best exemplified by increased pressures in areas below or adjacent to most of the implemented surface water bodies, leading to a complete reversal in the local fluid flow dynamics (Figs. 3.7 and 3.8). Compared to M1, where the upper hydraulic BC was derived based on measured groundwater heads, differences in the elevation of hydraulic heads up to $\pm 12.2\,\mathrm{m}$ ($\Delta p_{max} = 1.19\,\mathrm{bar}$) were implemented in the additional model realizations (M2 and M3). The resulting changes in hydraulic potential and pressure lead to modifications in the predicted local flow field, which is best illustrated at Lake Tegel. Here, a major low in prescribed hydraulic head representing a major discharge area obtained in M1, features a local potential high in M2 (influent, Fig. 3.5b). This in turn induces infiltration of surface water from the lake boundaries into the adjacent aquifers, as is typical for the region (Nützmann et al., 2014). Moreover, the resulting pressure changes also lead to strong uprising in the direct vicinity of the lake shore. These results, visualized by calculating the fluid pathways, show a general downward flow beneath the lakes. When entering the first aquifer, the flow field develops a horizontal component flowing parallel to the surface of the first aquitard encountered at depth and it finally rises to the surface into a major discharge area (Fig. 3.7c). The distribution of these flow paths mimics to some extent the observed local fluid dynamics, where intense groundwater pumping activities in these areas have led to considerably lower hydraulic heads (Fig. 3.5a,b). This caused an increase of infiltration of surface water from the lake into the aquifer which is in accordance with the observed hydraulics, where up to 70% of groundwater wells in Berlin are fed by surface water infiltration (Massmann et al., 2008).

From the results of this study, it appears clear that considering a simplified approach in deriving the hydraulic head distribution from measured groundwater heads, as is mostly done in these kinds of simulations (Viszkok, 2000; Person et al., 2008; Zlotnik et al., 2011, 2015; Anderson et al., 2015), will only hinder the model to capture the complex dynamics occurring in the subsurface (Fig. 3.7b,c). This can be seen clearly in the thermal signature, indicating changes in the groundwater dynamics as induced by the presence of major lakes reaching depths up to -4000 m a.s.l. (Fig. 3.9). This is far greater than for variations induced by seasonal fluctuation in surface temperature and/or human activities, illustrating the far reaching long term effects of importance for any further study focusing on the aforementioned parameters.

Considering major rivers in addition only leads to local modifications of the modeled hydraulic field. Indeed, even when rivers are hydraulically connected to the underlying aquifers, the overall magnitude of water exchange is comparatively small, reaching its maximum potential beneath areas of highest hydraulic gradients (Fig. 3.5b; Fig. 3.8a,b). Similarly to M2, these areas were predicted as discharge areas in M1 but are now featuring infiltration due to a local rise of

hydraulic potential, which enables the process of bank filtration in groundwater production which is established in vicinity of the surface water bodies (Fig. 3.8a,b, Massmann et al. (2007)). Additionally, modifications of the hydraulic field are identified in regions where rivers connect to lakes. Here, the increase in the hydraulic head at the rivers has the effect of smoothing out local gradients in the hydraulic potential between the different water bodies (e.g. Outlet Lake Stienitz: Reduction from 8.2 ° to 0.2 °, Fig. 3.5a,b) and therefore results in less vigorous infiltration of surface water in nearby locations. The overall depth influence of these modifications ($\geq$-1200 m a.s.l., Fig. 3.6e) is limited when compared to M2, however, it still encompasses the entirety of the shallow fresh water compartments.

The results obtained in this study also have a more direct and applied merit in the context of a safe fresh water management within the city of Berlin. As an example, M3 showcases the sensitivity of the shallow hydraulic field to major rivers. These results can then be used to analyze the influence of contaminants which are carried into the model domain or might even be coming from inside the model area, thus having a relevance to better quantify the danger of contamination of the fresh water aquifer. For instance, extensive lignite mining in the Lausitz (SE of model area) has led to the exposure of pyrite, which represents a major source of sulfur. This chemical component can be found in river water in the form of $SO_4{}^{2-}$ (e.g. Graupner et al., 2014), which is a major groundwater pollutant. Increased concentrations of this component have already been found in groundwater samples within the model area (e.g. Maeng et al., 2010). The source of the latter can either be by river-load or through groundwater circulation. This problem and the increased salinity of the shallow groundwater compartments, outlines the necessity of being able to represent the hydrodynamics near the surface and the related feedbacks to and from deeper groundwater circulation with the highest amount of details. The study presented here therefore depicts a step towards a systematic understanding of river-aquifer interactions in an urban environment. However, to make quantifiable predictions, local studies should be envisaged, depicting even higher resolutions and taking into account contaminant and solute transport.

The thermal field predicted by the models of this study displays heterogeneously distributed temperatures at the investigated elevation levels. At depths greater than -3000 m a.s.l. the thermal configuration is mainly controlled by conductive heat transport locally shaped by the structural configuration of the units with highest or lowest values for thermal conductivities, namely the Permian Zechstein and partly the Paleogene Rupelian. However, in the shallow model domain this general relationship is overprinted by a component of convective heat transport. At these depth levels ($\leq$-1000 m a.s.l.), locally colder temperatures are predicted, where major areas of recharge result in infiltration of cold surface water. In contrast, locally warmer temperatures are predicted below major discharge areas, where heated water from the deeper model domain rises to the surface. These findings are in general agreement with a previous study (Frick et al., 2016a) but show distinct differences in predicted temperatures, where focused down- and upward movement of groundwater (Fig. 3.7a) is predicted by the models presented here. This is illustrated by predicted temperatures differences at -500 m a.s.l., which are as high as $\pm$7.5 °C. These are likely linked to the increase in convective heat transfer, induced by local increases or

decreases of hydraulic gradients.

Using the predicted temperatures as a tracer for quantifying the effect of changes in fluid dynamics, the results show, that the implementation of lakes produced maximum temperature differences of ±5 °C, whereas colder temperatures are more common than warmer (Fig. 3.9c,e). These modifications are traceable down to -4800 m a.s.l. (mainly above -2000 m a.s.l., Fig. 3.9f). In comparison, thermal perturbations induced by the consideration of Rivers are only up to ±1.3 °C (Fig. 3.9d,e). The related modifications of the thermal configuration are traceable until -1200 m a.s.l., but mostly restricted to the very shallow model domain (≥ -200 m a.s.l., Fig. 3.9f). Combining the results of the two modified model scenarios, colder temperatures prevail (Fig. 3.9e). This likely derives from the general increase in hydraulic potential compared to the reference model. Consequently, most rivers and lakes represent losing conditions in M3, which is in accordance with observations (Massmann et al., 2008) and results partly from reduced hydraulic heads due to groundwater pumping.

The effects of urbanization and climate change on the subsurface thermal field has gained increased focus in the last decade (e.g. Taniguchi et al., 2007; Yalcin and Yetemen, 2009; Zhu, 2013; Menberg et al., 2015). The results of these studies show that the shallow subsurface in such areas has been highly modified, both thermally and hydraulically. These modifications are mostly represented by increased temperatures beneath urban centers connected to changes of surficial BCs, like surface sealing, industrial waste heat and climate change amongst others, commonly referred to as urban heat islands (Menberg et al., 2013). This excess heat has been proposed for geothermal utilization, providing heating for decades (Zhu et al., 2010). However, these studies are purely analytical or limited to 1d, therefore excluding 3D effects entirely. This study shows that the shallow geothermal field is controlled by numerous factors to which it reacts in a more or less sensitive manner. This in turn entails caution while performing any feasibility study for assessing the utilization of heat resources below major urban areas, where modifications in the local hydrodynamics as related to the aforementioned activities might have far-reaching and unexpected effects. This is supported by the results of this study, where local changes in hydrodynamics lead to temperature differences up to ±5 °C, which translates to strong variations in the extractable amount of heat, especially for shallow geothermal utilization. At the same time the results illustrate that these shallow thermal fingerprints might reach depths up to ≥-4000 m a.s.l., depending on the local hydrogeological conditions. All of these factors point towards a careful planning to set up possible city-wide energy provision from geothermal resources, which is especially relevant given that the thermal perturbations are well within the typical thermal breakthrough values during operational activities (Hähnlein et al., 2013). Therefore, an accurate description of the shallow hydraulics, here represented by more realistic hydraulic BCs, is of high importance. This is also evident in significant variations in the amount of extractable heat at a given place due to the changes in local hydrodynamics.

The models presented in this study focus on proposing and testing a conceptual physical model of the shallow to deep water dynamics beneath the area of the city of Berlin as based on a detailed geological model. This conceptual model underwent a quantitative and systematic calibration in terms of the gravitational response from the geological structuring, providing constraints on the

quality of our geological configuration and range of rock material parameters (Maystrenko and Scheck-Wenderoth, 2013). Additionally, it has been validated against the two only available deep temperature logs in wells, providing further constraints on the geological reliability of the models as well as their basic parameterization (Frick et al., 2016b). Moreover, all model parameters entered have been derived from either direct measurements (field, laboratory) or from literature research (Sippel et al., 2013; Frick et al., 2016b). On top of these data, the study integrates data on the shallow hydraulic conditions, most importantly the hydraulic BC, arriving at the most up-to-date understanding of the geological and hydrogeological configuration of the area beneath the capital city of Berlin. However, these types of studies might at best provide predictions about the system behavior within certain error bounds, which are indeed intrinsic in any study, whether based on extrapolation of measurements or on forward predictive physics based models. In detail, the models presented here could still be improved and will be, given the appropriate data, in terms of incorporating more information of the geological configuration (well logs, seismics), parameterization of model units (calibration, measurements) or hydraulic BC setup (cross border flow, denser database). However, we would like to emphasize that at this stage, under consideration of all available data, we are convinced by the robustness of the modeling results in representing the first order dynamics of the system, which are in accordance with published studies as outlined above.

The results of this study show, that lakes and rivers, under the assumption of ideal hydraulic connectivity, might reshape the fluid flow field considerably, especially where surface water bodies with large fluid volumes are involved. However, riverbeds (colmation layer) typically show a lower hydraulic conductivity than the surrounding aquifer, which would likely reduce the exchange of groundwater and surface water. Studies investigating this aspect are so far mostly restricted to local models (e.g. Engeler et al., 2011), and measurements of the physical properties of the colmation layer are rarely available. In the setting of the model area, river gradients, and therefore also fluid velocities are rather small, which would suggest a comparatively thick and stable colmation layer as opposed to higher energy settings (Ruf, 2007). Nevertheless, hydraulic gradients between surface water bodies and surrounding aquifers are comparatively high (Fig. 3.5b), which has been shown to be sufficient to cause leakage even through low permeability layers (i.e. Rupelian) independent of their thickness. To quantify these processes more accurately, ongoing studies are investigating the sensitivity of 3D thermohydraulic models to the implementation and parameterization of colmation layers. Additionally, the model is forced to present-day observed hydraulic head conditions and these are prescribed for 250 k yr of simulation time (after Sippel et al. (2013)). This implies (1) that we may overestimate advective cooling/warming effects looking at the evolution of temperatures (steady state after approximately 7 k yr) and (2) that we do not consider a "natural" state of the system as present day hydraulic heads also integrate current pumping activities, which are however not part of the model dynamics. Here, future studies should implement groundwater wells, as effects of the latter on local hydrodynamics, as well as connected thermics are still poorly studied and understood. Especially the impact on predicted shallow temperatures is of importance since current policies opt for a greater share of renewables in the energy mix, also including geothermal.

3.7. Conclusions

The implementation and consideration surface water bodies in 3D thermohydraulic modeling is of importance since it significantly influences the predicted hydraulic and temperature field. First and foremost, changes to the local thermohydraulics are most pronounced where differences in prescribed hydraulic heads are highest between the surface water bodies and adjacent aquifers. Accordingly, we observe more vigorous infiltration of cold surface water into the deeper model domain where hydraulic heads of rivers and lakes are higher than those of neighboring aquifers, leading to forced convective cooling. In contrast, where hydraulic heads of surface water bodies are lower than the surrounding aquifers, a change of the fluid flow direction from downwards to upwards is predicted, leading to higher calculated temperatures since heated waters rise up at these locations. The modifications induced by the implementation of lakes are mostly confined to areas in their direct vicinity since no directional hydraulic gradient is imposed. In contrast, the implementation of rivers might lead to changes in subsurface hydraulics in areas where the absolute hydraulic head remains constant, but a downriver hydraulic gradient is existent.

This study was able to outline the depth influence of surface hydrodynamics on coupled deep and shallow fluid and heat transport. Implemented lakes account for modifications of the hydraulic and thermal field down to an elevation of -4800 m a.s.l. and the consideration of rivers modifies these fields down to an elevation of -1200 m a.s.l. Herein, temperature differences of more than 5 °C are predicted down to an elevation of more than -500 m a.s.l., which translates to major modifications in depths of interest for shallow geothermal utilization. Additionally, these depth ranges encompass the entirety of shallow groundwater compartments, which underlines the importance of implementing surface water bodies, especially concerning the groundwater compartmentalization in connection with groundwater pumping or groundwater contamination from river load in the model area. Understanding the influence of all physical processes involved serves as basis for future simulations of thermohaline energy and solute transport looking both at the present state and future scenarios.

3.8. Acknowledgments

We highly appreciate the comments by the two anonymous reviewers, which helped increase the quality of this manuscript. This research is funded as part of the joint initiative of the research field energy of the Helmholtz Association “Energy System 2050”. We would like to thank the Senate Department for Urban Development and the Environment of Berlin (SenStadtUm), Berlin waterworks (BWB), Ministry of Rural Development, Environment and Agriculture of the Federal State of Brandenburg (MRDEA) and the Waterways and Shipping Office (WSA) for providing the data for this study. The 3D information on the structural configuration of the subsurface of Berlin was compiled, visualized and interpolated with the commercial software package Petrel (© Schlumberger). All data are available upon request from the listed sources above and simulation results are available from the first author upon request.

Supplementary Material

The following files support the conclusions of the manuscript at hand and contain information as follows.

Figs. 3.10 to 3.18 describe the structural setup of the model in much more detail than was necessary for the readability of the manuscript. We provide an overview of the utilized well database in accordance with Frick et al. (2016b) (Fig. 3.10). The resulting elevation (Figs. 3.11 to 3.14) as well as thickness distributions (Figs. 3.15 to 3.18) as derived from the structural modeling done by Frick et al. (2016b) are shown for all respective geological (model) units. These represent the input grids as produced with Petrel© with a resolution of 100x100 m. The only exception is the geological surface of the Holocene (topography) which was integrated with a resolution of 25x25 m as necessary for the scope of this study.

We also included a map view of the employed upper temperature boundary conditions, which were derived from measured and interpolated groundwater temperatures as described in Frick (2015) (Fig. 3.19).

Last, we also included map views for the presented model scenarios of recharge and discharge area distributions. These show an increasing alignment with proposed fluid dynamics (Massmann et al., 2007) but were deemed as less illustrative than the stream tracer analysis presented in the main body. Lastly, we include a map of recharge/discharge magnitudes predicted by the models, wherein the most common values are in alignment with reported values (Senate Department for Urban Development and Housing, 2013).

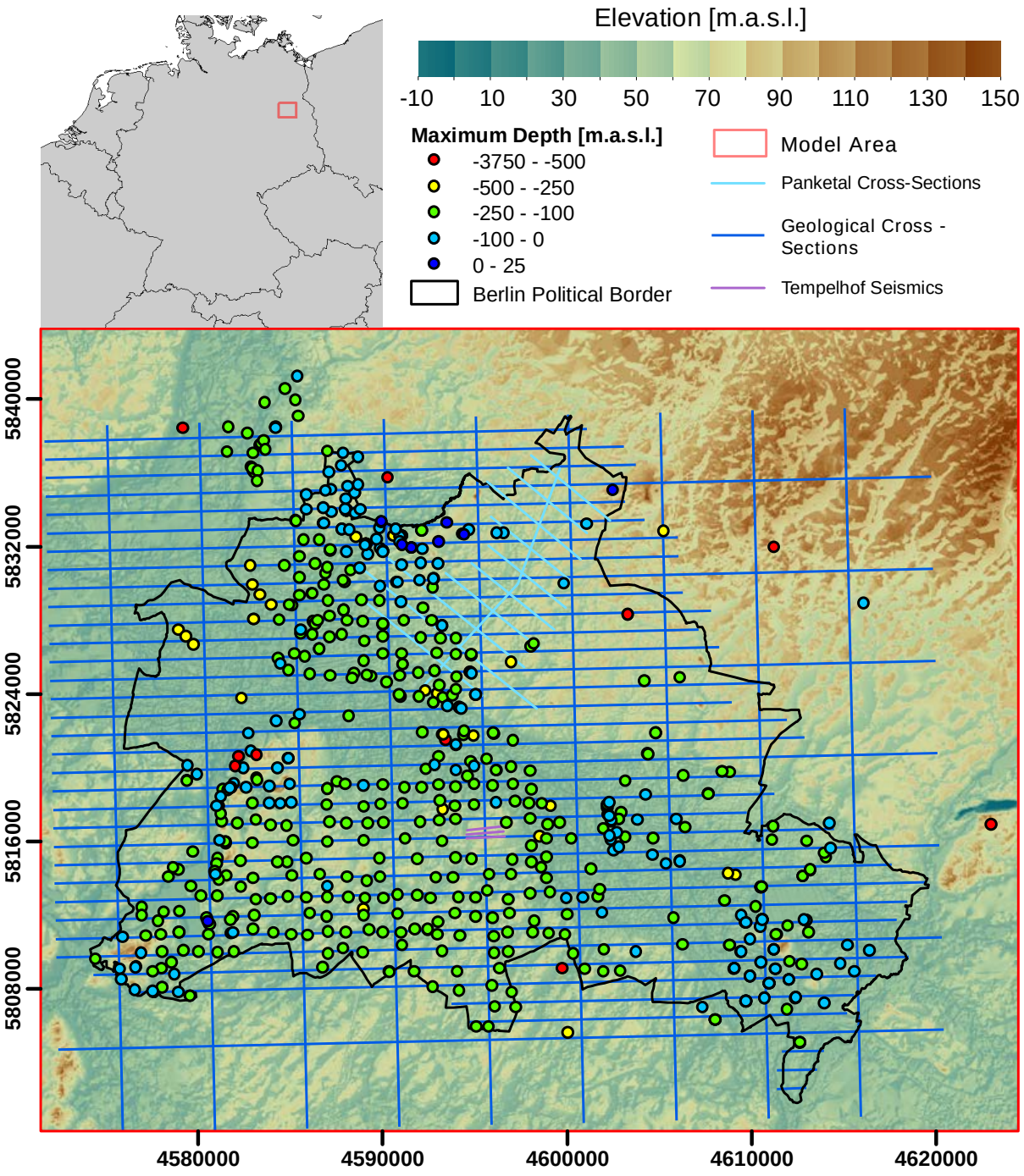

Figure 3.10.: Location of the model area in central Europe and database. As indicated, colored dots represent well positions inside the model area, dark blue lines show locations of the geological cross-sections (light blue lines show cross-sections cutting the Panketal aquifer), m.a.s.l.: meters above sea level; Coordinates [m] in Gauß-Krüger DHDN Zone 4. Please note, that larger scale 3D gravity constrained geological models were also utilized, especially, where no well data are available.

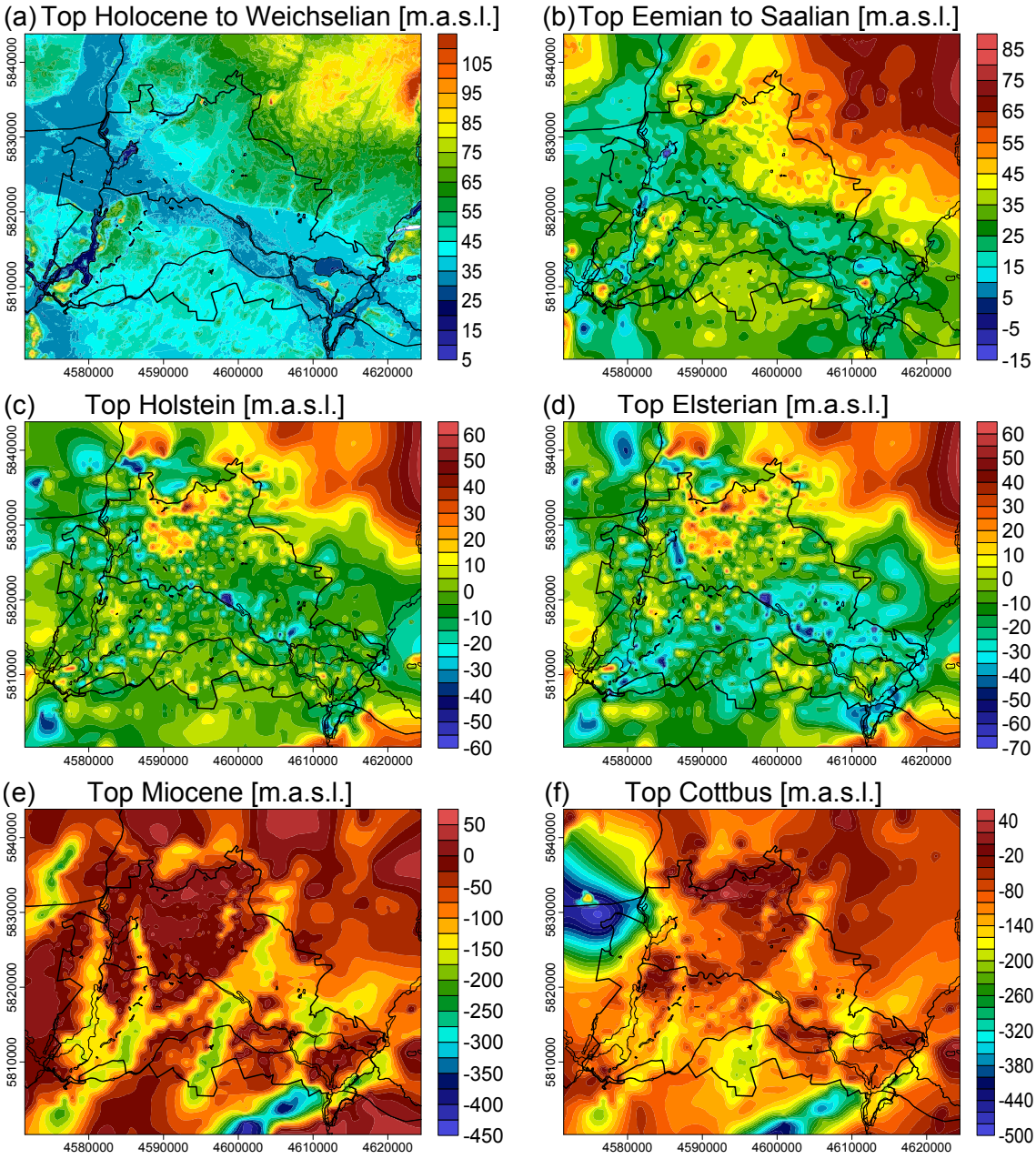

Figure 3.11.: Elevation of top surfaces of Quaternary Holocene to Tertiary Cottbus as used in the 3D structural model used for the thermal simulations. Coordinates [m] in Gauß-Krüger DHDN Zone 4. (a) Quaternary Holocene to Weichselian, (b) Quaternary Saalian, (c) Quaternary Holstein, (d) Quaternary Elsterian, (e) Tertiary Miocene, (f) Tertiary Cottbus. White areas depict where the unit is missing or very thin.

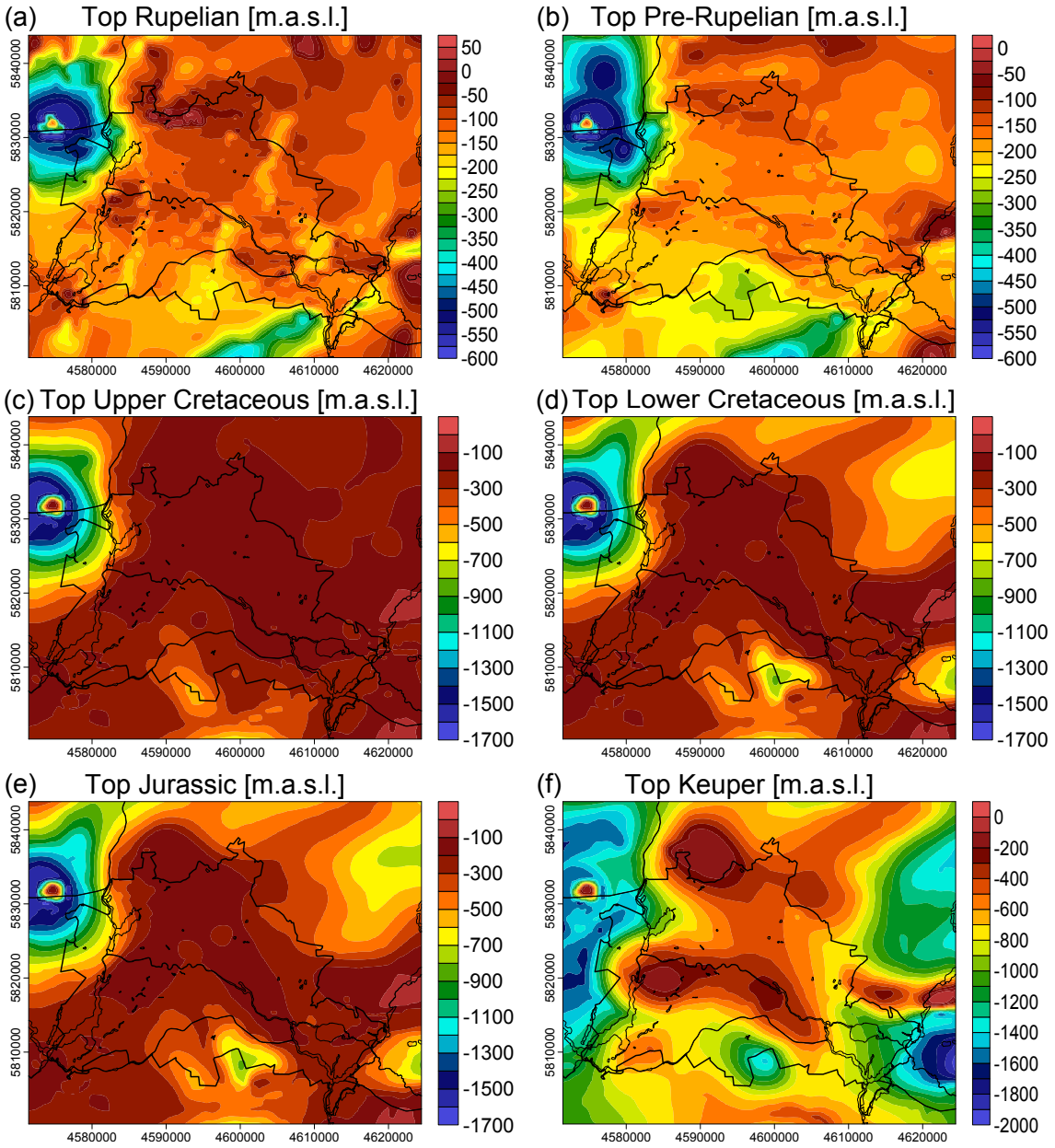

Figure 3.12.: Elevation of top surfaces of Tertiary Rupelian to Triassic Keuper as used in the 3D structural model used for the thermal simulations. Coordinates [m] in Gauß-Krüger DHDN Zone 4. (a) Tertiary Rupelian, (b) Tertiary Pre-Rupelian, (c) Upper Cretaceous, (d) Lower Cretaceous, (e) Jurassic, (f) Triassic Keuper. White areas depict where the unit is missing or very thin.

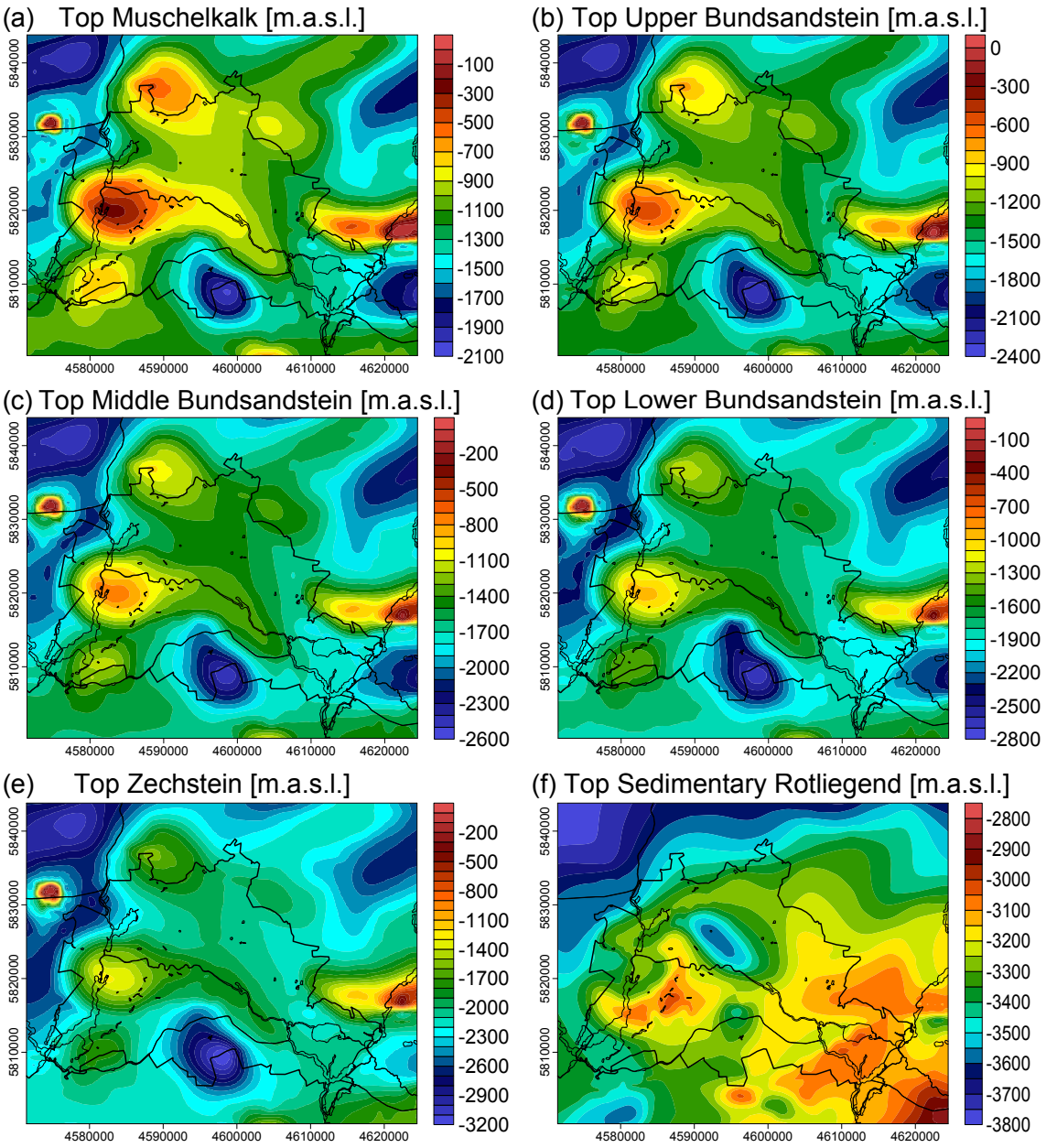

Figure 3.13.: Elevation of top surfaces of Triassic Muschelkalk to Permian Rotliegend as used in the 3D structural model used for the thermal simulations. Coordinates [m] in Gauß-Krüger DHDN Zone 4. (a) Triassic Muschelkalk, (b) Triassic Upper Buntsandstein (c) Triassic Middle Buntsandstein, (d) Triassic Lower Buntsandstein, (e) Permian Zechstein, (f) Permian Rotliegend.

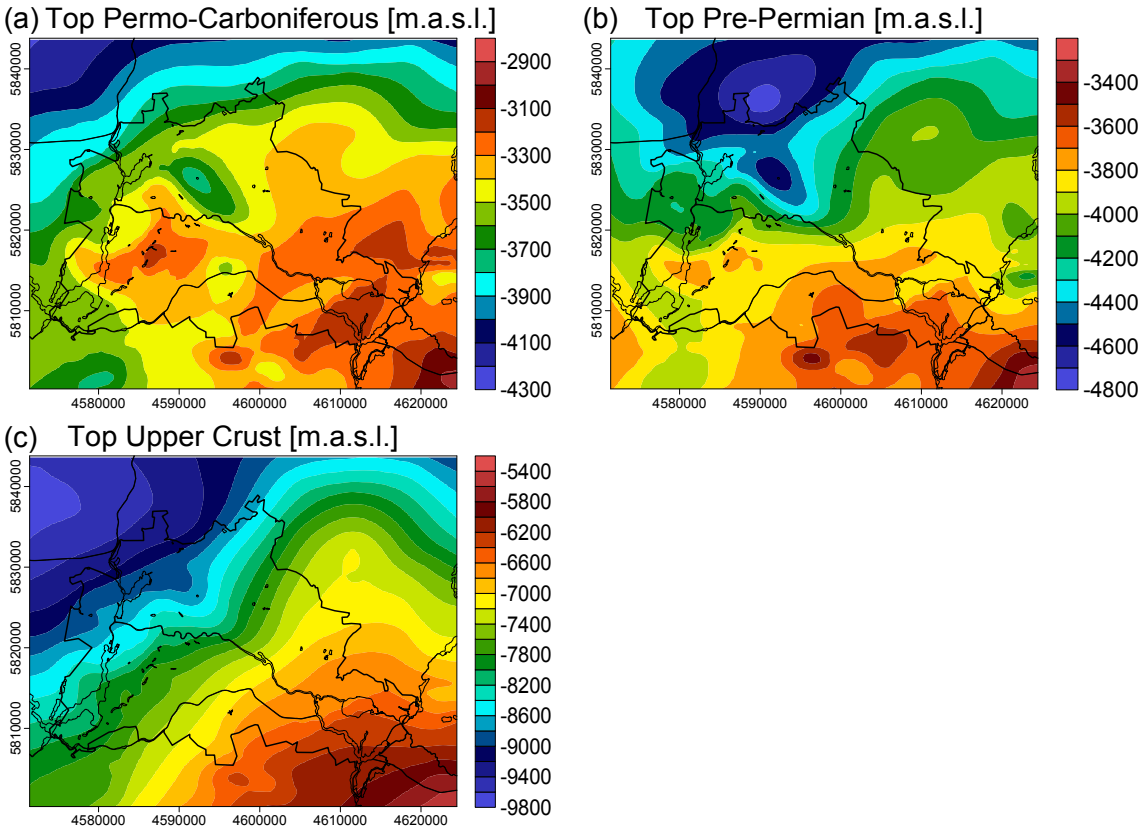

Figure 3.14.: Elevation of top surfaces of Permocarboniferous Volcanics to Lithosphere-Asthenosphere-Boundary as used in the 3D structural model used for the thermal simulations. Coordinates [m] in Gauß-Krüger DHDN Zone 4. (a) Permocarboniferous Volcanics, (b) Pre-Permian, (c) Upper Crust.

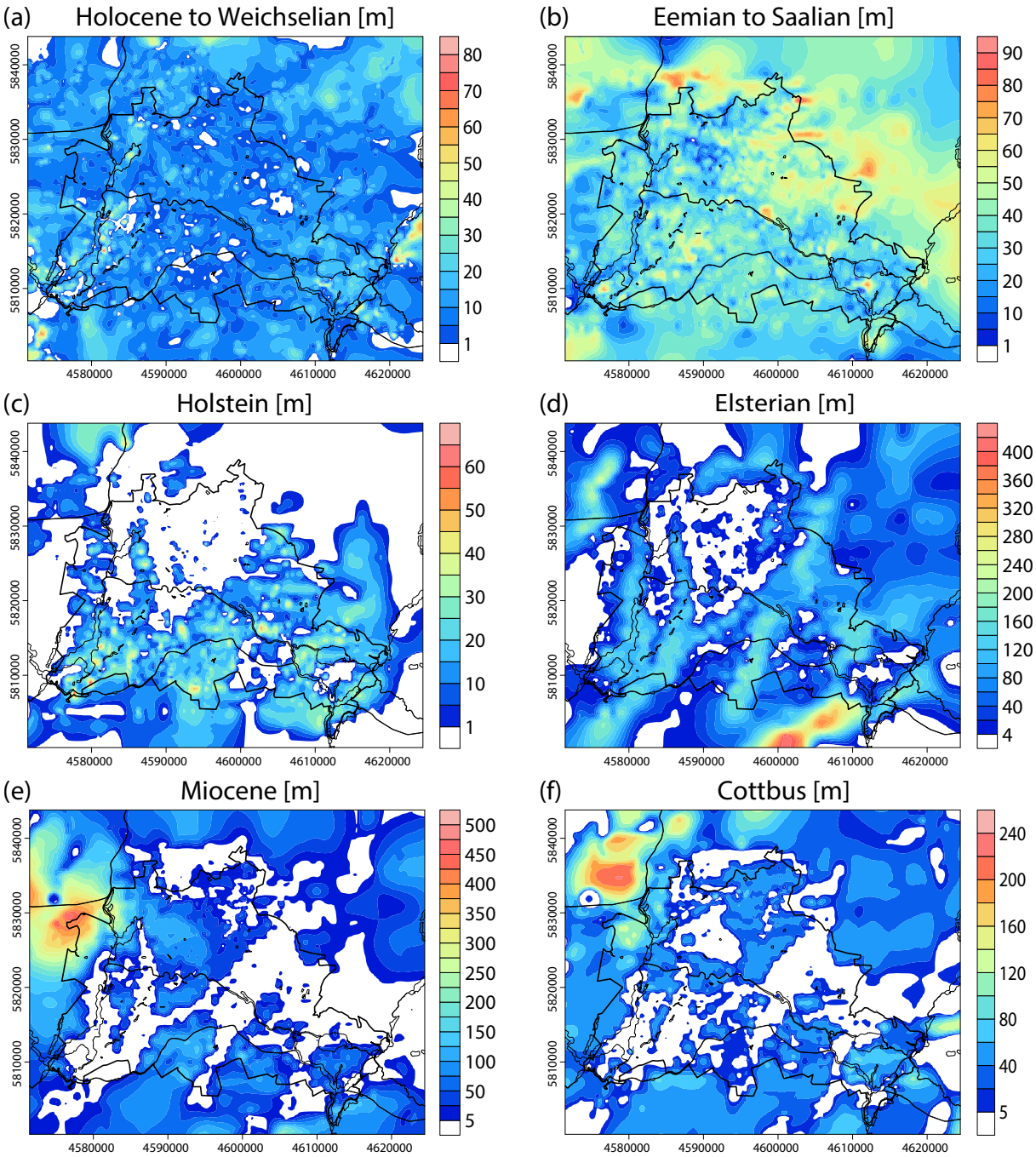

Figure 3.15.: Thickness distribution of Quaternary Holocene to Tertiary Cottbus as used in the 3D structural model used for the thermal simulations. Coordinates [m] in Gauß-Krüger DHDN Zone 4. (a) Quaternary Holocene to Weichselian, (b) Quaternary Saalian, (c) Quaternary Holstein, (d) Quaternary Elsterian, (e) Tertiary Miocene, (f) Tertiary Cottbus. White areas depict where the unit is missing or very thin.

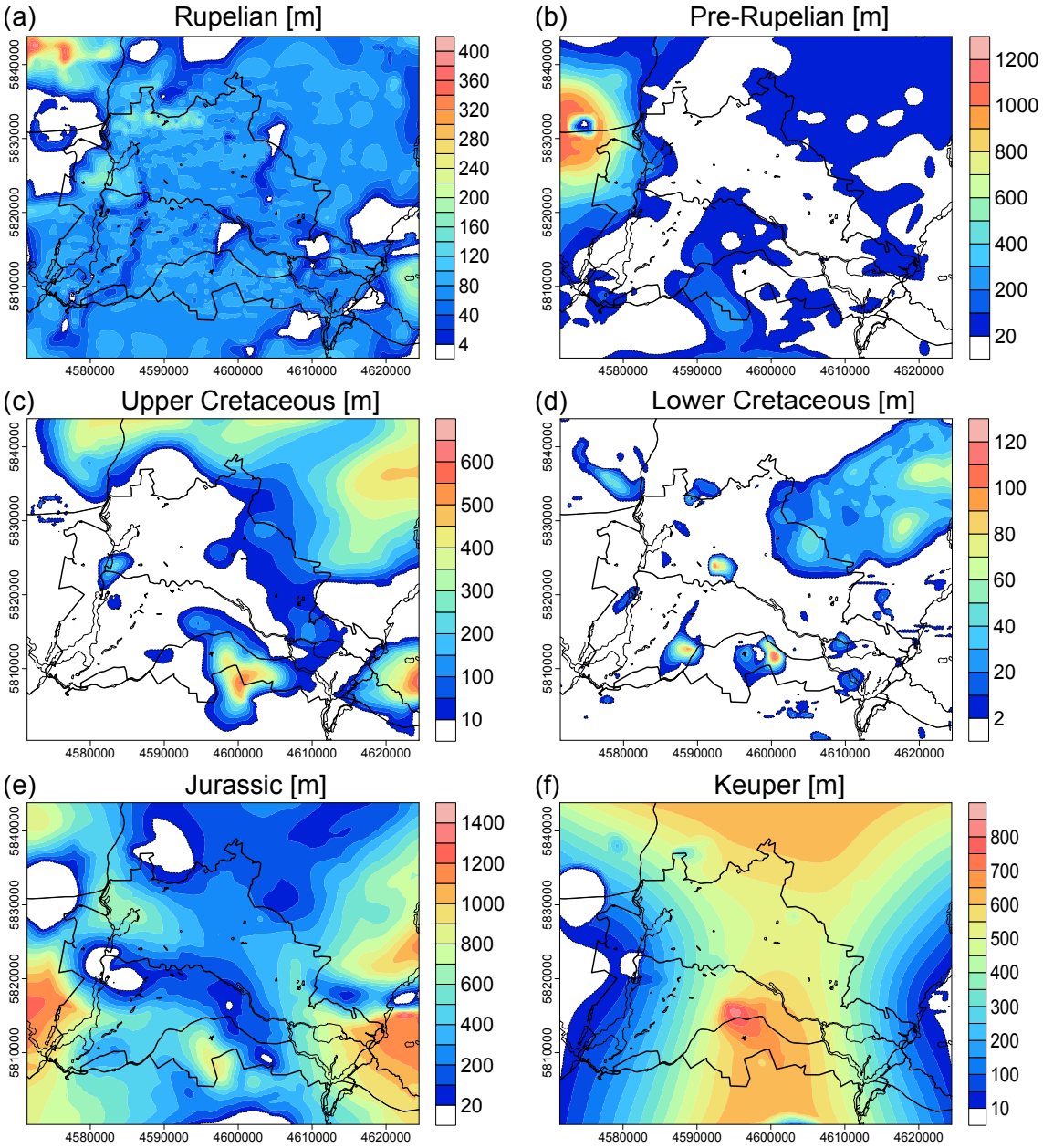

Figure 3.16.: Thickness distribution of Tertiary Rupelian to Triassic Keuper as used in the 3D structural model used for the thermal simulations. Coordinates [m] in Gauß-Krüger DHDN Zone 4. (a) Tertiary Rupelian, (b) Tertiary Pre-Rupelian, (c) Upper Cretaceous, (d) Lower Cretaceous, (e) Jurassic, (f) Triassic Keuper. White areas depict where the unit is missing or very thin.

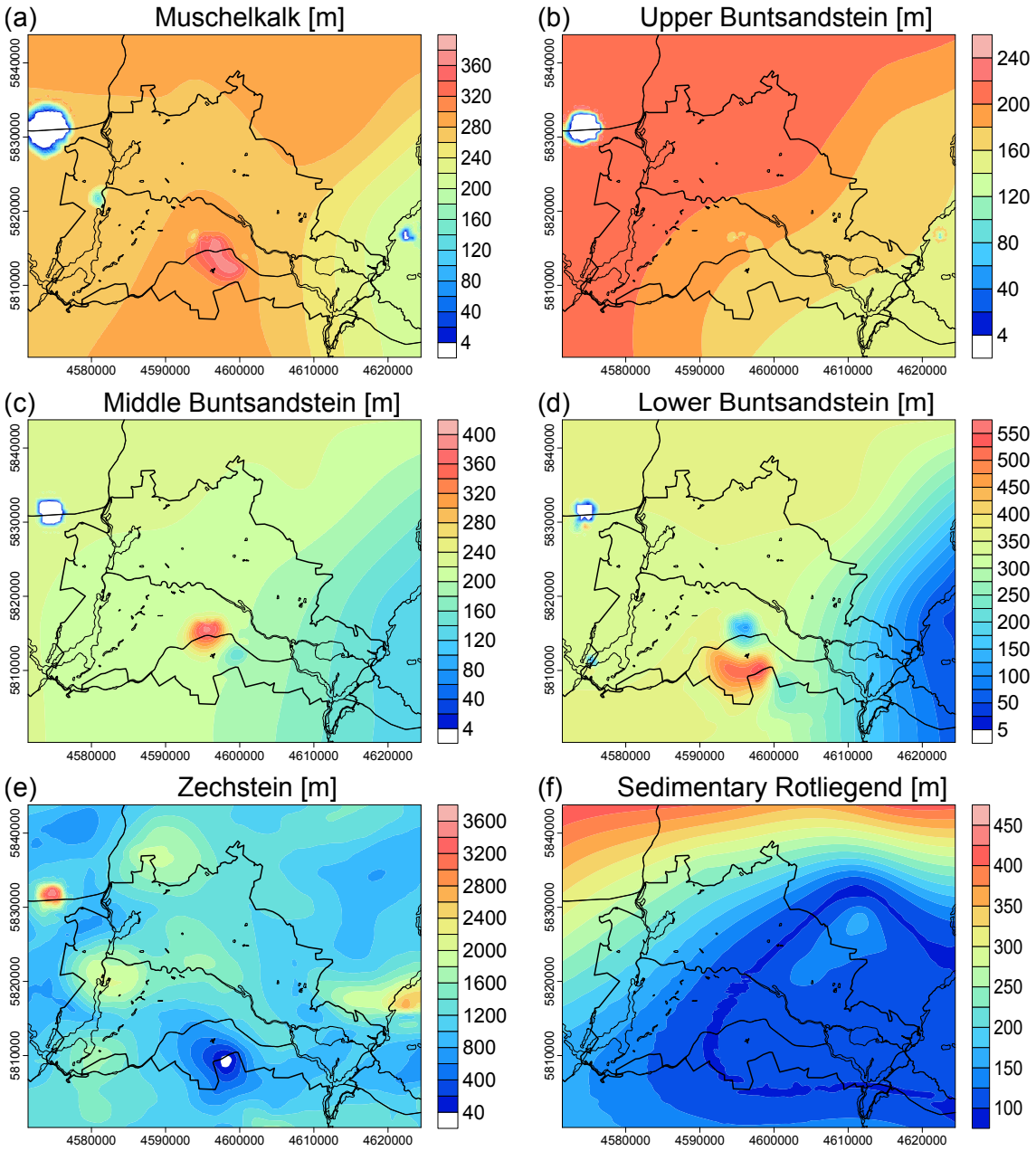

Figure 3.17.: Thickness distribution of Triassic Muschelkalk to Permian Rotliegend as used in the 3D structural model used for the thermal simulations. Coordinates [m] in Gauß-Krüger DHDN Zone 4. (a) Triassic Muschelkalk, (b) Triassic Upper Buntsandstein (c) Triassic Middle Buntsandstein, (d) Triassic Lower Buntsandstein, (e) Permian Zechstein, (f) Permian Rotliegend. White areas depict where the unit is missing or very thin.

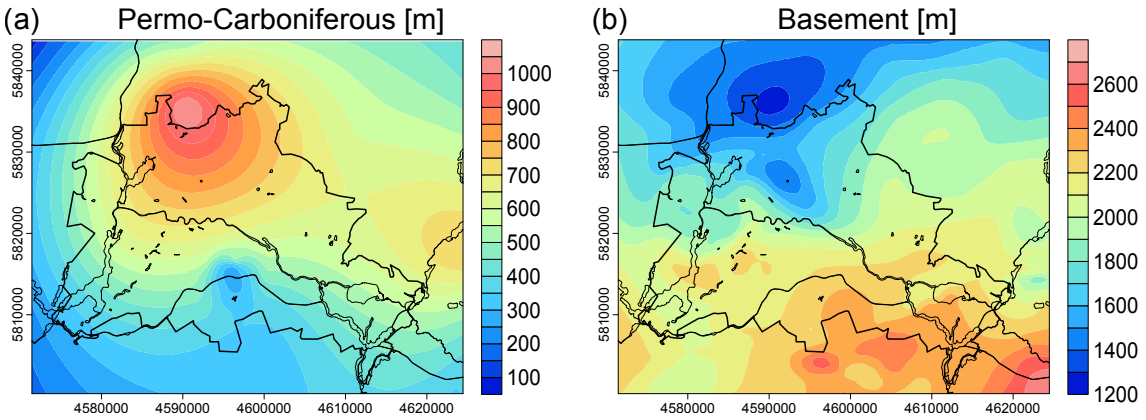

Figure 3.18.: Thickness distribution of Permocarboniferous Volcanics to Lithospheric Mantle as used in the 3D structural model used for the thermal simulations. Coordinates [m] in Gauß-Krüger DHDN Zone 4. (a) Permocarboniferous Volcanics, (b) Basement (Includes Pre-Permian and parts of the upper crust, compare to Fig. 3.14).

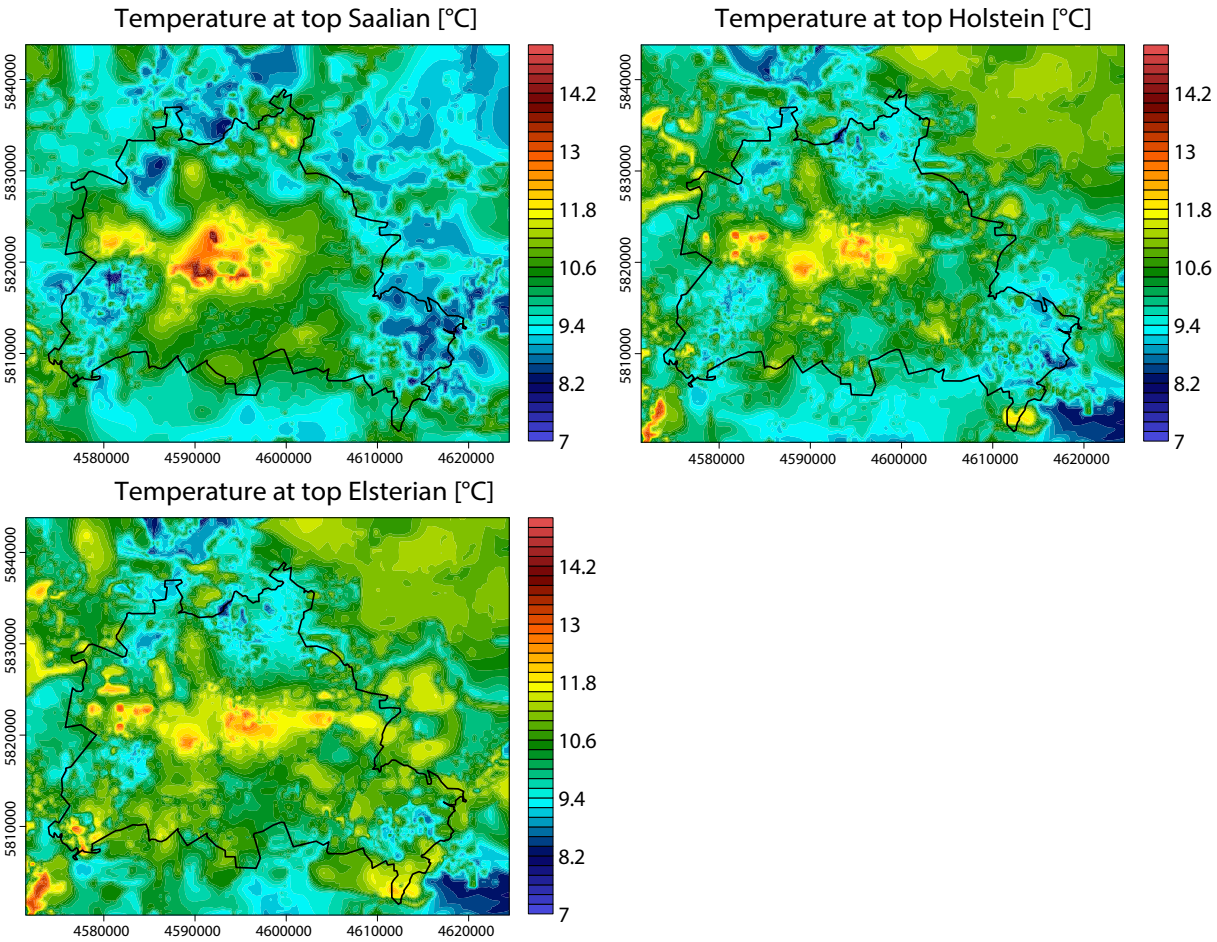

Figure 3.19.: Upper Temperature Boundary condition after Frick et al. (2015); (a) Temperature distribution at top Saalian, (b) Temperature distribution at top Holstein, (c) Temperature distribution at top Elsterian, Coordinates [m] in Gauß-Krüger DHDN Zone 4.

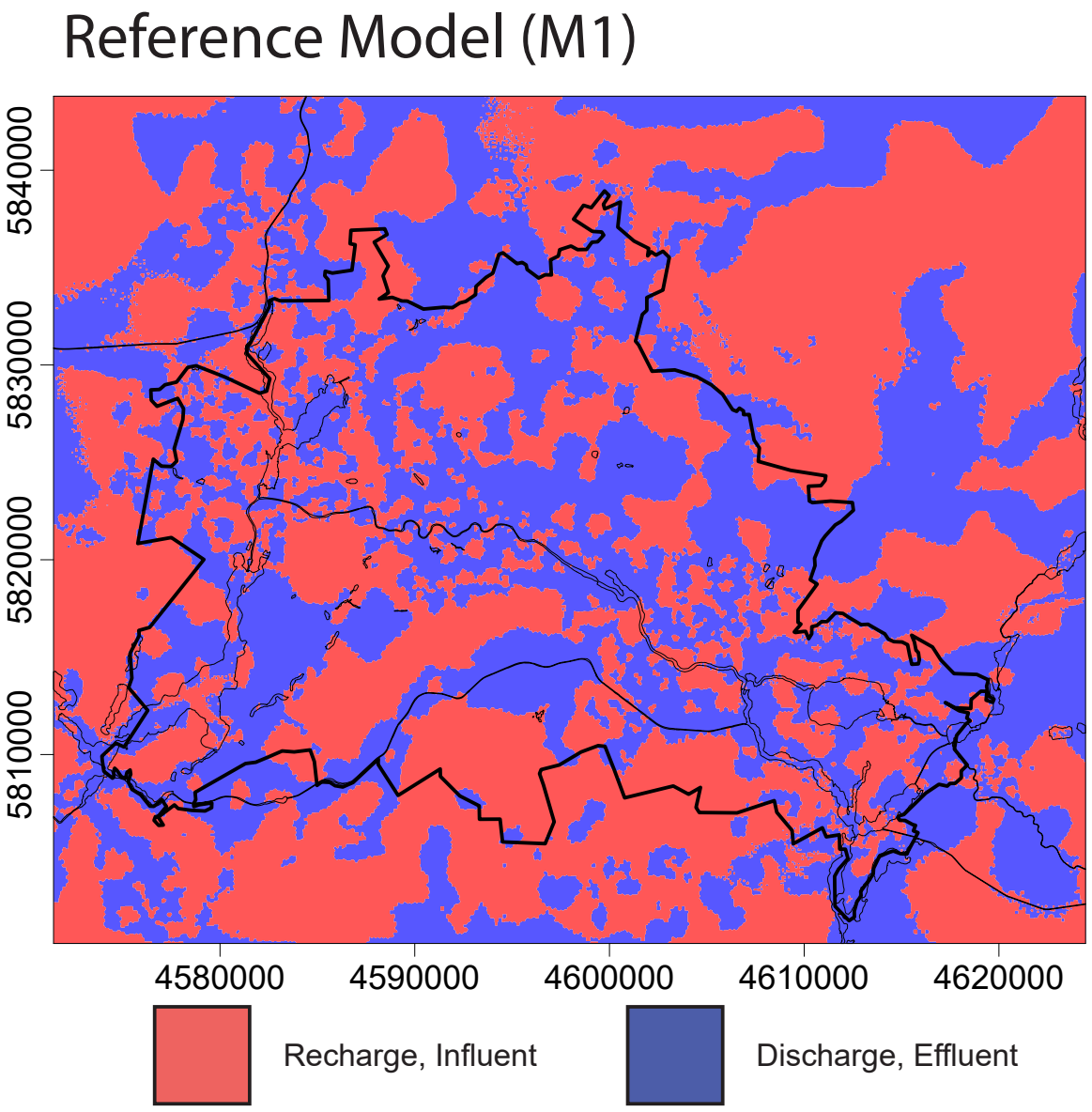

Figure 3.20.: Distribution of recharge and discharge areas for the Reference Model (M1); Coordinates [m] in Gauß-Krüger DHDN Zone 4.

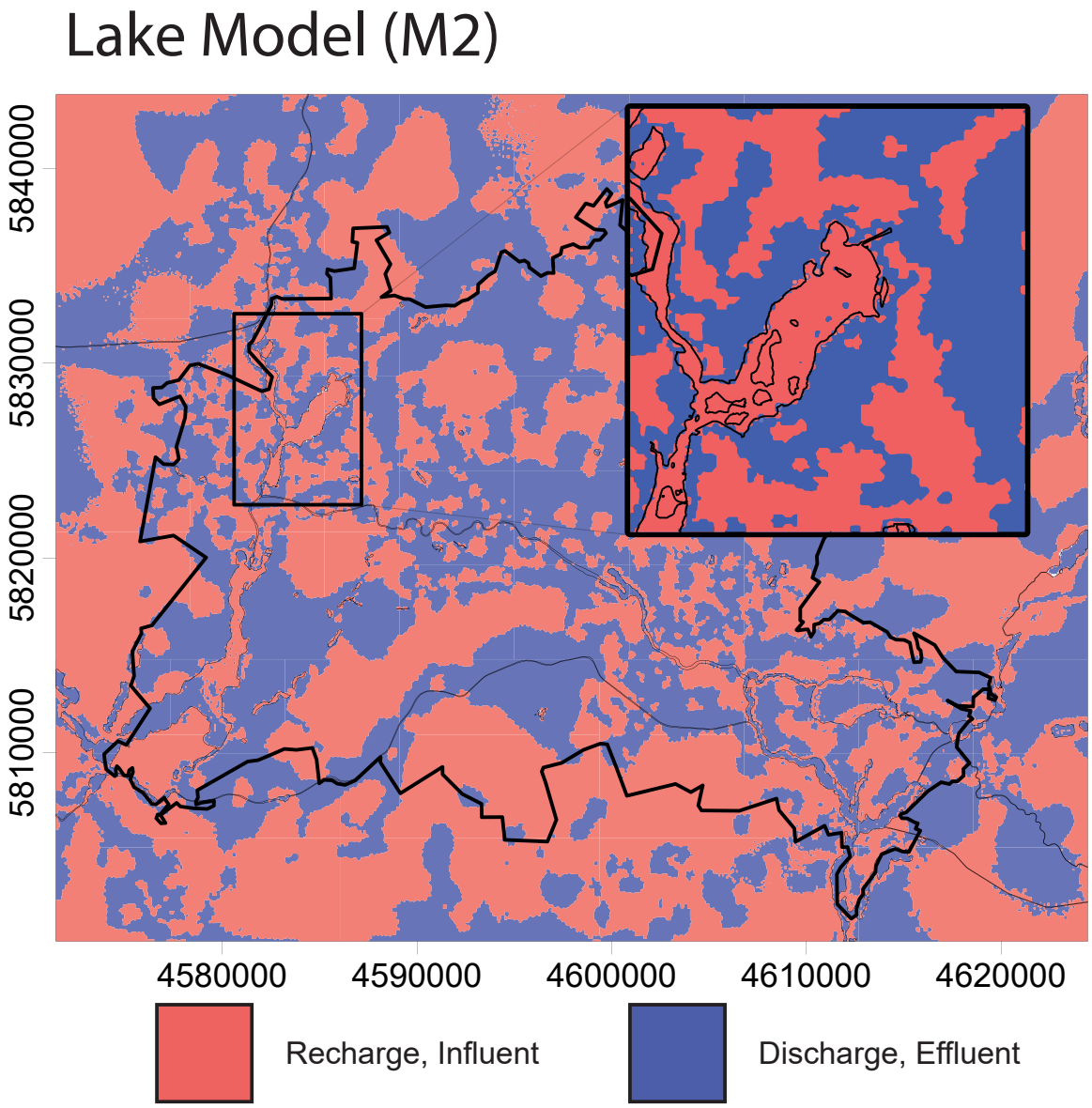

Figure 3.21.: Distribution of recharge and discharge areas for the Lake Model (M2); Coordinates [m] in Gauß-Krüger DHDN Zone 4.

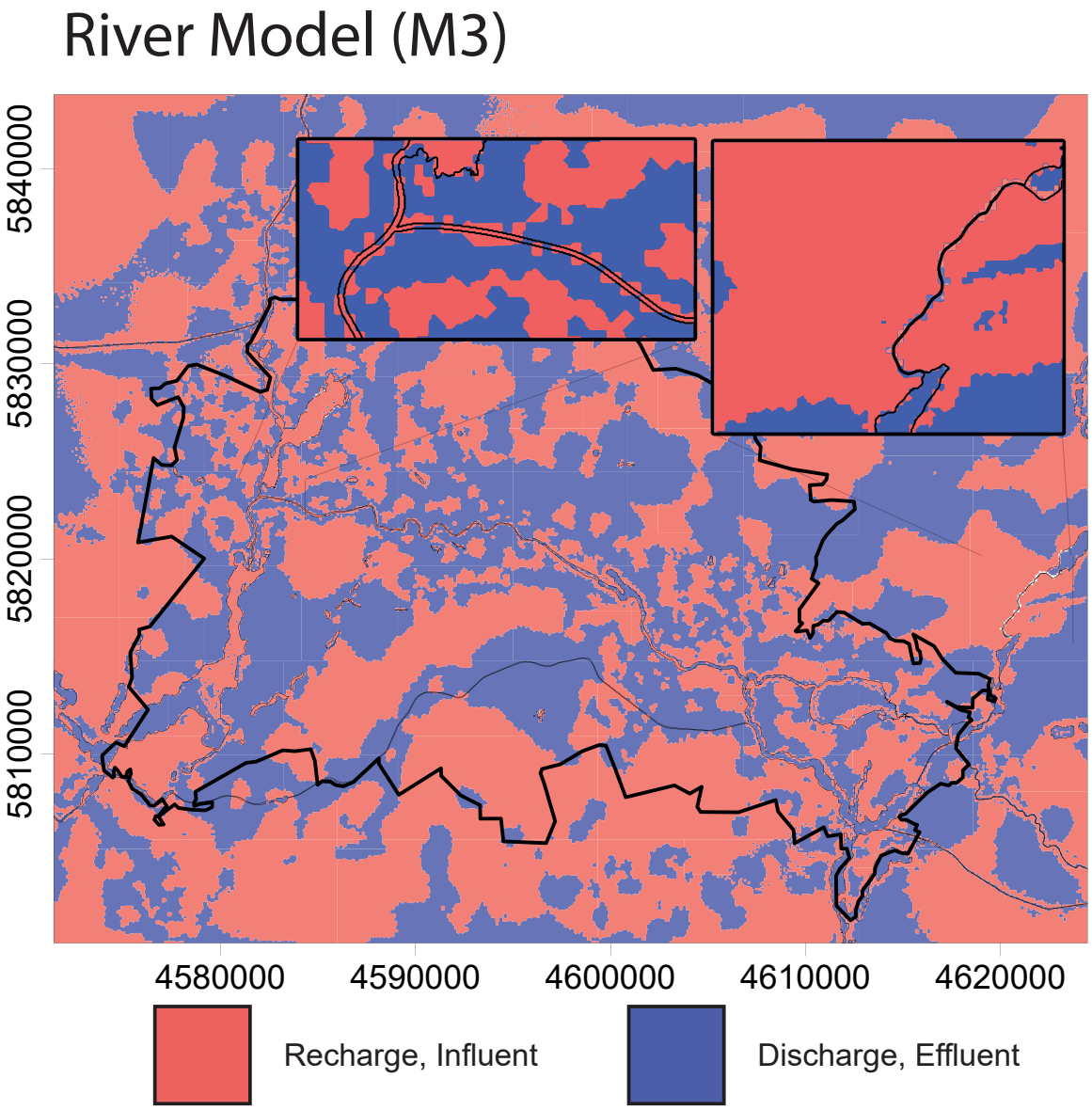

Figure 3.22.: Distribution of recharge and discharge areas for the River Model (M2); Coordinates [m] in Gauß-Krüger DHDN Zone 4.

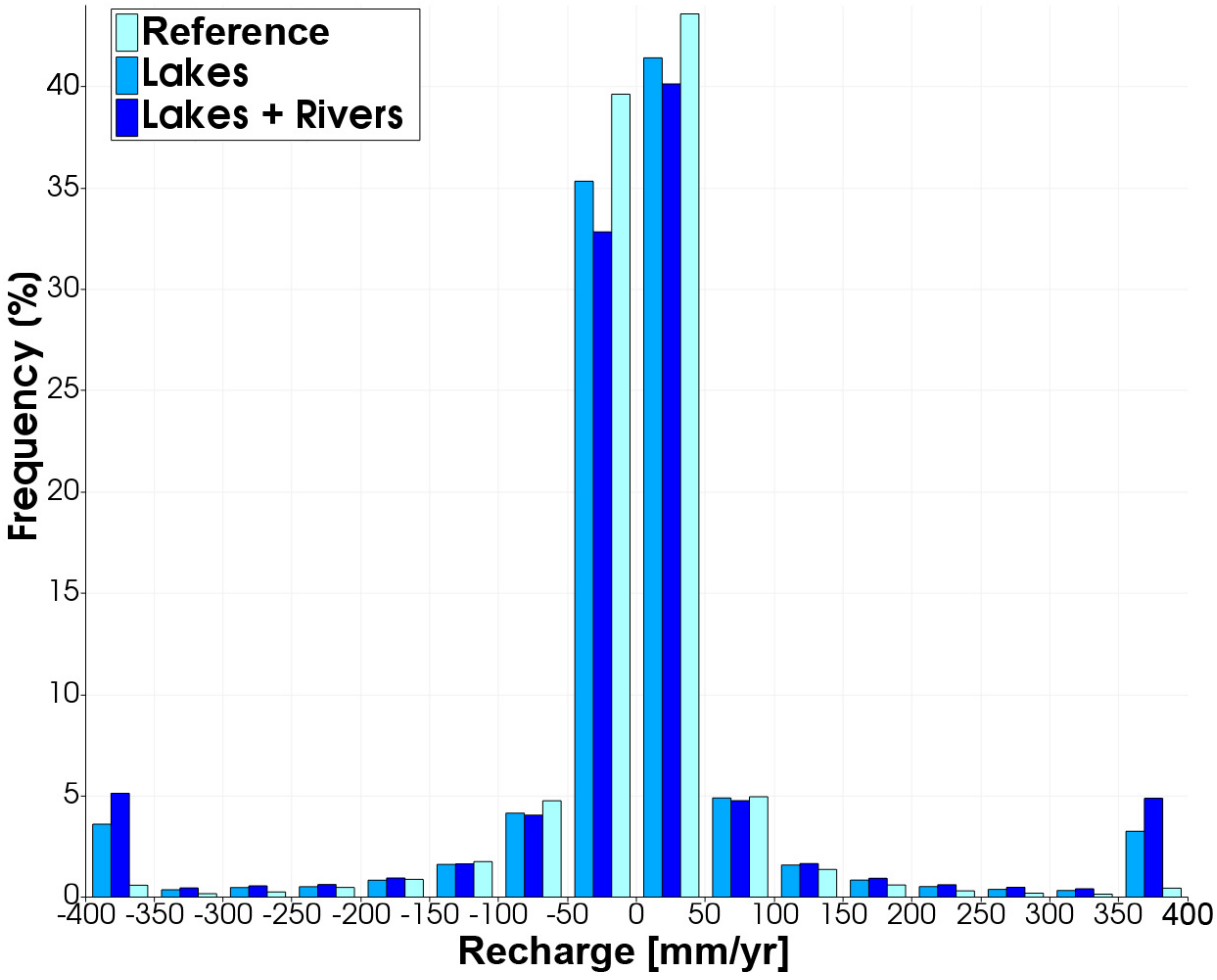

Figure 3.23.: Histogram of calculated groundwater recharge values. Bin-Size = 50 mm/yr.

4. 3D Simulations of Groundwater Utilization in an Urban Catchment of Berlin, Germany

Haacke, N., Frick, M., Scheck-Wenderoth, M., Schneider, M., and Cacace, M. (2018). "3-D Simulations of Groundwater Utilization in an Urban Catchment of Berlin, Germany." In: *Advances in Geosciences*. European Geosciences Union General Assembly 2018, EGU Division Energy, Resources & Environment (ERE) - EGU General Assembly 2018, Vienna, Austria, 8–13 April 2018. Vol. 45. Copernicus GmbH, pp. 177–184. DOI: 10.5194/adgeo-45-177-2018

Abstract

The objective of this study is to analyze the influence of groundwater pumping on predicted groundwater circulation below the urban center of Berlin, Germany, by 3D numerical models. Of particular interest are hydraulic head distributions, the related shallow-deep groundwater interactions and their scale dependency within an anthropogenically overprinted environment. At this purpose, two model scenarios are investigated. In the first model realization (Model 1), the effects of groundwater pumping are implemented by imposing a fixed, though spatially variable, hydraulic head distribution over the whole model area, therefore implicitly taking into account the effects of pumping activities. In the second model realization (Model 2), these effects are considered in an explicit manner by imposing variable production rates in locations where pumping activities are ongoing.

The results of this study show, that both models predict similar hydraulic head distributions on the regional scale (i.e. urban wide). Locally, differences in the extent, volume and depth of emerging depression cones can be observed. This is manifested in differences in predicted fluid flow patterns supporting or refuting the possibility of contaminant transport in an area of importance for groundwater production (Lower Havel). Herein, the second model approach outlines the necessity of implementing wells as an active parameter to reproduce observed fluid pathways.

4.1. Introduction

The aim of this study is to investigate the effects of groundwater pumping wells on the regional shallow to deep groundwater dynamics in a densely populated area, as exemplified by the capital of Germany, Berlin. For this purpose we created two model scenarios, each depicting a different set of hydraulic upper boundary conditions.

In detail, in Model 1 (M1 hereafter) we apply a fixed in time hydraulic head distribution (first order boundary condition) over the whole spatial extent of the model domain. The hydraulic head distribution has been derived from previous studies (Frick et al., 2017) and takes into account, though implicitly, the secondary effects related to pumping activities on the surface

to subsurface hydraulics. In a second model realization (M2 hereafter) the effects of pumping activities on the groundwater dynamics have been implemented in a more realistic manner by explicitly integrating production wells with variable rates as active boundary conditions in the model. The initial state, that is, the "natural state" before commissioning of the wells has been derived based on the assumption that surface hydraulic features as represented by major lakes and rivers can be considered as representing preferential discharge areas characterized by the lowest hydraulic potentials. The reliability of this working assumption is tested by quantifying the ability of this second model set up to provide a first order representation of the regional and local subsurface hydraulic field as constrained by available hydraulic data (as implemented in M1).

The results from the modeling exercise are analyzed both regarding the regional (urban wide) and local characteristics. On the regional scale we discuss and quantify the reliability of computed groundwater dynamics to capture first order aspects of the observed hydraulic head trends over the whole model area. On a more local scale, we focus on a specific area of interest as represented by the Lower Havel, a lake-like lowland river in the west of Berlin (Fig. 4.1). The Lower Havel has been chosen because of recent measurements demonstrating increasing amounts of pollutants nearby active wells (Galleries Rupenhorn and Schildhorn in Figs. 4.1 and 4.2), the origin of which is still under debate. It is likely that pollution of the groundwater might originate from a nearby sewage farm (Karolinenhöhe, KH in Figs. 4.1 and 4.2) located on the western side of the river, which has been active for more than 100 years (Hasch, 2014). In addition, an undercurrent river connection between the sewage farm and the well galleries has also been proposed in previous studies (Jarmersted, 1992). In order to test these hypothesis, we include an additional component of non-reactant contaminant transport in the model and investigate to which degree the hydrodynamics of these contaminants are affected by the hydrogeological setting and the local groundwater circulation as overprinted by anthropogenic activities. Understanding the aforementioned dynamics is of specific relevance for the area under investigation, given the fact that the city of Berlin produces all of its drinking water supply on wells utilizing groundwater resources within the limits of the urban area, where inflowing groundwater and bank infiltration represent the major constituents (Möller and Burgschweiger, 2008).

4.2. Hydrogeological Setting

The 3D structural model used here, is based on the study of Frick et al. (2016b). It differentiates 20 geological units, 8 Cenozoic, 8 Mesozoic and 2 Paleozoic, for the sedimentary succession and 2 units for the underlying basement.

The presented Mesozoic sediments are mainly composed of consolidated clastics, carbonates and sandstones with clay and silt. However, the Middle Muschelkalk contains of evaporites, thereby representing an aquitard. The overlying Cenozoic sediments are predominantly composed by unconsolidated clastics (Frick et al., 2016b) which contain the main shallow aquifer system utilized for the water supply of Berlin (Limberg and Thierbach, 2002). This upper aquifer system has a total thickness of 150 m and can be subdivided into four different aquifers, with the second

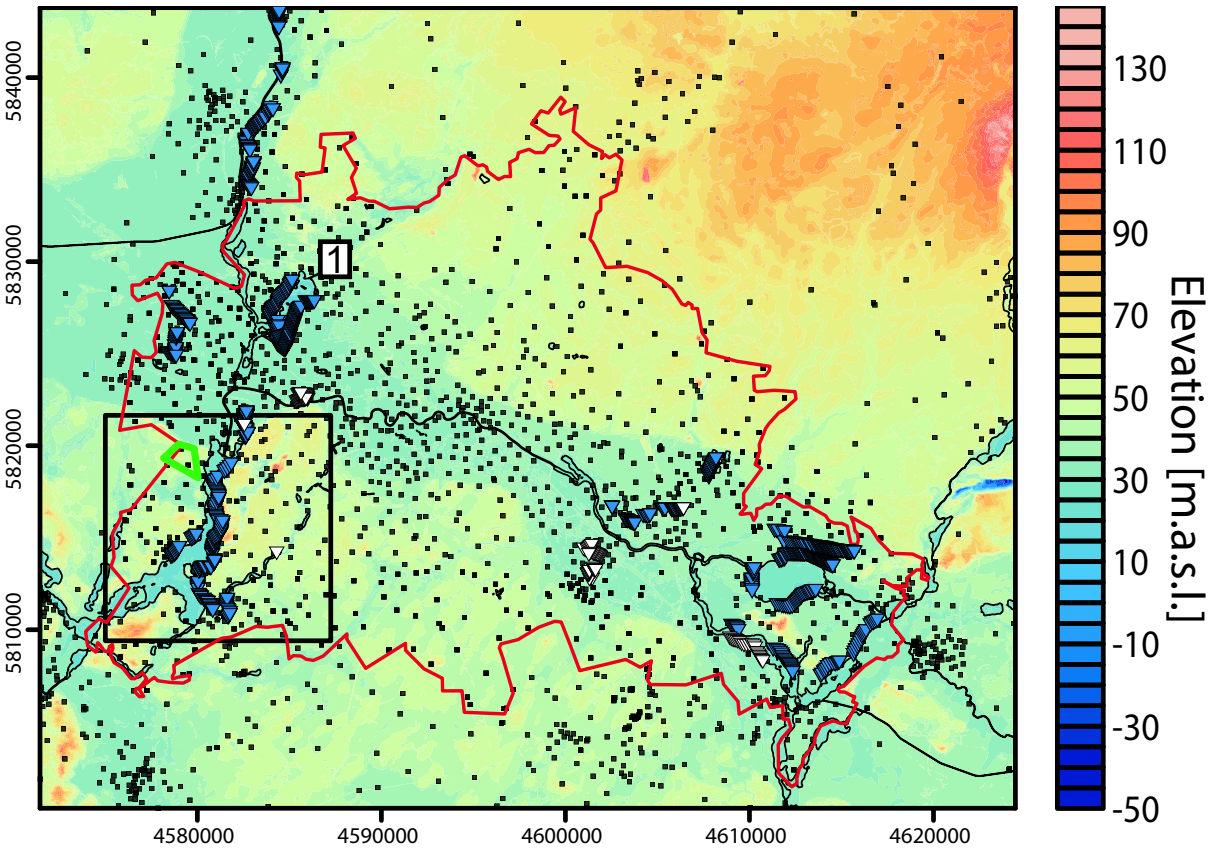

Figure 4.1.: Topography of the model area. Small black box = Lower Havel site, red line = political border of Berlin, black outlines = surface water bodies, black dots = hydraulic head measurement positions, triangles = well positions: blue = active, white = inactive, bright green outline = sewage farm Karolinenhöhe (KH), 1 = Lake Tegel. m.a.s.l. = meter above sea level. Coordinates [m] in Gauß-Krüger DHDN Zone 4. Database supplied by Senate Department for Urban Development and the Environment of Berlin (SenStadtUm), Ministry of Rural Development, Environment and Agriculture of the Federal State of Brandenburg (MRDEA) and the Waterways and Shipping Office (WSA).

aquifer regarded as the most important (Limberg and Thierbach, 1997). The upper fresh water aquifers are separated from the lower brackish to saline aquifers by the Rupelian aquitard, a clay-rich layer of Oligocene age. Locally, where the sediments of the Rupelian are eroded through incision of glacial channels, a hydraulic connection between both aquifer systems is possible (Limberg and Thierbach, 1997; Limberg and Thierbach, 2002). Within the context of the present study, these areas are of particular interest since they might provide preferential pathways for intra-aquifer fluid circulation and related mixing of fresh and saline water as locally enhanced by groundwater production from existing active drinking water wells.

4.3. Modeling Method and Scenarios

4.3.1. Hydrogeological Model

3D coupled fluid, heat and mass transport simulations have been carried out relying on the commercial software FEFLOW©. The base hydrogeological model resolves the geological subsurface as well as the surface hydrology, including major lakes and rivers.

Table 4.1.: Properties of the geological units as used for the calculations. Properties of Cretaceous and older units after Sippel et al., 2013. $c^{(s)}$ = heat capacity of solid, ϕ = porosity, κ = hydraulic conductivity, Q_r = radiogenic heat production, $\lambda^{(b)}$ = bulk thermal conductivity; Values were derived from Norden and Förster, 2006; VDI, 2010; Otto, 2012; Norden et al., 2012; Das, 2013; Sippel et al., 2013; Devlin, 2015.

	Geological unit	$\lambda^{(b)}$ $[W/m/K]$	Q_r $[W/m^3]$	$c^{(s)}$ $[kJ/kg/K]$	ϕ $[-]$	κ_{xy} [m/s]
Neogene	Colmation Layer	1.64	1.3E-06	1.81	0.237	3.23E-06
	Holocene to Weichselian	2.71	0.9E-06	1.57	0.32	1.42E-03
	Eemian to Saalian	2.59	0.9E-06	1.58	0.314	4.04E-04
	Holstein	2.17	0.9E-06	1.67	0.296	1.91E-06
	Elsterian	2.35	0.9E-06	1.61	0.304	8.98E-05
	Miocene	2.47	1.0E-06	1.56	0.301	6.88E-05
Paelog.	Cottbus	2.62	1.3E-06	1.7	0.305	1.15E-04
	Rupelian	1.64	1.3E-06	1.81	0.237	3.23E-06
	Pre-Rupelian	2.48	1.3E-06	1.7	0.297	6.56E-05

In comparison to earlier models (Frick et al., 2017), we include a colmation layer as a 1m thick layer at the base of the surface water bodies, thinning out towards the shoreline. As based on previous analysis (Beyer and Banscher, 1975; Karpf, 2012), this layer is assumed to be mostly impermeable, being composed of organic matter and fine grained sediments of the riverbed. In order to parameterize this layer, we relied on a previous sensitivity analysis (Haacke, 2018) where the range of variations of the permeability have been constrained by laboratory test data (Schälchli, 1993) and field measurements (Beyer and Banscher, 1975; Ingerle, 1991). The best fitting value here corresponds to the characteristics of the Oligocene Rupelian (Frick et al., 2016b, Table 4.1).

The horizontal resolution of the model is on average 10x10 m. In detail, surface water bodies were discretized in accordance with their respective shape to ensure their precise representation in the models. Each geological unit (20 in total) was subdivided into at least two computational layers to guarantee a good vertical to horizontal element size ratio. The implementation of a colmation layer in the structural and numerical models leads to a total of 57 computational layers with ∼33,000,000 elements.

The derived geological model was imported into FEFLOW© to solve for fluid flow and heat and non-reactant mass transport. Details about the mathematical background can be found in Diersch (2014). Mass transport in all models was realized by simulating saturated saline water (345 g/l) as a proxy for poorly absorbing and adsorbing substances by means of a constant mass concentration boundary condition limited to the extent of the sewage farm KH (Fig. 4.2). The set of boundary conditions for the temperature consists of: (i) A spatially variable temperature distribution at the surface as derived from the long term average annual temperature data Senate Department for Urban Development and Housing (2001) ranging from 7° C up to 10° C with local maxima in the center of the model area (Frick et al., 2018b). (ii) A fixed temperature distribution at the base of the model as derived from a previously published study by Noack et al. (2010), which shows variations from 196° C to 220° C gradually increasing from northwest to southeast. Given that the topic of the study is to test the sensitivity of the model results to different sets of surface hydraulic boundary conditions, their description is detailed in the following paragraph.

The parameterization of all Cenozoic units is listed in Table 4.1. To reproduce sufficiently large

flow rates in the vicinity of well localities it was necessary to increase the hydraulic conductivity of the Cenozoic units compared to earlier studies (e.g. Frick et al., 2017, Table 4.1). However, the resulting values are considered to be realistic as they lie well within literature values reported in this region (e.g. Limberg and Thierbach, 2002; Norden, 2011). In addition, an anisotropy ratio of 10:1 ($\kappa_{xx,yy} : \kappa_{zz}$) was taken into account. All lateral boundaries are closed to both, fluid and heat flow. For fluid flow, this assumption is supported by the location of the region in the middle of the North German plain. Here, no mountainous terrain is adjacent and therefore cross-boundary flow is likely to be very small and was neglected in this study.

4.3.2. Model Scenarios

To investigate the effects of groundwater pumping wells on the regional shallow to deep groundwater dynamics, two different model scenarios have been simulated, each featuring a different set of hydraulic boundary conditions. They both have in common that all lateral boundaries are closed to fluid, heat and mass transport. We apply this approach since constraints on cross boundary flow are not available and the study areas location in the middle of the North German plain where no mountainous regions are at the borders, likely linking to very small, negligible, cross-boundary flow.

The first model scenario (M1) depicts a setting, where the hydraulic head boundary condition is based on measured groundwater head (Fig. 4.1, Fig. 4.2a) and surface water level data (Fig. 4.2a) which have been implemented as fixed hydraulic head boundary condition across the entire model area. Thus, M1 includes the effects of present day water production, though implicitly. Accordingly, extensive depression cones induced by pumping activities can be observed in several locations, most prominently at Lake Tegel and the Lower Havel (Fig. 4.2a). These have been shown to lead to drastic modifications of the local fluid flow regime (Frick et al., 2017). For the simulation run, the pressure and temperature initial conditions for M1 were derived by solving for heat and fluid transport decoupled in steady state. The model was then solved for coupled fluid and heat transport in transient until reaching quasi-steady-state conditions after $\sim 275\,\mathrm{k\,yr}$ final simulation time. The resulting pressure and temperature distribution was used to finally solve for mass transport for a simulation time of 100 yr, which is the time period of irrigation of treated sewage water.

The second model scenario (M2) utilizes a different setup of the hydraulic boundary condition. Here, the natural distribution of the hydraulic heads and temperature before commissioning of the wells was used as an initial condition. In detail, the boundary condition nodes for the extent of anthropogenically influenced areas were removed (Figure 4.2b), thus enabling the groundwater table to adjust freely, based on the computed hydraulic potential. These areas were determined by identifying areas where groundwater levels are lower than that of adjacent surface water bodies, indicating lowering through pumping activity (Fig. 4.2). In a further step, the effect of pumping activities on the groundwater dynamics and the connected contaminant transport as based on available data for the last 100 yr of production (Figure 4.2c,d) was considered. These were implemented as discrete features with a point-wise sink/source character with fixed flow rates at the bottom for the entire model run (Table 4.2).

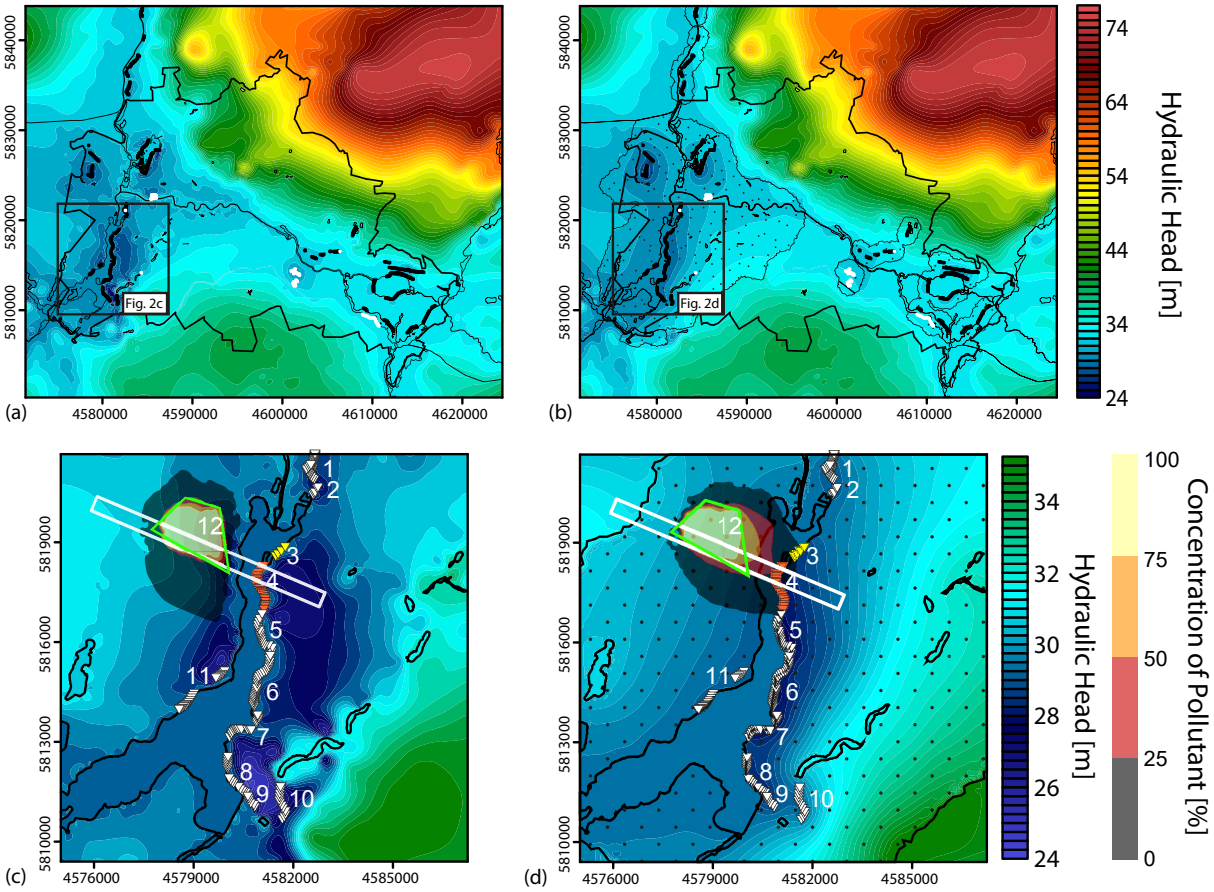

Figure 4.2.: Regional and local distribution of hydraulic heads for M1 and M2. (a,b) Hydraulic head distribution for entire model area for (a) M1 and (b) M2, black dots = active wells, white dots = inactive wells. (c,d) Hydraulic head distribution for Lower Havel for (c) M1 and (d) M2, triangles = implemented wells: yellow = Rupenhorn, orange = Schildhorn, white = further (Table 4.2); white box = extent of Fig. 4.3; green outline = sewage farm KH. (b,d) Dotted area represents extent of depression cones induced by pumping wells used for hydraulic boundary condition setup of M2; Colored plumes represent areas of increased concentration (lower threshold 1 g/l) of saline water.

4.4. Results and Discussion

For the results and discussion part, we firstly investigate the regional hydraulic head distribution for the entire model area (Fig. 4.2a,b) and for the Lower Havel (Fig. 4.2c,d) for all scenarios. Then we show the results of local fluid dynamics (Fig. 4.2c,d) along a cross-section (Fig. 4.3) perpendicular to the river shores of the Lower Havel, parallel to the expected flow direction. We analyze the distributions of modeled hydraulic heads (Fig. 4.2) with respect to the extent and depth of simulated depression cones. For the local analysis, special focus was given to the well galleries Rupenhorn and Schildhorn on the east bank (Fig. 4.2c,d, Fig. 4.3).

The hydraulic head distribution for the first model scenario follows the elevation distribution of the model surface quite closely. Maximum hydraulic heads (up to 75.5 m) are observed in the northeast, south and the northwest, where higher than average topographic relief is found (Figs. 4.1 and 4.2a). Accordingly, lowest heads (up to 24.7 m) are found in the central model domain, namely the Greater Spree Valley (northwest-southeast striking valley in the center) and large parts of the western model domain, where low topographic relief is encountered (Fig. 4.1,

Table 4.2.: Pumping rates of the wells implemented in M2 for the local study site. Pumping rate = average (2005-2014), Pumping rate/well = Pumping rate gallery / number of wells. Data provided by Berlin waterworks (BWB).

Waterworks	Gallery	Active Wells	Pumping Rate $[m^3/a]$	Pumping Rate/Well $[m^3/a]$	Pumping Rate/Well $[m^3/d]$
Tiefwerder	1 - Gallery N	16	1941859.7	121366.2	332.5
	2 - Gallery S	18	3078456.9	171025.4	468.6
	3 - Rupenhorn	5	2245068.4	449013.7	1230.2
	4 - Schildhorn	20	6225842.8	311292.1	852.9
Beelitzhof	5 - Lieper Bucht	15	8648613.3	576574.2	1579.7
	6 - Lindwerder	25	8461800.1	338472.0	927.3
	7 - Großes Fenster	19	5986246.6	315065.6	863.2
	8 - Wannsee	15	5644629.5	376308.6	1031.0
	9 - Wiesenleitung	6	1306607.4	217767.9	596.6
	10 - Rehwiese	12	3669781.7	305815.1	837.9
Kladow	11 - Kladow	18	1295527.0	71973.7	197.2

Fig. 4.2a). Additionally to this natural relationship, where lakes and rivers normally display discharge areas, anthropogenically overprinted areas are found in the model area, induced by groundwater pumping. These were identified by their respective hydraulic heads being lower than that of the adjacent surface water body level. Most prominently these are located in the western model domain, i.e. near Lake Tegel, in Spandau and for this study most importantly at the Lower Havel and feature an artificial low in hydraulic heads, manifested in the lakes and rivers changing to recharge areas (Fig. 4.2a,c). The identified overprinted area depicts a horizontal extent of 6.1E+08 m^2 with maximum drawdown of 5.16 m and a volume of 1.85E+08 m^3.

The initial condition for model M2 displays a head distribution where anthropogenically induced depression cones have been replenished completely. Hence, lowest elevations in this scenario are 26.5 m whilst highest elevations remain the same (75.5 m). Moreover, all lakes and rivers display discharge areas in this setting, as opposed to results obtained from M1 and M2. The hydraulic head distribution of M2 depicts similar trends to those predicted in M1 which can be seen in the large scale variations (min: 24.7 m, max: 75.5 m, Fig. 4.2b). Additionally, the maximum drawdown of M2 of 4.17 m as well as the horizontal extent of the depression cones of 5.75E+08 m^2 follow the results of M1 closely, however, the overall volume of 8.67E+07 m^3 is considerably smaller. These differences likely derive from comparatively high flow rates towards the well galleries initiated by the hydraulic conductivity setup which supports horizontal flow as opposed to vertical. This regional observation is cross-checked in the following (local regime, Fig. 4.2c,d, Fig. 4.3).

At the local scale, simulated distributions of hydraulic head for M1 at the Lower Havel show extensive depression cones in the east and west of the Lower Havel (Fig. 4.2c). Lowest hydraulic potentials can be found in close proximity to the surface water body and range from 24.6 m to the east, near the well gallery Wannsee, to 26.2 m in the west. Furthermore, a connection between the aquifers below the east and west bank is indicated by an extensive depression cone along the west bank likely being the result of pumping at the galleries Rupenhorn and Schildhorn in the east (Figure 4.2c). The difference between the water level of the Lower Havel (29.32 m) and the lowest hydraulic potentials leads to influent conditions along the river bank and thus induces the process of bank filtration which is in agreement with observed fluid flow patterns (Möller and Burgschweiger, 2008). In comparison, the hydraulic head distribution predicted by M2 also shows

lowest hydraulic potentials of 27.6 m in an extensive depression cone along the east bank of the Lower Havel (Fig. 4.2d). However, only a less developed depression cone is evident to the west of the Lower Havel. Comparing these model results, differences between the depression cones predicted by the different models becomes more apparent, wherein, M2 shows a comparatively smaller horizontal extent of the depression cones due to the same reasons as outlined above.

To validate whether the model results obtained in M1 and M2 reproduce observations concerning local pathlines and contaminant transport, we investigated the results for a representative 3D cross section (Fig. 4.3). Here, a predominantly gravity-driven groundwater circulation in the shallow groundwater system above the Rupelian is predicted for M1, whereby a west-east directed groundwater flow along the pressure gradient dominates, discharging in areas of lowest hydraulic potentials, here represented by the depression cones (Fig. 4.3a). At these locations, a strong uprising of groundwater shows a significant influence on the advective groundwater flow as a result of pumping activities. These groundwater dynamics would lead to a contaminant transport from the sewage farm KH towards the western shore of the Lower Havel, mainly discharging and accumulating in the depression cone at this location. These results would argue against the hypothesis of a hydraulic connection between the sewage farm KH and the well galleries Rupenhorn and Schildhorn. Instead a southward movement of the contaminants in direction of the depression cones on the west shore is predicted (Fig. 4.3a). Hence, a static implementation does not allow to capture these proposed fluid flow patterns (Jarmersted, 1992). In comparison, the cross sectional view for M2 (Figure 4.3b) also shows a fluid flow pattern dominated by infiltration in the west quickly changing to horizontal flow. This strong component of horizontal flow discharges focused at the east shore of the Lower Havel where the implemented wells are located. Here, a strong undercurrent below the surface water body can be observed. Comparing M1 and M2, a general increase in volumetric flux at well gallery locations (10^3-fold increase) can be observed for M2, deriving from the hydraulic forcing induced by well pumping. This also suggests, that the influence of groundwater pumping on the resulting groundwater hydrodynamics is only crudely approximated in M1. Additionally, implementing the well galleries as an active parameter in M2 leads to a lateral flow of contaminants, where up to 10-20% of the initial concentration reaches the well galleries (Figure 4.2d) in the time frame of sewage farm activity (Liese et al., 2007). This is also in accordance with the proposed fluid pathlines of Jarmersted (1992).

4.5. Conclusions

The model scenarios presented in this study, (1) illustrate the influence of groundwater pumping on predicted groundwater circulation. (2) Pollutant transport depends mainly on the hydraulic forcing. (3) This natural transport can be accelerated by pumping activities.

Hydraulic head distributions of M2 are generally fitting observations well (regional), however, on the local scale misfits in both lateral extent and overall volume can be observed. This likely derives from comparatively high flow rates towards the well galleries initiated by the hydraulic conductivity setup which supports horizontal flow as opposed to vertical. For the Lower Havel,

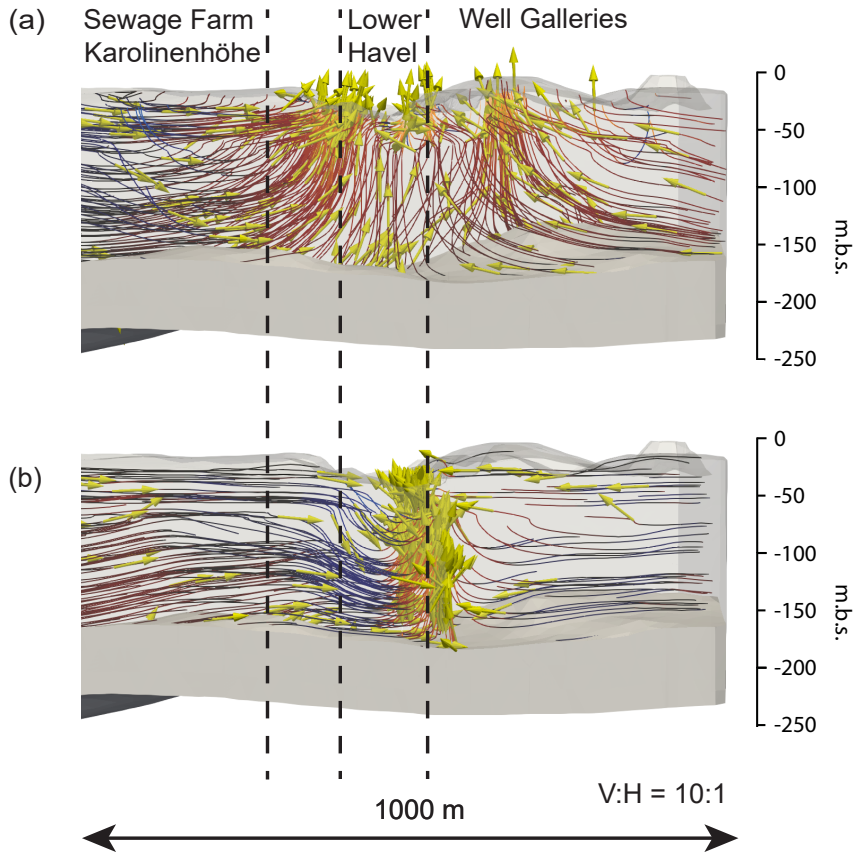

Figure 4.3.: 3D-cross-section through Lower Havel. Groundwater flow lines in M1 (a) and M2 (b); m.b.s. = meter below surface; Colored flow lines represent downwelling (Blue) and upwelling (Red) groundwater calculated with Paraview's stream tracer filter (Squillacote et al., 2007); Yellow arrows = groundwater flow direction; Gray layer = Rupelian unit.

M2 was found to match observations most closely concerning fluid pathways and contaminant transport, indicating both an undercurrent of the surface water body Lower Havel as well as a pollutant transport in the time framing of the activity of the sewage farm KH (100 yr). However, the way pollutant transport is modeled here, represents a strong simplification as dispersion and diffusion values of site-specific contaminants were not considered. This could be investigated in future work as well as including higher resolution of the hydrogeological subsurface. Furthermore, measured hydraulic head distributions indicate a more complex anthropogenic overprinting then modeled here, hinting at the necessity of implementing time sensitive pumping rates to provide a more reliable base model for groundwater management and sustainability.

Data availability

The datasets generated during the current study are available from the corresponding author on reasonable request. The database is partly confidential and can therefore not be shared at this point in time. For further information on the model setup and database please refer to Frick et al. (2016b, 2018a).

Author contributions

NH and MF constructed the mentioned 3-D models, conducted the coupled simulations, and drafted the manuscript. MSW and MC helped to draft the manuscript. MSW, MS and MC participated in the design of the study and contributed with the discussions and interpretation of the results. All authors read and approved the final manuscript.

Competing interests

The authors declare that they have no conflict of interest.

Special issue statement

This article is part of the special issue "European Geosciences Union General Assembly 2018, EGU Division Energy, Resources & Environment (ERE)". It is a result of the EGU General Assembly 2018, Vienna, Austria, 8–13 April 2018.

Acknowledgments

This research is funded as part of the joint initiative of the research field energy of the Helmholtz Association "Energy System 2050". We would like to thank the Senate Department for Urban Development and the Environment of Berlin (SenStadtUm), Berlin waterworks (BWB), Ministry of Rural Development, Environment and Agriculture of the Federal State of Brandenburg (MRDEA) and the Waterways and Shipping Office (WSA) for providing the data for this study. The 3D information on the structural configuration of the subsurface of Berlin was compiled, visualized and interpolated with the commercial software package Petrel (© Schlumberger). We want to thank the anonymous reviewers for their contributions which helped improve the quality of this manuscript significantly.

5. Overcoming Spatial Scales in Geothermal Modeling for Urban Areas

Scheck-Wenderoth, M., Frick, M., Cacace, M., and Sippel, J. (2017). "Overcoming Spatial Scales in Geothermal Modeling for Urban Areas." In: *Energy Procedia* 125, pp. 98–105. DOI: 10.1016/j.egypro.2017.08.080

Abstract

A major component in the transition from fossil to renewable energy is the demand for district heating where geothermal energy can be a substantial option. We present results on the controlling factors for the deep thermal field below a large urban area, the city of Berlin. Therefore we analyze 3D thermal models considering conductive and mixed convective heat transport mechanisms as well as different boundary conditions. Of the controlling factors, heterogeneous thermal and hydraulic physical properties of geological units at different depths are key. That data density decreases with depth poses challenges for model assumptions for which we propose solutions.

5.1. Introduction

In the course of the transition from fossil and nuclear energy to renewable energy, the production of geothermal energy becomes of increasing importance (Breisig et al., 2015) . In particular, in areas with pronounced seasonal temperature fluctuations a major demand of energy is related to the provision of heat needed during the cold season. Today for many large urban areas heating of buildings relies almost entirely on fossil energy (Lund et al., 2014) . This is also the case for the city of Berlin, where more than 90% of heating is accomplished via burning of fossil energy resources such as natural gas, petroleum or coal (Wasserwirtschaft, 2015; S. Berlin-Brandenburg, 2016). One possible alternative source that could play an important role in the future energy mix is geothermal energy (Huenges and Ledru, 2011). Indeed, earlier work has explored the deep geothermal potential as based on a first generation of 3D models for the subsurface geological configuration (Sippel et al., 2013; Kastner et al., 2013; Kastner et al., 2015). More recently, the quality of the shallow configuration of Cenozoic sedimentary units has been improved and a second generation of geothermal models has therefore emerged (Frick et al., 2015, 2016b). On the basis of all previous and relatively new modeling results, we hereby present how deep and shallow influencing factors control the deep geothermal field below Berlin.

Understanding heat transport in the subsurface requires assessing the impact of different physical coupled processes occurring in the underground. Of these, conductive heat transport is usually regarded as the dominant transport process being controlled by variations in the heat budget (mainly from crustal origin) and the heterogeneous distribution of thermal conductivity

of the sedimentary sequence (Clauser, 2006; Jaupart et al., 2007; Bjørlykke, 2015). In addition heat transport may be influenced by advective and convective transients in the upper few km of the crust (Lampe and Person, 2002; Kaiser et al., 2011; Noack et al., 2013). A major problem in quantifying this influence by means of geothermal modeling is the lack of knowledge on the thermal and hydraulic conditions at the model boundaries and the relatively high uncertainties in the model parameters and their distribution with depth. A constant temperature or heat flow is often assigned as the lower thermal boundary condition assuming an average geothermal gradient of 30°C/km. However, the average geothermal gradient is either measured or calculated by the individual layer dependent geothermal gradients and their thicknesses. Therefore, assuming a constant geothermal gradient of 30°C/km may lead to significant errors if the deep structure is heterogeneous (Van Balen et al., 2002; Norden et al., 2008; Stephenson et al., 2009; Cacace et al., 2010; Scheck-Wenderoth and Maystrenko, 2013). Considering that the subsurface is composed of different lithological units, conductive heat transport will be influenced by the lithology-dependent distribution of thermal properties (e.g. thermal conductivity and radiogenic heat production) and by variations of heat input from the crust and the mantle (Scheck-Wenderoth et al., 2014). In addition advective heat transport related to regional groundwater flow patterns in the porous geological units of the subsurface may affect the system to different degrees (Noack et al., 2013; Kaiser et al., 2013b). Thereby, the dynamics of fluid flow are again controlled by the regional structural and hydrogeological setting on the basin-scale over several tens to up to hundreds of km. Examples for such structural heterogeneities are salt structures and their deformed cover layers or large faults. In response to these variations, large lateral temperature differences may be present at a certain constant depth level.

5.1.1. Geological Setting

Geologically, the city of Berlin is located in the southeastern part of the Central European Basin System, an area that subsided over the past 300 million years above a heterogeneous crystalline crust and lithosphere. Accordingly, Berlin is underlain by a sedimentary succession that is up to 5 km thick and contains clastic deposits and a thick unit of Permian Zechstein salt (Scheck-Wenderoth and Lamarche, 2005; Scheck-Wenderoth et al., 2008; Sippel et al., 2013).

The latter has been mobilized during the past 150 million years to form salt pillows and diapirs. This resulted in a highly irregular subsurface structural setting (Fig. 5.1a) which is important for the thermal field as salt is twice as thermally conductive compared to the surrounding clastic sediments. As a result the salt structures represent thermal chimneys while the clastic sediments in turn have an insulating effect and lead to thermal blanketing (Jensen, 1990; Norden et al., 2008; Stephenson et al., 2009; Noack et al., 2012; Sippel et al., 2013). Two large salt diapirs piercing their cover layers are present near the western and eastern boundaries of Berlin, where the salt is up to 3600 m thick and reaches very shallow depths indicated by circular anomalies (“1” in Fig. 5.1a) in the depth map of the top salt surface. Furthermore three larger, up to 2 km thick salt pillows are located beneath the western part of Berlin (“2” in Fig. 5.1a) whereas the salt has been withdrawn from below the central southern part of the city as well as from the NE and NW corners of the study area (“3” in Fig. 5.1a). These domains instead are filled with

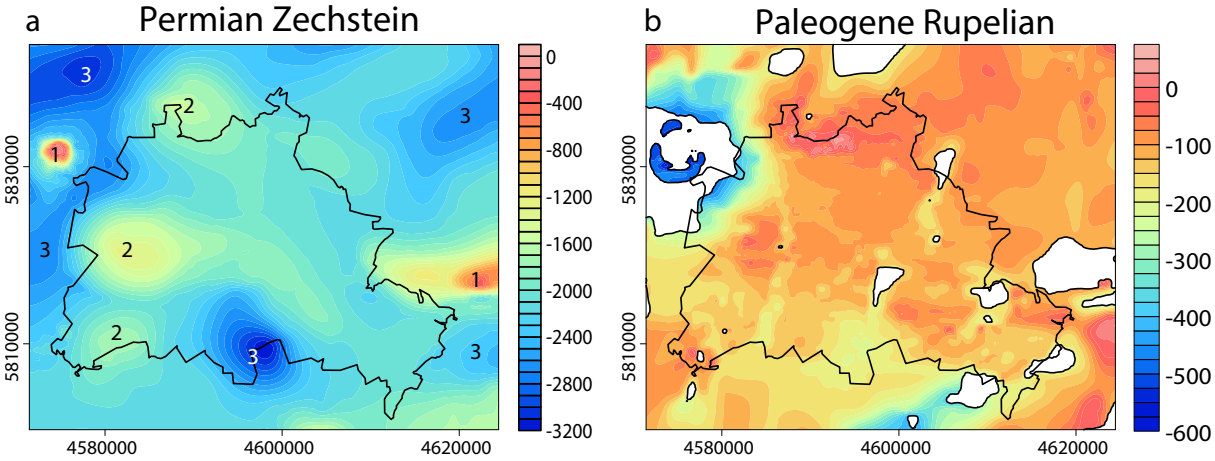

Figure 5.1.: Elevation of the top salt surface according to the structural model of Sippel et al. (2013) and Frick et al. (2016b), both in meters above sea level; Numbers indicate specific structures referred to in the text, Coordinates [m] in Gauß-Krüger DHDN Zone 4.

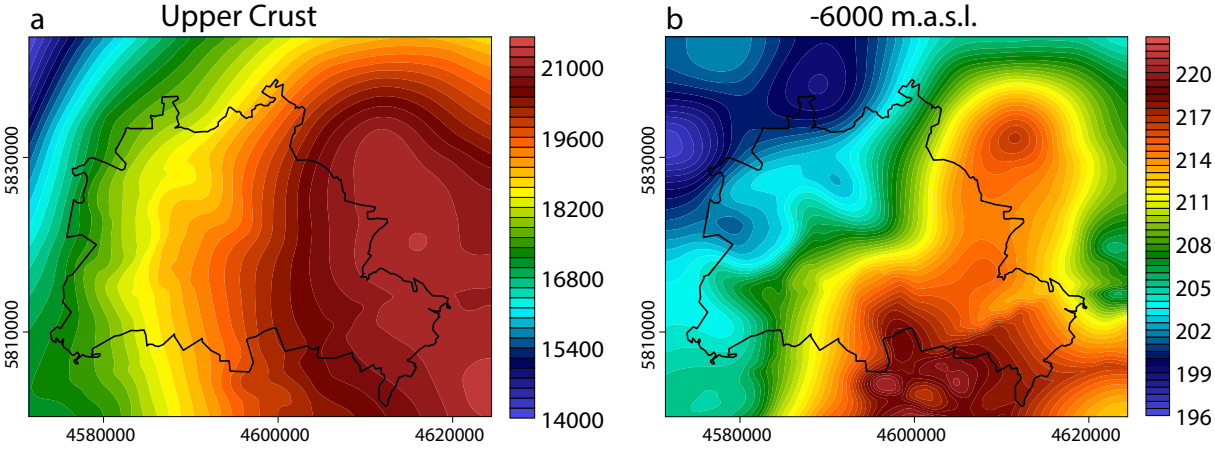

Figure 5.2.: (a) Thickness of radiogenic upper crystalline crust; (b) lateral variations in temperature at -6 km.a.s.l. predicted by the conductive lithosphere-scale model that was used as lower thermal boundary condition for the coupled simulation of heat and fluid transport.

clastic insulating sediments.

A second important factor for the thermal field is the nature and configuration of the crystalline crust below the sedimentary units as especially the upper crystalline crust is rich in radiogenic elements and may significantly contribute to the heat budget (Jaupart et al., 2007; Clauser, 2011; Scheck-Wenderoth and Maystrenko, 2013). Geophysical data and models (Krawczyk et al., 2008; Maystrenko and Scheck-Wenderoth, 2013) indicate that the crystalline crust below Berlin may be grossly subdivided in two layers: a more radiogenic silicic upper crustal unit and a less radiogenic mafic lower crustal unit. Interestingly the upper crustal unit is a few km thicker below the eastern half than below the western half of the city of Berlin (Fig. 5.2a). This provides more basal heat input to the eastern part of Berlin than to its western part resulting in higher temperatures at depths below the sedimentary fill (Fig. 5.2b).

A third factor influencing the thermal field in the upper few km below Berlin is the flow of underground water in the porous clastic sedimentary units. Previous work (Frick et al., 2016b)

showed that this dynamic component is mainly influenced by two factors below Berlin: (1) the, often not accurately known, upper hydraulic conditions and (2) the distribution of the Rupelian clay (Fig. 5.1b), an aquitard separating the upper fresh water compartment from the deeper saline aquifers. As a result of glacial erosion (Kaiser et al., 2013b) the Rupelian clay is locally discontinuous (e.g. white domains in map of Fig. 5.1b, Frick et al. (2016b)). In those areas where this unit is missing hydraulic communication between the shallow and deep groundwater compartments may occur (Kaiser et al., 2013b). This may result locally in cold surface fresh water entering at large depths in the subsurface beneath major recharge areas and in rise of hot deep saline water in discharge areas. In summary, thermal models should consider the cumulative effects of these factors, which requires a workflow that integrates processes from the scale of the lithosphere to the scale of shallow sediments.

5.1.2. Methods and Input Data

The workflow combines lithosphere-scale 3D conductive modeling with basin-fill-scale modeling of coupled fluid and heat transport. To calculate the steady state 3D conductive thermal field the heat equation is solved using a Finite Element Method (FEM) for a 3D structural model resolving the main sedimentary units, two crustal units and the lithospheric mantle. From this model the temperature distribution at -6 km.a.s.l. (Fig. 5.2b; (Sippel et al., 2013)) is extracted and prescribed as lower thermal boundary condition for the simulations of coupled heat and fluid transport using the software FEFLOW©(Diersch, 2014). The physical and numerical background of the method is described in Sippel et al. (2013) and Frick et al. (2016b). Accordingly, initial conditions were calculated for steady state conditions in the case of the coupled model, separately for fluid flow and heat flow. The simulation time for the transient simulations in the coupled case were chosen such that quasi-steady state conditions were established. This was the case for a simulation time of 250 thousand years. Physical properties (thermal conductivity, radiogenic heat production, heat capacity, porosity, permeability, Fig. 5.3b) as well as the upper thermal and hydraulic boundary conditions are chosen identical with the ones described by Frick et al. (2015) and Fig. 5.3 illustrates the respective hydraulic head observed at the groundwater table.

5.2. Results

In the following we describe the superposed effects of variations in upper crustal thickness, of the distribution of conductive salt versus insulating sediments and of fluid flow in response to variations in permeability and in hydraulic head. All these factors together lead to significant differences in temperature causing lateral variations and partly even inversion in the temperature trends with depth.

This is illustrated in Fig. 5.4 for two representative depth levels: at -300 m a.s.l. and at -3000 m a.s.l. Most impressive is the opposite temperature trend at the shallow and the deeper level. A large part of this pattern is controlled by the conductive heat transport as evident by direct comparison of the temperature pattern predicted by the conductive model (left panel in Fig. 5.4) with the one predicted by the coupled model (right panel in Fig. 5.4). At -3000 m a.s.l.

a

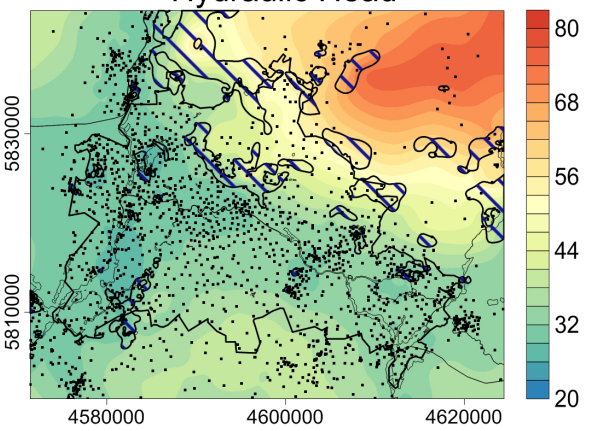

b

	Geological unit	λ^b [W/mK]	Q_r [W/m³]	c^s [J/kgK]	Φ [-]	κ [m/s]
Quaternary	Holocene to Weichselian	2.71	9.0E-06	1570	0.32	1.42E-05
	Eemian to Saalian	2.59	9.0E-06	1580	0.31	4.04E-06
	Holstein	2.17	9.0E-06	1670	0.30	1.91E-08
	Elsterian	2.35	9.0E-06	1610	0.30	8.98E-07
Tertiary	Miocene	2.47	1.0E-05	1560	0.30	6.88E-07
	Cottbus	2.62	1.3E-05	1700	0.31	1.15E-06
	Rupelian	1.64	1.3E-05	1810	0.24	3.23E-08
	Pre-Rupelian	2.48	1.3E-05	1700	0.30	6.56E-07
	Upper Cretaceous	2.82	6.0E-06	2290	0.11	4.81E-07
	Lower Cretaceous	2.36	1.5E-05	2290	0.11	4.81E-07
	Jurassic	2.71	1.5E-05	2250	0.19	4.81E-07
Triassic	Keuper	2.35	1.6E-05	2320	0.13	9.62E-09
	Upper Muschelkalk	2.3	1.0E-05	2250	0.15	9.62E-09
	Middle Muschelkalk	2.3	1.0E-05	2250	0.04	impermeable
	Lower Muschelkalk	2.3	1.0E-05	2250	0.12	5.77E-10
	Upper Buntsandstein	3.0	1.8E-05	2190	0.03	6.44E-09
	Middle Buntsandstein	2.0	1.8E-05	2390	0.14	5.84E-07
	Lower Buntsandstein	1.84	1.8E-05	2390	0.05	1.25E-09
Permian	Zechstein	4.5	4.0E-06	1940	0.01	impermeable
	Sedimentary Rotliegend	3.0	1.4E-05	2180	0.08	5.06E-08
	Permo-Carboniferous	2.5	2.9E-05	2600	0.03	8.66E-10
	Basement	2.2	2.8E-05	2300	0.01	impermeable

Figure 5.3.: (a) Hydraulic head [elevation in m a.s.l.] prescribed as upper hydraulic boundary condition in the coupled model obtained from groundwater measurements at numerous wells (black dots). (b) Physical properties and units for the geological units resolved: thermal conductivity λ^b; radiogenic heat production Q_r, heat capacity c^s, porosity ϕ, hydraulic conductivity κ.

differences between the two models are small, as the influence of fluid flow decreases with increasing depth. This is due to a reduction of porosity and permeability of sedimentary rocks in response to increasing compaction with depth.

The general trend of higher temperatures below the eastern half of the city at -3000 m a.s.l. partly follows the variations in basal heat input (Fig. 5.2), but the pattern strongly deviates from the one imposed by the lower thermal boundary condition (Fig. 5.2b). Accordingly these variations must be caused by the heterogeneities in thermal properties considered in the sedimentary succession. The strongest contrast in thermal properties in this context is the one between salt and clastic sediments. A comparison between the top salt surface (Fig. 5.1a) and the modeled temperature distributions (Fig. 5.4) reveals a spatial correlation between the position of salt structures and thermal anomalies: at shallow depth (-300 m a.s.l.) highest temperatures are predicted above the two salt diapirs ("1" in Fig. 5.1a and Fig. 5.4) and the salt pillows ("2" in Fig. 5.1a and Fig. 5.4). In contrast, negative thermal anomalies are associated with salt diapirs and pillows at larger depth as visible in the temperature maps for -3000 m a.s.l. This inverse pattern of high temperatures above and low deep temperatures below salt structures is caused by the more efficient heat transport within the conductive salt compared to the insulating surrounding sediments. The heat therefore is extracted towards the surface, but cannot reach the latter as the salt structures are covered by insulating sediments. This results in heat storage above the salt causing the positive circular temperature anomalies above the diapirs and the larger positive anomalies above the salt pillows. In contrast, in areas where the salt has been replaced by insulating clastic sediments ("3" in Fig. 5.1a and in Fig. 5.4), heat storage affects the entire sedimentary succession causing positive thermal anomalies at larger depth.

In addition to these salt-related temperature variations the temperature pattern predicted by the conductive and the coupled models is considerably different at shallow depth (-300 m a.s.l.). These differences illustrate the influence of heat transported by moving fluids. In domains where the Rupelian aquitard separating shallow freshwater and deeper saline waters is discontinuous

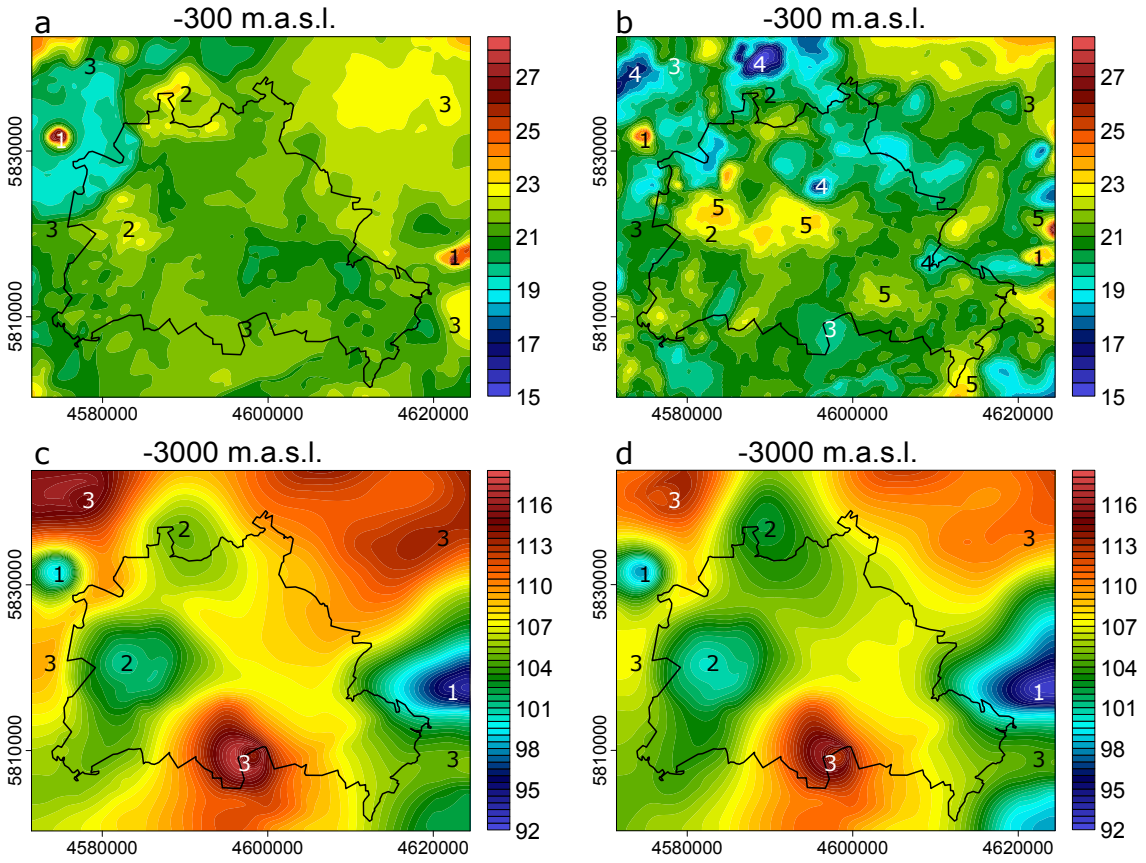

Figure 5.4.: (a) Temperature distribution at -300 m a.s.l. predicted by steady-state conductive model; (b) temperature distribution predicted by coupled simulation of fluid and heat transport at -300 m a.s.l.; (c) temperature distribution predicted by the steady-state conductive model at -3000 m a.s.l.; (d) temperature distribution predicted by coupled simulation of fluid and heat transport at -3000 m a.s.l. Numbers indicate specific structures that are referred to in the text.

(Fig. 5.2b) and where the hydraulic gradient is high (Fig. 5.3), cold surface water flows to deeper levels leading to local negative thermal anomalies (indicated as "4" in Fig. 5.4). Inversely, where the hydraulic head is low and the separating aquitard is continuous and shallower than -300 m a.s.l., hot deep water may rise and cause positive thermal anomalies at shallow depth (indicated as "5" in Fig. 5.4).

Comparing the purely conductive model predictions for -3000 m a.s.l. (Fig. 5.4c) with the temperatures at the same depth predicted by the coupled model (Fig. 5.4d), shows that the general pattern is very similar but the coupled model indicates a more complex hydrodynamics affecting the shallow temperature distribution and resulting in a net cooling effect induced by fluid flow and relatively colder conditions.

5.3. Discussion and Conclusions

The results of this study illustrate, that physically meaningful predictions of subsurface temperatures in areas of potential geothermal energy production need to consider influencing

factors acting at different scales. First-order influences are to be expected from the deep crustal and lithosphere structure that need to be explored in order to capture variations in the basal heat input. In addition lithological heterogeneities in the upper few km may overprint the basal heat signal in two ways: (1) large contrasts in thermal conductivity as between salt and clastic sediments may focus heat flow to preferential directions and depth levels and (2) advective heat transport may lead to significant local cooling or heating.

For the area of Berlin, highest shallow temperatures are expected beneath the central western part of the city based on the conductive and the coupled models, where up to 24°C are reached at -300 m a.s.l. according to the predictions of the coupled model. Such areas would be interesting targets for shallow geothermal energy production. In contrast local low-temperature anomalies may be encountered as well, like below the NE part of Berlin where only 15 °C may be reached at -300 m a.s.l.. Such areas should be avoided if shallow geothermal energy production is planned. An important conclusion from the work presented is that the pattern of shallow temperatures is not representative for deep temperature anomalies and the deep temperature anomalies may even be inverted with respect to the shallow temperature pattern.

Areas with the best potential for deep geothermal energy production are located in the central southern part of the city and in the eastern half of the city in general. There thick successions of insulating and permeable clastic sediments have accumulated in salt rim synclines and could be best targets for the production of deep geothermal fluids. High temperatures combined with high heat flow are expected within the upper portions of the Zechstein salt structures. These domains are however tight as salt is impervious. Therefore closed system borehole heat exchangers may be the technology suitable for exploitation of deep heat in these domains.

These results show that considering geothermal heat as a potential contributor to the future energy mix and in particular to urban heating is a realistic option. However, simple concepts of a uniform average temperature increase with depth in the subsurface will definitely fail to predict the geothermal potential. Even if the scale of a city is small with respect to the thickness of the crust or lithosphere, the thermal field may be considerably influenced by regional heat transport processes. This is not only true for the basal heat input coming from the deeper crust and mantle but also for the heat transported in the subsurface by differently conductive rocks and by moving groundwater in the shallower levels below the urban area. Accordingly, exploration concepts related to the utilization of geothermal energy in urban areas should assess the geological and hydrogeological heterogeneities first and consider possible regional influences. In addition to these natural conditions also socio-economic factors as the need for energy in a specific district need to be evaluated. Finally, the assessment of the natural situation and of the areal demand for energy should be complemented by the anticipation of consequences and feed-back processes induced by the production of deep fluids.

Acknowledgments

This study is part of the project Energy System 2050 a joint initiative of the research field energy of the Helmholtz Association and was supported with data by the Senate Department for Urban

Development and the Environment of Berlin (SenStadtUm) and by Berlin waterworks (BWB) which is gratefully acknowledged.

6. Geothermal Potential

Frick, M., Lewerenz, B., Kastner, O., Scheck-Wenderoth, M., Schneider, M., and Cacace, M. (In Preparation). "The Geothermal Potential of the Subsurface of Berlin"

6.1. Introduction

This chapter is part of a paper that is currently in preparation. For the sake of keeping this chapter short and avoiding repetition, the introduction has been reduced to the essentials. I hereby extend the discussion opened in the previous chapter (Chapter 5, Scheck-Wenderoth et al., 2017) by further investigating promising areas for geothermal exploration. Therefore, the regional geothermal potential is used as a different quantitative indicator. One of the main results from the previous chapter has been to identify two main geological horizon as being the most promising from an energetic point of view. These two areas show a different prospect for the utilized extracted energy, being located at different depth levels. Indeed, I have already identified the target use of each of these areas, if only based on the available temperature and depth location of the local reservoir. The central and northeastern areas of the model domain provide favorable conditions for geothermal operations at relatively shallow depth levels ($\sim -300\,m\,a.s.l.$), while the southern and northwestern areas present favorable geothermal conditions at greater depths ($\sim -3000\,m\,a.s.l.$). Based on this information supported by the available temperature at the specific depths, I concluded on the possibility of making use of the energy extracted from shallower levels for mainly district heating purposes, while the deeper reservoirs likely have the potential for electricity production.

6.2. Modeling Method

In the following I present a more targeted approach along the lines of the studies by Kastner et al. (2013) and Kastner et al. (2015). This method calculates the available heating power of deep aquifers by considering the maximum production mass flux, needed pumping energy, minimum well separation at maximum mass flux and the resulting coefficient of performance. Here the fundamental principle assumes that a virtual hydrothermal heat plant delivers heat $\dot{Q}$ and consumes electrical power $\dot{W}_{el}^{P/I}$ to drive the production and injection pumps. In the following the main equations behind the method together with the modifications to the originals approach are described. More details can be found in the literature Kastner et al. (2015) and Kastner et al. (2013). All symbols used are explained in Table 6.1.

Essentially, we assume a hydrothermal plant consisting of two wells: injection and production. Following this setting, the limiting production mass flux $\dot{m}_{limOP}$ represents a production level that can maintain absorbing well conditions at the injection well. It can be expressed as:

$$\dot{m}_{limOP} = \frac{2Z_{\infty}\rho\pi\tau}{ln(2D/R)} \tag{6.1}$$

Table 6.1.: List of symbols and parameters used for the calculation of all relevant properties.

Symbol	Description
$\dot{m}$	Mass flux
$\dot{m}_{OP}$	Mass flux at operation point
Z_∞	Natural hydraulic head
ρ	Fluid density
τ	Transmissivity
D	Half doublet separation
rf = 2D	Final injected fluid radius, well separation
R	Borehole caliber = 0.065 m
a	Plant life time, for the calculations in this manuscript set to 30 years = 946080000 seconds
M	Effective reservoir thickness = Absolute thickness
ϕ	Porosity
W	Lamberts Function
k	Permeability (MBS = 6E-14 m^2, SR = 5.19E-15 m^2)
η	Dynamic fluid viscosity =$8.90 \cdot 10^4 Pa \cdot s$
$\dot{Q}$	Heat flux
$\dot{Q}_{OP}$	Heating power at operation point
c_f	Mass-specific heat capacity of fluid
T	Temperature
T^P	Production Temperature
T^I	Injection Temperature = 45°C
W_{OP}	Working power at operation point
g	Gravitation constant
COP	Coefficient of performance, see limitations in the text

wherein the required well separation ($2D$, representing the thermal breakthrough, that is, the first arrival of the injected thermal front at the production well) is defined by:

$$2D = \sqrt{\frac{\dot{m}a}{\rho\pi M\phi}} \tag{6.2}$$

This quantity is calculated for a scenario where a lifetime of 30 years is assumed. Therefore, the distance between injection and production well depends on the mass flux as well as the reservoir properties.

Eq. (6.1) and Eq. (6.2) then combine to the mass flux for the production well:

$$\dot{m}_{op} = \frac{2\beta}{W(2\beta e^{-2\alpha})} \tag{6.3}$$

with $\alpha = \frac{1}{2} ln\left(\frac{R^2\rho\pi M\phi}{a}\right)$ and $\beta = 2Z_\infty\pi\rho\tau$ where $\tau = M\frac{k\rho g}{\eta}$

This production mass flux can be used to express the thermal heating power in operation by:

$$\dot{Q}_{op} = \dot{m}_{op}c_f(T^I - T^P) \tag{6.4}$$

and the working of the production pump in operation:

$$\dot{W}_{op} = \dot{m}_{op}g|Z_\infty| - g\frac{\dot{m}_{op}^2}{\rho}\frac{1}{2\pi\tau}ln\frac{R}{2D(m_{op})} \tag{6.5}$$

From Eq. (6.4) and Eq. (6.5) we can then derive the coefficient of performance:

$$COP = \frac{Q_{op}}{W_{op}} \tag{6.6}$$

COP is a theoretical measure of the ratio between the energy extracted from the hot brine and the energy needed to lift the brine to the power plant at the surface. It is a coefficient usually adopted to quantify the level of performance of heat pumps.

Changes that have been implemented in comparison to Kastner et al. (2015) mostly concern the parametric setup of the model. In detail, we refrained from differentiating between nominal and effective thickness (in (Kastner et al., 2015) effective thickness = nominal thickness * sandstone fraction) because this differentiation is not resolved in the underlying geological and numerical model. Moreover, the hydraulic properties of the reservoir have been assigned to the entire thickness of the unit in the numerical model (compare to Table 3.1), which is then in agreement with the calculations done here. In this context, the depth dependency of the porosity and permeability of the reservoir units was removed and replaced by the same fixed values used in this thesis. We used the newly predicted temperatures of the models produced in this thesis to provide an estimate of the influence of different parameters on the extractable heating power, also depicting the most up to date estimate of the latter.

The model adopted for this study (as described in detail in Chapter 4) depicts a highly heterogeneous distribution of burial depths (meter below surface), between 180 m and 2650 m

with a thickness between 0 and 400 m for the Middle Buntsandstein (Fig. 6.1a,b). The reservoir temperature of the unit then lies within a range of 20 °C and 100 °C, whereas highest temperatures are found in the south, northeast and -west and in the southeast, correlating with large burial depths (Fig. 6.1a,c). The deeper reservoir of the Sedimentary Rotliegend has burial depths between 2950 m and 4050 m with thicknesses from 90 m to 430 m (Fig. 6.1d,e). The temperature at this depth ranges from 95 °C in the east and southeast to 135 °C in the northeast and -west (Fig. 6.1f) representing a mixture of burial depth, heat input from the crust and heat withdrawal through the chimney effect of the Zechstein salt.

6.3. Results and Discussion

With these input data we can derive the relevant properties for the potentially producible heating power by a power plant utilizing a doublet system for the Middle Buntsandstein. The first of these properties is represented by the production mass flux, which ranges between $0\,\frac{kg}{s}$ and $75\,\frac{kg}{s}$. The maximum flux is predicted in the south and correlates spatially with the maximum temperature therefore giving minimum values of fluid density and viscosity. It correlates positively with the thickness distribution as well, which relates to the increased effective transmissivity of the reservoir section at those localities (Fig. 6.1b and Fig. 6.2a). A similar distribution is calculated for the production pump working power, whereas values range in between 0 kW and 300 kW (Fig. 6.2b). Here, the maximum power derives from the high mass flux and large burial depth of the reservoir across the southern border. The critical well separation of the virtual doublet lies between 440 m and 645 m for the Middle Buntsandstein reservoir. Highest values in this regard are located at highest reservoir temperatures and vice versa (Fig. 6.2c). Under consideration of all of the values mentioned up until now, we can then predict the geothermal potential for every lateral node of the targeted reservoir. For the Middle Buntsandstein this means a range of extractable heating power between 0 and $\sim 10\,MW_{th}$, whereas close to no potential is predicted above the Zechstein diapirs and pillows, due to the low temperature and mass flux at these localities (Fig. 6.2d). The more promising sites are located where we predict high mass fluxes as well as high temperatures. These are namely, in the south (south of Tempelhof) and in the northwest (Krämer forest). For a first glimpse on the effectiveness of producing geothermal fluids from this reservoir a simple ratio between the predicted heating power and the pumping power needed to get it to the surface was calculated. Based on this simplified approach the highest "coefficient of performance" is located where above average geothermal potentials correlate spatially with comparatively low pumping power (Fig. 6.2e). This means that the area targetable for exploitation becomes larger than by identifying the heating power alone.

The deeper reservoir of the Sedimentary Rotliegend shows comparatively low mass fluxes between $2\,\frac{kg}{s}$ and $14\,\frac{kg}{s}$ (Fig. 6.3a). Like for the Middle Buntsandstein, it correlates strongly with the thickness and therefore transmissivity distribution and to a lesser degree with the temperature since the latter shows a smaller range of variation than that of the shallower reservoir. Hence, largest values are found in the entire northern sector of the model area, where highest transmissivities are found. The same holds true for the pumping power predicted,

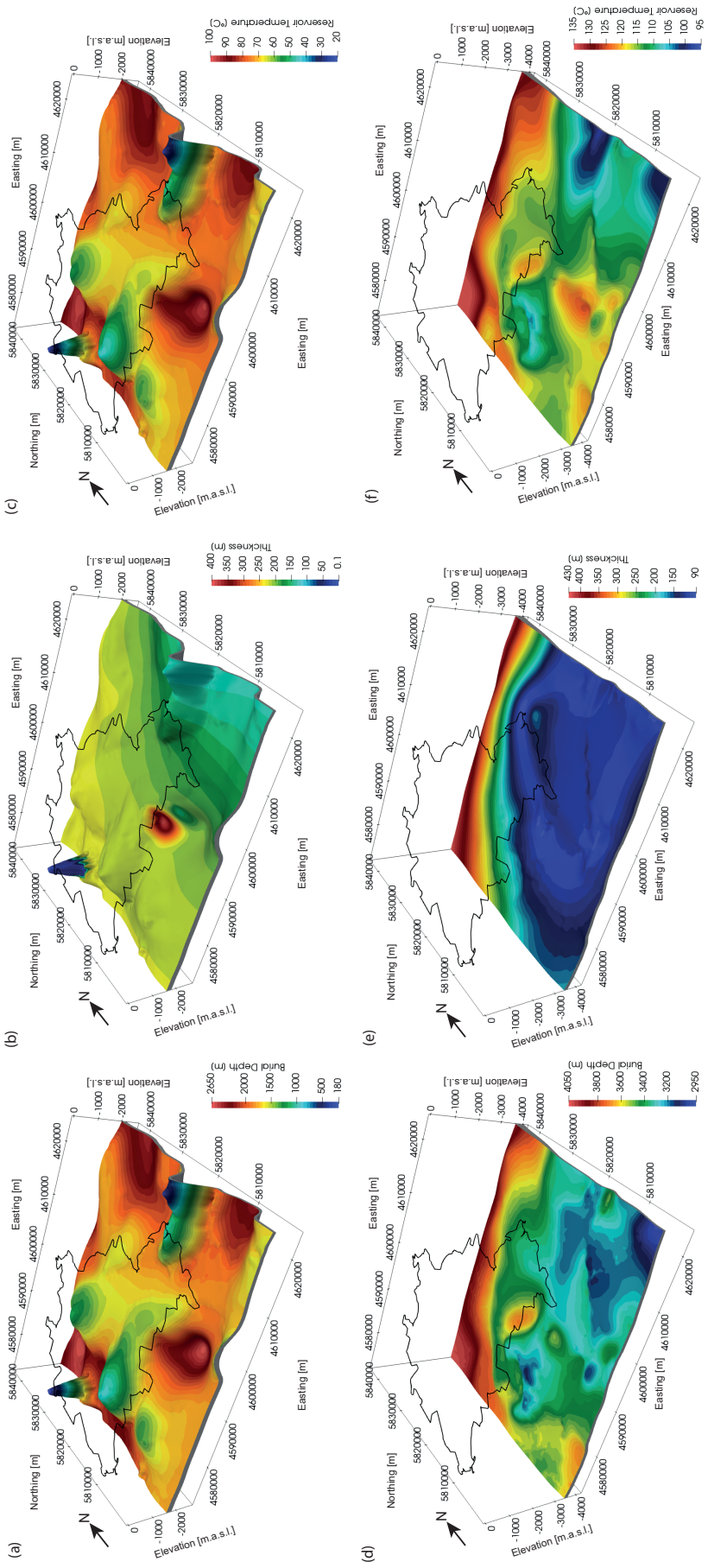

Figure 6.1.: Input data for the calculation of geothermal potential properties. (a-c) Middle Buntsandstein, (d-f) Sedimentary Rotliegend. (a,d) Burial Depth, (b,e) Thickness, (c,f) Reservoir Temperature (Half way between top and bottom). m.a.s.l.: meters above sea level; Coordinates [m] in Gauß-Krüger DHDN Zone 4.

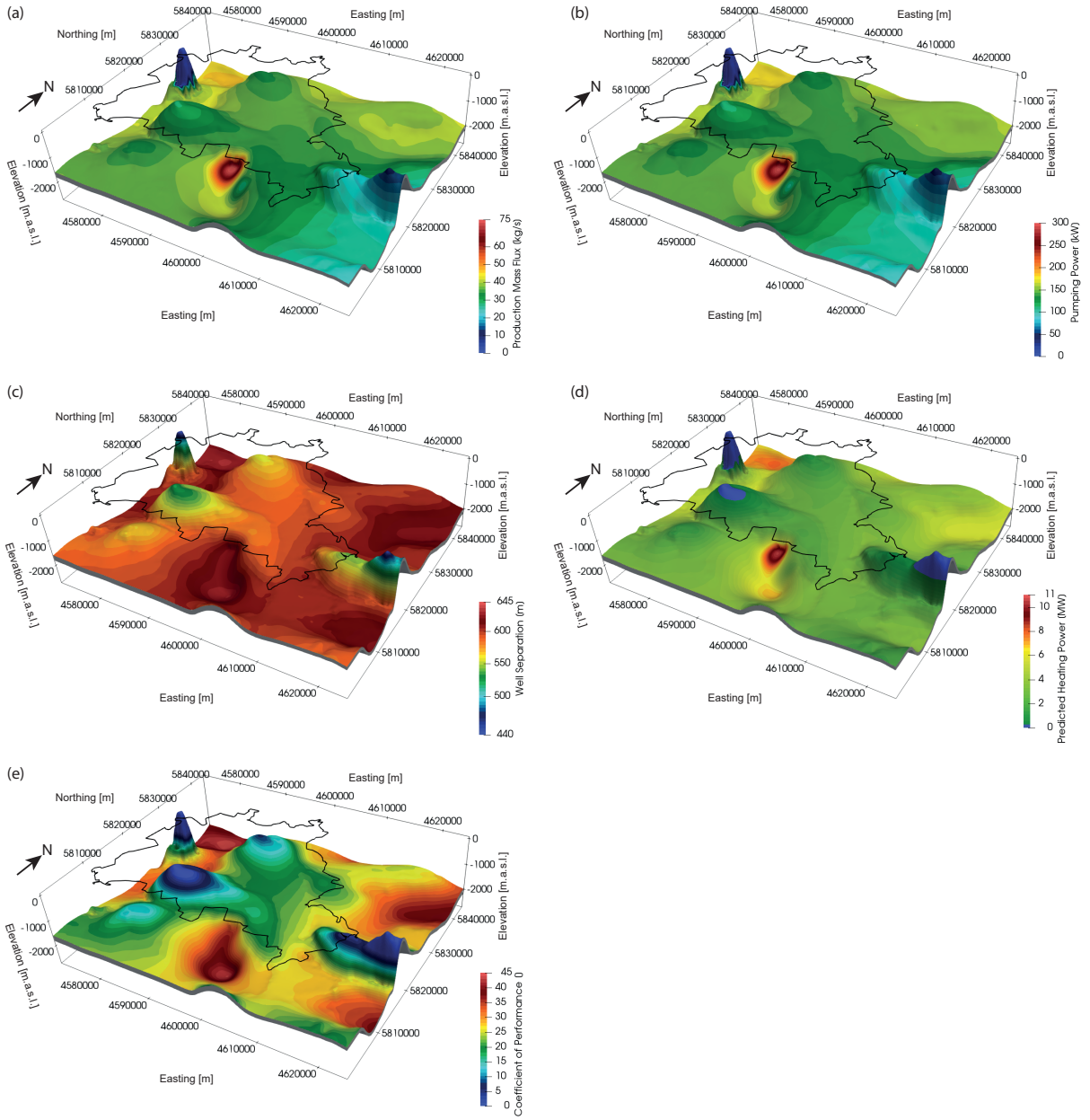

Figure 6.2.: Output data of the calculation of geothermal potential properties for the Middle Buntsandstein reservoir. (a) Production Mass Flux, (b) Pumping Power (extraction pump), (c) Well Separation, (d) Predicted heating power, (e) Coefficient of Performance. Coordinates [m] in Gauß-Krüger DHDN Zone 4.

whereas values range between 0 kW and 90 kW (Fig. 6.3b). The critical well separation of the Sedimentary Rotliegend lies within a narrow range of 275 m to 320 m with values correlating well with the reservoir temperature distribution because of the coupled fluid density (Fig. 6.3c). The resulting heating power for the deep reservoir is considerably smaller, showing maximum values of $\sim 4\,MW_{th}$ only (Fig. 6.3d). This can be explained by the considerably smaller mass fluxes which can not be compensated by the higher reservoir temperature. Maximum potentials are found in the north where highest mass fluxes coincide with high reservoir temperatures. If we then take these data and derive the efficiency via the coefficient of performance again, the low heating power gets combined with even lower pumping power than for the Buntsandstein, resulting in rather high efficiencies of up to 60 (Fig. 6.3e). Comparing the areas identified by the heating power only with the areas where an above average efficiency is predicted we can see that the latter is again larger.

The values reported above should be regarded with caution, being only indicative of the exploitability of these reservoirs, since a validation or calibrations is not possible at this stage of research. However, as stated in the introduction section of this thesis, an estimation of the potential of geothermal energy should be carried out under consideration of all available data. These values stand representative of the most up to date temperature predictions for the subsurface which in turn integrate all available data concerning structure and physical parameterization for the municipality of Berlin. The importance of updating the models concerning all of these parameters becomes evident when looking at the development between the publication by Kastner et al. (2015) and recent estimates provided by this thesis. In (Kastner et al., 2015) the range of predicted heating power from the Middle Buntsandstein was $0\,MW_{th}$ to $\sim 6\,MW_{th}$ and for the Rotliegend $0\,MW_{th}$ to $\sim 0.2\,MW_{th}$. Both the distribution and magnitude of those values are comparatively lower than those predicted by the models of this thesis which derives from the improvements of the underlying models in accordance with all available data. With these results, an even higher potential than previously assumed is predicted which outlines a possible future utilization of these underground resources. To put the potential into perspective, a single geothermal power plant utilizing the Middle Buntsandstein could provide up to $\sim 10\,MW_{th} = 0.28 * 10^{15}\,J$ (assuming 8000 h production) which translates to 0.63% of the overall heat demand of Berlin (S. Berlin-Brandenburg, 2018d).

To get a first estimate the potential for the Middle Buntsandstein for the entire model area we crudely assume an inter-well distance of 1150 m (= 2*average well separation) to avoid any interference tween two virtual doublets. With this approach, 1786 locations in the model remain, which are regularly gridded, with a resolution of 1150x1150 m. The summed up geothermal potential of these localities is then on the order of $\sim 4610\,MW_{th} = 133 * 10^{15}\,J$. Applying the same approach to the Sedimentary Rotliegend, an inter-well distance of 600 m is assumed, which translates to 6336 possible locations. These then sum up to a theoretical potential of $\sim 6770\,MW_{th} = 195 * 10^{15}\,J$. Combining these estimates for the two reservoirs, this results in an overall geothermal potential of $327.7 * 10^{15}\,J$. Comparing this value with the 2015 heat energy consumption of $44 * 10^{15}\,J$ outlines that it is by far in excess. Despite physically sound, these estimates represent upper limiting theoretical values, which might not reflect real practical

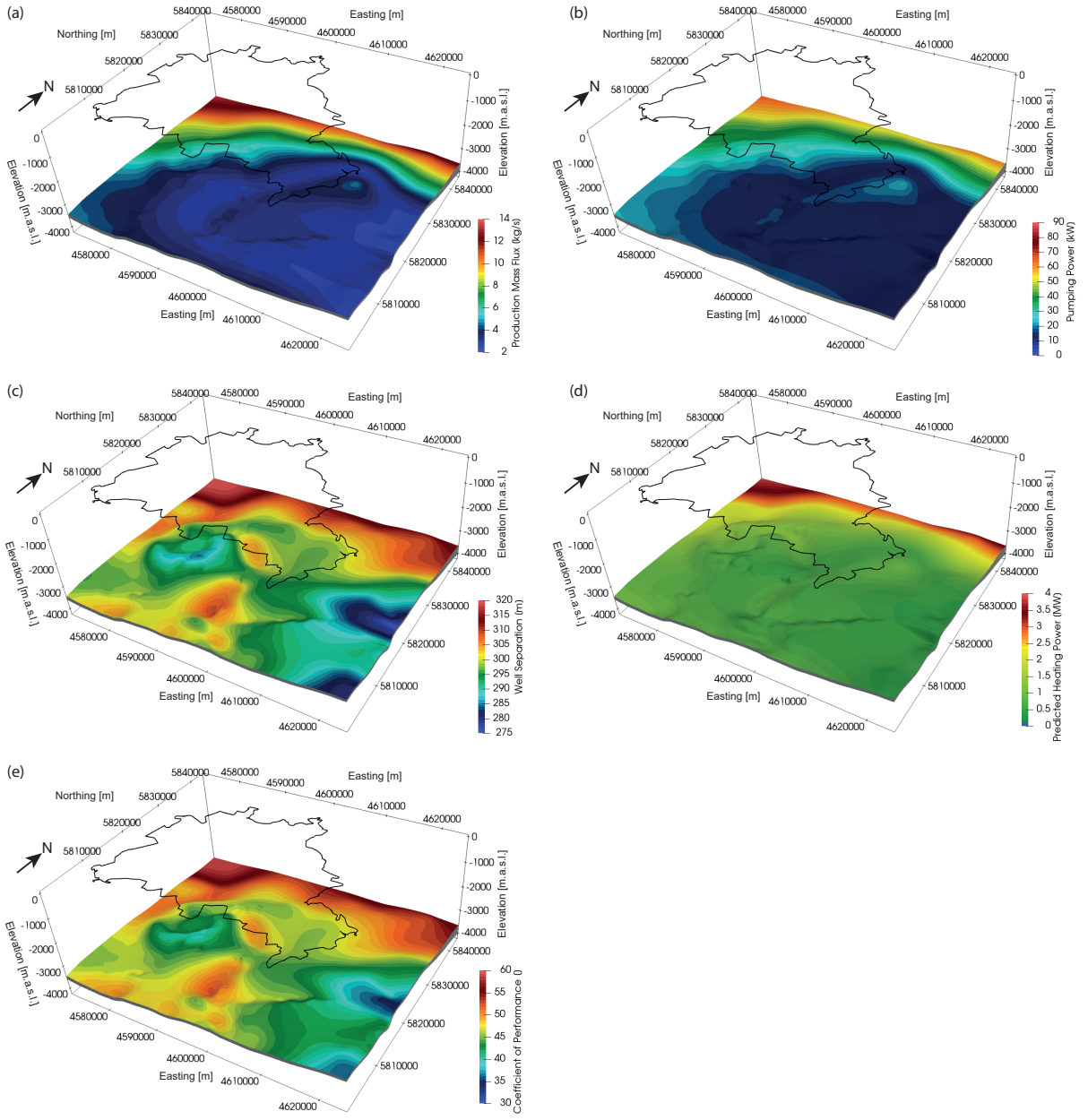

Figure 6.3.: Output data of the calculation of geothermal potential properties for the Sedimentary Rotliegend reservoir. (a) Production Mass Flux, (b) Pumping Power (extraction pump), (c) Well Separation, (d) Predicted heating power, (e) Coefficient of Performance. Coordinates [m] in Gauß-Krüger DHDN Zone 4.

scenarios. The limitations that have to be taken into consideration lie in the economical feasibility (i.e. drilling cost versus producible energy) as well as engineering and governmental limitations (i.e. (sub)surface utilization). This is why I would like to conclude at this stage on the need to further develop this approach opting for a multi-criteria analysis to spatially distribute a best case scenario of subsurface utilization. Moreover, uncertainties in the physical property representation should not be neglected and their effect investigated as soon as new data become available.

7. Discussion and Outlook

In Germany in general and in Berlin in particular, the need for sustainable environmentally friendly energy provision gained increased focus throughout the last decades. The decision to terminate energy supply by nuclear and decreasing the use of fossil fuels has strengthened this focus, and encouraged the switch to renewables such as wind, photo-voltaic and geothermal, amongst others (Sellner and Fellenberg, 2011). For geothermal energy a strong emphasis lies on the fact that we need to characterize all physiochemical processes in the shallow to deep subsurface in order to understand and identify the distribution of heat and groundwater circulation (Hebig et al., 2012; Huenges et al., 2013a). This is especially true for urban environments, which might have been anthropogenically overprinted and therefore display an even higher complexity than other regions with a comparable geological subsurface configuration (Menberg et al., 2013). There has been significant development on both, identifying deep geothermal resources on the basin scale and exploring shallow geothermal resources, specially beneath cites. However, linking these two and identifying which processes are involved in this complex setting has been rarely attempted. To provide first steps in bridging this gap has been the main motivation for this thesis. As recorded in the previous chapters, I have been able to demonstrate which processes and rock and fluid parameters exert an influence in distributing the temperature and pore pressure with depth. Moreover, I could show to which degree the resulting dynamics and hydrothermal configuration are sensitive to improvements in the model components, being those of natural origin (i.e. surface body waters) or induced by human activities (pumping).

In the following, I will make use of the results presented in the thesis to answer the open scientific questions raised at the beginning of the study. This will be followed by a broader discussion on the implications derived from the study aiming at embracing all the basic findings into an overarching final discussion.

7.1. Surface Water - Groundwater - Interactions

Open scientific question: Surface Water - Groundwater - Interactions: What are the main hydrogeological characteristics of these interactions at depths of their dynamics and what are the main consequences for groundwater management and sustainability within an urban area?

In order to approach this question, I questioned and revisited a long lived assumption that has ruled the standard approach in the regional hydrogeological modeling community. This assumptions stems from approximating in a regional context the hydrodynamic potential at the surface by means of the resolved variability in the topographic relief (constant pressure or constant load BC on the topography). While such an assumption permits to represent the regional characteristics of the groundwater potential (hydraulic gradients), it always leads to (i) overestimation of the amount of the surface pressure loading acting on the system, (ii) great fluid mass imbalance (especially for simplistic model configurations), and (iii) neglect the interactions

between surface water features (lakes and rivers) on the local to regional groundwater circulation (i.e. Marklund and Wörman, 2011; Kaiser et al., 2013b; Frick et al., 2015). In order to specifically quantify the latter point, I implemented rivers and lakes as distinct physical 3D elements in all model realizations as described in Chapter 3. This was done following a step-like approach, by gradually introducing the level of complexity of the models to enable a proper quantification of the effect of each modification as well as of their interactions. The base, starting model configuration of this thesis considers a hydraulic head boundary condition, which was derived from interpolated grids of groundwater levels after SenStadtUm (2013b). Hereby, smoother undulations of the groundwater levels are imposed, orders of magnitude lower than would be present at topographic level, which leads to a reduction of forced convective cooling (Frick et al., 2015). However, this approach holds a major limitation if applied in an urban environment, where hydraulic heads have been significantly altered because of drinking water production. In Chapter 3 I demonstrated how a mere interpolation of measured groundwater heads (partly overprinted by human activities) deviates significantly from the present day hydraulic setting. The relevance of this particular relationship becomes evident when considering the classical hydrological textbook picture representing areas of high elevation as recharge areas and lowlands, featuring rivers and lakes, as discharge areas. In a natural setting locally disturbed by human made operations (a typical situation within urban areas) this relationship might not hold true for extensive areas and leads to erroneous predictions concerning subsurface hydrology and temperature distributions.

An alternative is to rely on more data, and a data driven approach, as done in this thesis by implementing all major surface water features and by investigating the resulting hydrodynamics. This is particularly crucial while investigating settings as Berlin, where most of the produced drinking water is supplied through bank infiltration from surface water bodies (Möller and Burgschweiger, 2008). The results show that modeled fluid pathways can reproduce the current hydrodynamics to a higher fidelity, depicting strong infiltration from surface water bodies of higher hydraulic potential towards artificially lowered hydraulic heads in their direct adjacency. A major finding connected to the models presented here is that these modifications are not only limited to the shallow subsurface, but might be traced down to depths of $-4800\,m.a.s.l.$ and have a lateral spread of up to 4 km. This is connected to both, pressure as well as temperature differences. Concerning pressure differences the implications of the models are, that in order to depict the groundwater circulation patterns in the subsurface of urban areas, only considering groundwater heads as a hydraulic boundary condition, is likely insufficient. In such setting, the natural hydraulic regime is closely connected to anthropogenic activities, which in turn can lead to a complete overprinting of the natural dynamics as envisaged in reversal in expected flow directions. Despite these discussion points having been derived from a study centered on a specific setting, their relevance to other settings (given similarities) can be easily discussed further. This latter aspect points to the fact that a safe and sustainable utilization of the natural water resources underneath major urban centers should benefit from similar applied studies bringing a more in depth understanding of the shallow to deep groundwater dynamics and interactions. Moving back to the specific study case of Berlin, the thermal perturbations caused by anthropogenic overprinting are on the order of thermal breakthrough for classical

shallow geothermal utilization which calls for a careful planning in this respect. Moreover, the correct representation of rivers depicts parts in the model area showing losing conditions (river water infiltrates into the subsurface). This presents an important dynamic aspect, since riverine pollutant transport has been reported in Berlin (Massmann et al., 2004) and is also typical for industrial areas connected to urban centers. These pollutants might then be carried on into the groundwater, thus posing a threat to drinking water production as well as groundwater ecology.

As a final word on this first point, I would like to add a short discussion on the current limitations of the study in its present state. Those are mainly related to two assumptions, that is: (1) a perfect hydraulic connection between the surface water bodies and the groundwater and (2) depicting the component of anthropogenic overprinting only as a second order parameter. For point (1) there is evidence of some degree of decoupling in the residence times of groundwater derived from the produced water in production wells (Massmann et al., 2004) likely connected to clogging layers. Therefore, as also will be outlined in the following paragraphs, future studies should try to better constrain and integrate such clogging layers in their resolution (Chapter 4). A specific merit deserves the assumption delineated at point (2). In this regard, it is highly uncertain whether and to which degree representing the effects of groundwater pumping activities in the light of imposed cones of hydraulic depressions could suffice to fully depict the effects and consequence of such dynamics on the natural system. Realizing that, prompted me to question the validity of the second assumption in the first family of model realizations and let me to open a second scientific question, which I will tackle in the following paragraph, related to Chapter 4.

7.2. Groundwater Pumping and Natural State

Open scientific question: Natural versus anthropogenic forcing and their influence on the hydraulic and thermal subsurface configuration in urban areas: How to quantify their respective influence?

This question has already been introduced in the previous paragraph, as it naturally originates from the discussion opened above. It once again deals with a proper use of the modeling efforts to discriminate the effects of physical processes of different origin (natural versus human induced in this specific case), and to consider their nonlinear interactions and the results of the latter on the dynamics of a natural system. In order to address this problem, I followed once again a step-like approach. I therefore firstly focus on reproducing (in terms of the physical processes responsible for it) the theoretical natural hydrodynamic state in the study area. This state is representative for the hydraulic configuration of the time before commission of the pumping wells started. In a second stage, I made use of this result to investigate its sensitivity to the full available history of pumping activities. The focus of the latter modeling stage, was not only a mere reconstruction of the present observation by matching, but rather to make use of the comparison between model results and observations in order to get insights of the dynamics and stability of the groundwater configuration underneath Berlin. These models show that we are able to reproduce the present day state as well as reconstruct a pre-water-production "natural" state. More importantly, the models show an even more pronounced component of anthropogenic

overprinting of the subsurface fluid flow, and also thermal field, in the respective time frame.

In detail, I have identified extensive areas influenced by an anthropogenic signal, identified here as areas of lower hydraulic head values than that of adjacent surface water bodies. By removing the hydraulic head constraint in these locations, that is, letting these nodes being free parameters in the model, I could also observe a gradual, but continuous replenishment of water in these domains. This process reaches steady state conditions after approximately 100 years. This replenishment leads to a distribution of hydraulic heads and gradients in agreement with the classically expected spatial extent of recharge and discharge areas before any human action. Therefore, lakes and rivers present discharge areas in this model scenario, while the plateaus and hills are predominantly recharge areas. Building on this state, the following model implements all wells which are presently active. A production period of 100 years was modeled, since this is on the one hand the time it took to reach quasi steady state in the natural scenario, but more importantly it represents the time period of extensive production in the municipality of Berlin. The model then depicts, that active pumping of groundwater leads to extensive modifications of groundwater circulatory patterns. Groundwater flow towards the wells leads to a large drop in heads in their direct vicinity but also in more distal areas. High gradients between surface water bodies and the well heads develop, leading to bank filtration, which is in agreement with observations (Massmann et al., 2004). Therefore, production wells develop as major discharge areas, drawing in water from extensive areas, but most importantly from the surface water bodies. The implications arising from these circulatory patterns of the groundwater go along the lines discussed in Chapter 3. Threats to the safety and security of groundwater might be connected to the infiltration of riverine pollutants. Another source of anthropogenic pollution are sewage farms, which were also investigated in relation to pumping activities. These installations have been active for the last 100 years in Berlin, recharging treated sewage water to the groundwater. This infiltration water accumulates the low amount of pollutants it carries in the subsurface and likely links to increased pollutant concentrations in some production wells in Berlin (Chapter 4). Here the models were able to capture a connection between a sewage farm on one shore of the Lower Havel to production wells on the opposing shore, a concept first proposed by Jarmersted (1992). These dynamics could not be captured by the models in Chapter 3, highlighting the importance of a dynamic implementation of the effects of groundwater production.

For the most up to date models, I also introduced a colmation layer as an additional free parameter in the problem. This layer stands representative for the lowly permeable sediments at the bottom of all major surface water bodies, disconnecting the surface waters from the groundwater to a certain degree. The results of this thesis then show that it is necessary to consider such a layer which is lowly permeable (same value as Rupelian) to allow for a reproduction of the observed hydraulic head decrease through pumping activities (Chapter 4). Realistic depression cones will only develop if there is a contrast in hydraulic conductivities between the colmation layer and the connected aquifer. However, high enough flow rates through the clogging layer must be allowed in order to prevent groundwater wells from falling dry. These observations open possibilities for future activities which should focus on providing a more observational base to properly parameterize magnitude and anisotropy in the permeability

values of the respective components. Indeed, as a first attempt, I also found that by considering a 10:1 ratio of anisotropy (horizontal to vertical) for the whole Cenozoic succession would allow for high enough flow rates towards the well galleries. To validate these values, in situ measurements would be necessary and are not available as of now, however, all values used for the models in this regard are derived from grain size distributions after Devlin (2015) and Devlin (2017) and are well within the range reported for the region (Manhenke et al., 2001; Limberg and Thierbach, 2002). Concerning the hydraulic properties presented in this chapter of the thesis, a large range of values has been tested to assess how far the overall conclusions are valid. In particular the key geological unit Rupelian has been parameterized very low conductivity (0.1 mD $\approx$ 9.6E-10 m/s, Sippel et al. (2013)) to low conductivity (33.6 mD $\approx$ 3.23E-07 m/s, after Devlin (2015)) wherein always keeping a contrast in permeability between the Rupelian and the over- and underlying clastics.

The models produced for answering the second question of this thesis depict the most up to date representation of the subsurface of Berlin as a whole in terms of considered physics, geometry of model units and boundary conditions. However, there are still open questions remaining which can be seen in the extent and depth of the predicted depression cones locally diverging from the present day situation. While the models already depict a high degree of complexity, especially in the shallow model domain, geological data show even more complex structures (Zech and Stoltmann, 2012). These complexities are of special relevance given the already high degree of utilization of the subsurface and the possibility of interactions not yet resolved in the models. An increase in the complexity of the hydraulic boundary conditions is another aspect that should be taken into account for future studies. Especially groundwater recharge and cross-boundary-flow might influence the model result significantly, but are difficult to constrain and implement, given the scarcity of data and opting for a balanced model. Moreover, groundwater production has been considered on this scale for the first time, but was generalized to a certain degree. Therefore, time series of different well galleries should be considered in order to fully elucidate time sensitive effects on groundwater circulation and subsurface temperatures. Another major component of the system which is likely connected to groundwater pumping - groundwater contamination - should also be investigated in more detail and is discussed in a separate section Section 7.4.

7.3. Geothermal Potential

Open scientific question: Geothermal potential and geothermal exploration: Can we make use of numerical models as effective additional tools?

In order to answer this question, I will first provide a short review on the physical processes controlling the temperature distribution in the subsurface of Berlin to different degrees. While describing those physics I will also reiterate the links with respect to the first two discussion points in a way that will help better addressing the proposed question.

7.3.1. Controls on Temperature Distribution

The main practical outcome of the work presented in this thesis is to provide a substantial basis to further elaborate, on a more quantitative base, on the potential for heat provision from the geological subsurface in Berlin. The city is herein to be taken as a working example for a complex urban area. With this particular point in mind, the following paragraph will focus on an exhaustive, though brief discussion on the thermal subsurface regime, in the light of the results presented so far. The point here is to discuss the regional to local patterns of the temperature distribution at depths with reference to its potential economic usage. Therefore, attention will be mainly at explaining the thermal characteristics via the causative processes and their interactions with the hydrogeological structures of regional interest. The thermal configuration beneath Berlin is controlled by three factors: (1) the geometry of model units and connected heterogeneous distributions of thermal rock and fluid properties, (2) the thermal boundary conditions describing the amount of heat entering from the deeper components into the basin system (basal bc) and the sensitivity of shallow temperature to surface loadings (upper bc), and (3) the relevant heat transport mechanisms, being conduction and advection. As discussed in the previous chapter, with regard to the geological configuration, an extremely important unit is represented by the Zechstein salt layer. This unit displays higher thermal conductivities than the surrounding clastics. In addition, rock salt is also characterized by relatively low permeability values, close to impervious conditions and it shows a high level of structuration as evident in numerous pillows and diapirs revealed by seismic observations. Therefore, this sequence exerts a first order control on the city wide thermal configuration and hydraulic patterns. Within a purely diffusive thermal regime, i.e. when no additional heat transport components are considered, the temperature distribution around major salt structures shapes itself into a dipole anomaly with higher than background thermal gradients at the base of the salt dome and lower than background gradients at its top. These aspects are also clearly visible on a regional level, as for the temperature distribution extracted at constant depth levels from the 3D model. Below and inside major salt domes of the Zechstein, colder temperatures are predicted, because heat is carried upwards efficiently here (chimney effect) and warmer temperatures are found where the Zechstein is thin. The opposite trend can be observed above the Zechstein. Here, maximum temperatures are found at thickness maxima, because the excess heat carried from below is stored here by thermal blanketing resulting from the suprasalt sediment cover, and lowest temperatures are found where the Zechstein is thin.

The second controlling factor is the thermal boundary condition set-up. First of all, a differentiation between the upper and lower thermal boundary condition is necessary. The lower thermal boundary condition should represent the heat input coming into the sedimentary sequence from the deeper (crustal and mantle) subsurface. Given the relatively long time scale of diffusive crustal and mantle processes, its temporal variations could be neglected in models targeting the thermal regime from within the sedimentary pile. However, it is of utmost importance to set proper magnitudes of heat incoming from the deeper domains below the basement, since this heat in place corresponds to the whole energy budget available within the sedimentary cover. For this reason, I make use of a multistage workflow in order to set up a

proper basal thermal boundary condition. This follows a two-stage modeling approach, where I make use of a full lithosphere scale conductive model (including the deeper crustal and mantle lithosphere domains). This model is cut to extract the temperature distribution at the base of the sedimentary cover to then enforce a spatially variable thermal boundary condition for the coupled simulations. The upper thermal boundary condition should represent the effect of surface loading (climatic and human induced) on the surface and shallow subsurface temperature. Given the shorter time scales of the processes responsible for those variations, the assumption of constant and fixed through time values can be questioned. In order to include these aspects in the models, I opted for two different realizations. The first utilizes fixed temperatures derived from groundwater temperature measurements for the uppermost four geological interfaces. This was done in order to represent the present day state of the subsurface most accurately for the steady state simulations. The temperature distribution depicts increased temperatures below heavily populated regions, and lower temperatures below forests and sparsely populated areas. The second approach implements heterogeneously distributed temperatures at the surface, derived from long term air temperature measurements, depicting a similar distribution compared to the one described previously. Elevated temperatures (above rural average temperatures) are the result of a processes commonly referred to as urban heat islands (Menberg et al., 2013). Interestingly, these surface thermal anomalies can be traced at greater depths ($\geq 100\,m.b.s.$), an observation that testifies the relevance of other than diffusive processes being active in the subsurface. They have however little influence on the deep geothermal field and therefore also for the two reservoirs under study for this thesis. For this reason, I opt not to carry out any sensitivity analysis on the influence of temporal variations in surface temperature on the subsurface thermal field in this thesis.

Of major importance for the temperature distribution in the subsurface and the observations described above are the different heat transport mechanisms at work. These are conduction, advection and convection, each showing different wavelengths and depth dependencies. As stated above, conduction of heat can be considered in such tectonic inactive settings as the the background heat transport mechanism, which, depending of the specific hydrogeological conditions, can be locally overprinted by the other two mechanisms. The latter two processes are mainly effective in the shallow model domain, where less compacted sedimentary rocks still display high enough permeability values for groundwater transport to be effective on a regional scale. Because rock permeability decreases with depth, due to compaction and additional fluid chemistry reactive processes, the relevance of advection and convection in the overall thermal budget decreases also with depth. This leaves conduction as the dominant transport mechanism at greater depth levels. One of the most important factors while modeling these nonlinear transport phenomena related to fluid (groundwater) motion is the set up of the hydraulic boundary conditions. Indeed, the hydraulic gradient imposed at the uppermost surface level provides the force for groundwater to move into the sedimentary pile, thus effectively influencing the depth and lateral extent of the aforementioned mechanisms in the subsurface. With this in mind, and also recalling the previous discussions, I carefully and systematically tested different realizations of hydraulic boundary conditions in the present work, thus arriving at a quantification

of their respective influence on the resulting hydrodynamics and thermal configuration. The main observation in this regard is that any changes in the hydraulic forcing represented by the hydraulic gradient of the boundary condition are also reflected in the thermal field. Areas where the hydraulic gradient increases show lower temperatures at depth and vice versa in comparison to surrounding areas. This aspect has been discussed in detail in Chapter 4, where I have demonstrated how the distribution of shallow temperatures connects closely to forced uprising of warm water at well galleries and in low hydraulic potential areas, where also high temperatures are predicted. Low temperatures are predicted where strong infiltration is caused by high hydraulic potentials or gradients, also as a side-effect caused by groundwater pumping. The depth influence of this general forcing additionally depends on the parameterization of model units (poro-perm relationship) and their respective geometry. This is best exemplified by the Rupelian aquitard, which if parameterized as fully impervious, acts as an internal no flow boundary thus inhibiting any hydraulic connections between the supra- and sub-aquifers but in direct vicinity of areas of discontinuities (hydrogeological windows). Intra-aquifer connection across this clay layer has also been found to be more vigorous than expected if a proper, that is, more realistic parameterization of the aquitard is considered, thus resembling to a closer level field observations (Tesmer et al., 2007; Möller et al., 2007).

7.3.2. Predicted Temperatures and Geothermal Potential

The term "urban heat islands" recently gained increased focus, as the energy policies of major urban centers have been gradually switching towards a more substantial portion of renewable resources. In detail, most studies first focus on identifying the urban heat island and its effects in general (Taylor and Stefan, 2009; Yalcin and Yetemen, 2009; Westaway and Younger, 2016) and only few studies focus on identifying the so called "heat in place" (Menberg et al., 2015) connected to such an anomalous thermal configuration. Since these estimates rely on a few parameters only, the need for additional studies, which permit to model the complex behavior of groundwater and heat in 3D is still an open demand. As shown by the results of this thesis, any changes adopted in either the hydraulic or thermal characteristics (i.e. boundary conditions) might have far reaching effects. Therefore, any planning of utilizing the very shallow geothermal resources should be done with caution, also given the sensitivity of the system to groundwater pollution.

The same accounts for the identification and utilization of the deep geothermal potential. As outlined in this thesis, the salinization of the freshwater compartments might already be initiated through groundwater pumping in connection with drinking water production. Consequently, any deep geothermal utilization should be planned carefully. In this regard, the modeling workflow adopted in this thesis might provide an additional powerful tool at the hands of experts and decision makers to best plan activities for deep and shallow geothermal heat production. In this regard, possible detrimental effects onto the regional to local groundwater circulation patterns are considered. This is testified in this work, by making use of the modeling results to compute an estimation of the geothermal potential in place at different depth levels beneath the city of Berlin (Chapter 5). In this respect, the models have shown, that highly heterogeneous temperature

distributions are predicted for all depth levels, deviating significantly from the commonly used assumption of a diffusive background thermal gradient of 30 $\frac{K}{km}$. The complex geometry of model units, their heterogeneous physical properties and the resulting heat transport mechanisms lead to this rather complex temperature distribution. In the shallow model domain (-300 m.a.s.l.) promising areas are predicted in the central western part of the city, where up to 24°C are reached and therefore present interesting targets for shallow geothermal utilization. Low geothermal potential is predicted for areas like the northeast of Berlin, where only 15°C are predicted for the same depth and should therefore be considered as energetically less favorable areas (considering open systems). Worth mentioning is that at these depth levels, the thermal configuration is strongly affected by transient processes including heat advection by groundwater. This has been clearly demonstrated in this thesis by quantifying the effect of each modification to the model setting (hydraulic boundary conditions) on the resulting shallow thermal field and related geothermal potential. The deeper model domain (-3000 m.a.s.l.) shows a different pattern of temperature anomalies. Here, the central southern as well as the eastern half of the city, display temperatures up to 116°C, making those regions promising. This is especially the case under major rim synclines, where relatively thick clastics sequences mark these regions as promising targets for deep geothermal utilization.

In order to provide more quantitative estimates of the potential of specific identified areas, Chapter 6 focused on the results of predictions for potential geothermal wells by considering virtual geothermal doublets. In this regard, I followed and modified the approach outlined in Kastner et al. (2015). Based on the temperatures predicted by the models, along with the physical parameters of the reservoirs under study, quantitative predictions about the potential at each targeted point in the model have been determined. These potentials show that the nominal producible heat is distributed in a highly heterogeneous manner with maxima around $\sim 10\,MW_{th}$ for the Middle Buntsandstein and $\sim 3MW_{th}$ for the Rotliegend. Taking the critical well separation of the geothermal doublet as a minimum theoretical distance into account, an overall geothermal potential of the model area for these two aquifers would sum up to $11.4\,GW_{th}$. This theoretical value represents the technical potential only to some extent and does not take the economical factor into account. However, it stands representative for the energy that could physically be produced from two deep reservoirs in certain bounds. As stated in Chapter 6, these estimates depend on a series of assumptions, which need to be further quantified to make robust predictions, the most important of which is represented by the uncertainty in permeability. Once suitable places have been identified in this way, the implementation of thermal wells in the 3D models could be envisaged, the results of which could be shared with local governmental bodies. This methodology could also be easily applied to existing 3D models or temperature fields given data availability and would represent a powerful tool in identifying promising areas worth further investigation.

7.4. Groundwater Salinization

In connection with the reliable provision of clean energy from geothermal installations, another important aspect, especially in Berlin, is the possibility of contamination of fresh water resources. Fresh water supply in Berlin relies extensively on a Cenozoic regional aquifer system separated from the lowermost Mesozoic brackish to saline aquifers by a clay enriched unit, namely the Rupelian Clay aquitard. The effective sealing capacity of this aquitard is still a subject of debate, thus representing a topic of current discussions in the scientific community as well as in the governmental agencies and water suppliers. Here, two competing hypotheses are proposed: saltwater uprising (1) through hydrogeological windows featuring an impermeable Rupelian and (2), in areas of low hydraulic potential or active waterworks, independent of hydrogeological windows, with a low permeability Rupelian. Therefore, recent studies focused on investigating the influence of its geometry, as well as physical properties on the resulting fluid flow field and pore pressure distribution. Here, not only a more continuous lateral character with only few discontinuities has been proposed (Sippel et al., 2013; Frick et al., 2016b), but also an increase in the utilized hydraulic conductivity (Frick et al., 2015, 2016b). These improvements show that local connections between the compartments are likely strongest where the Rupelian is discontinuous, but might also occur in areas where high hydraulic gradients are present at the surface. These results are in agreement with chemical investigations done by Tesmer et al. (2007), outlining that there is a high degree of mixture of meteoric waters below the base of the Rupelian, conceptualized by considering across formational flow. This investigation also supports observations of local salinization above the top of the unit, even in locations where no discontinuity is present (Cai et al., 2015). In this case, especially high flow rates towards groundwater production wells could be problematic, as far reaching modifications related to the latter can be observed in the models. First observations concerning this process have already been measured and should therefore be investigated thoroughly (Möller et al., 2007; Tesmer et al., 2007; Cai et al., 2015). These conclusions are drawn on the fluid circulation alone but do not consider mass transport as of now. Simulations concerning this topic should be envisaged for the future, opting for reproducing already observed uprising of saline water including identifying the responsible processes (natural vs. anthropogenic). The results could then also be used for making predictions of how future utilization scenarios (geothermal, hydraulic), would impact these processes. These investigations are of utmost interest because of the heavy reliance on groundwater for the drinking water production of Berlin. Due to the general trend of decreasing precipitation and therefore groundwater recharge, a drop in groundwater levels is also to be expected, outlining the sensitivity of water supply in the region. The models of this thesis and their successors could therefore be used to develop strategies to mitigate possible water scarcity or contamination for the municipality of Berlin.

7.5. Anthropogenic Overprinting

Concerning anthropogenic overprinting, I suggest to discuss the specific situation in Berlin in more detail. The most important consideration is that most measurements that can be obtained

(i.e. temperature, pressure/hydraulic head) show different degrees of modification in comparison with expected natural distributions. The degree of overprinting in this regard can be correlated with different observables. For the temperature distribution in the shallow subsurface, this means that increased temperatures are mostly observed where a high amount of surface sealing is prevalent, also connecting to heat input from housing and industry and recently to climate change (Henning and Limberg, 1995; Henning and Limberg, 2012). To implement these observations in the models to some degree, two ways were chosen as described in Chapters 3 and 4. These implementations both show that elevated surface and shallow subsurface temperatures can be observed even at greater depths, due to advective heat transport processes, extending the depth of penetration and the lateral spreading of this anthropogenic overprinting. A more dynamic approach, opting for capturing the development of the elevated subsurface temperatures to then be able to also move forward in time would be to consider the proposed causes (Limberg, 2018). In detail this would require adding surface sealing in terms of hydraulics and thermics, as well as artificial heat sources to the models. An effect that is already considered in the models of Chapter 4 are elevated surface temperatures (derived from mean air temperatures). However this system is a lot more complex and should be considered separately if opting for a more detailed representation which could be of importance for the shallow subsurface and therefore also shallow geothermal utilization. An interesting aspect of the anthropogenically overprinted shallow temperature field is represented by the steadily increasing amount of shallow geothermal heat pumps. As mentioned in the introduction, more than 7000 of those are already installed (mostly closed loop systems), but their effect on the fluid flow and temperature field has not been systematically investigated. This is of particular interest since $\sim 10\%$ of those show some form of leakage (Limberg, 2018), which might have considerable effect, locally, and also regionally when considering cumulative effects.

In terms of anthropogenic overprinting of groundwater circulation, several factors are of importance. The most prominent one amongst them is groundwater pumping, represented in the models via lowered hydraulic heads or directly as production wells. Here, significant modifications in the pore pressure fields and the resulting groundwater circulations can be traced to depths up to -4800 $m.a.s.l.$ and spatially cover almost the entire model region in accordance with their respective catchments (Fig. 10 in Möller and Burgschweiger, 2008). This also leads to temperature differences on the order of interest for geothermal exploitation, especially in the shallow domain. Another aspect is represented by artificial groundwater recharge which is not considered in the models as of now, but would lead to an increase in the hydraulic load and therefore stronger infiltration of cold surface water. Not necessarily man made, but an anthropogenic effect nonetheless is also the decrease in groundwater recharge due to climate change which would have considerable impact on the groundwater levels and therefore circulation as well.

All of these observations are of particular interest, since they outline to which extent future utilization of the subsurface might impact and interact with the different groundwater compartments, also with respect to contamination and climate change (e.g. reduction in groundwater recharge) and therefore calls for a careful planning of any activity in the urban subsurface. However, this should not discourage any utilization, given the enormous potentials

outlined in this thesis.

7.6. Summarizing Discussion

In the general framework of subsurface utilization and the provision of clean energy an in depth understanding of the complex interplay of the different processes in the subsurface is of major importance. This thesis therefore targets questions concerning this topic, opting for producing a most up to date representation of the subsurface of Berlin and the processes therein.

In this, the models of this thesis show how different components of the system exert influence on different temporal and spatial scales. In the context of geothermal utilization of the subsurface it was shown, that to make reliable predictions to some extent, a variety of factors have to be taken into consideration. Especially the impact of overprinting due to human activities as well as the re-examination of the representation of shallow geological units shows, that far reaching effects can be induced by local changes in the system. The modification of the hydraulic boundary condition through human action causes a high degree of redistribution of re- and discharge intensities which should be taken into consideration for municipalities relying to large parts on groundwater for drinking water production. In this regard, modelers should aim for a most dynamic implementation of this component. The same holds true for the thermal overprinting (urban heat islands) where increased groundwater temperatures likely have far reaching effects on groundwater ecology and quality, but only minor impact on groundwater circulation. However, the occurrence and management of this phenomenon has gained increased attention recently and represents a significant component in the shallow subsurface which should be represented in any geothermal utilization modeling efforts.

In terms of the provision of heat from the shallow to deep subsurface, this thesis outlines the enormous theoretical potential. Given the temperature field predicted by the models of this thesis, temperatures of interest are reached at technically feasible depth ranges. Combined with suitable hydraulic properties encountered at depth, the amount of producible heating power for a single geothermal doublet in the model amounts up to $\sim 10\,MW_{th} = 0.28{*}10^{15}\,J$ which is equivalent to the annual heating demand of $\sim$ 19000 households. Given the fact, that Berlin features good, but not exceptional characteristics for geothermal utilization, this value is likely even higher for cities located in "hotter" regions (i.e. Munich, Frankfurt, Hamburg). These estimates are only for a single power-plant, and given the fact that the spacing (at least from the subsurface perspective) below two of these installations can be as small as less than a kilometer, the cumulative potential is theoretically of considerable size. The bottleneck in this kind of scenario is the technical and economical aspect which reduces these estimates in their feasibility. Due to the fact, that nuclear and coal based provision of heat and electricity is discontinued, aided by technological developments in the geothermal sector, the feasibility will likely increase in the near future. To fasten this process, precise knowledge of promising areas for geothermal utilization and the understanding of the involved processes need to be ensured, particularly to reduce the involved risks.

8. Conclusion

This thesis shows the need for highly detailed state of the art 3D models of the geological structure and connected physical parameters in order to make reliable predictions of the shallow to deep distribution of heat and fluids in the subsurface. This need involves updating as well as considering more detailed representations of the present state, as well as reconstructing a state before any human action. The models presented in this thesis therefore show different controlling factors and implications for the understanding and sustainable utilization of the geological underground below urban centers, such as the city of Berlin:

1. The distribution of heat and pore pressure in the subsurface of Berlin derives mainly from the geometry of model units and the resulting distribution of hydraulic and thermal properties in space, as well as the choice of boundary conditions. Here, the deep subsurface is dominated by conductive processes, while the shallow subsurface is strongly overprinted by a regime of mostly advective but also convective heat transport.
2. The shallow thermal and hydraulic configuration of the subsurface is highly modified by human actions connected to the urban environment. In detail, both, the groundwater circulation and the temperature distribution are modified by groundwater pumping for the former, and surface sealing for the latter. These are represented as boundary conditions in the models of this thesis and show significant influence on the modeling results.
3. Major surface water bodies have a significant influence on the shallow to intermediate geothermal and hydrogeological setting especially where connected to areas of anthropogenic overprinting. As a large share of groundwater production relies on the process of bank filtration, forced infiltration from surface water bodies is observed in reality and has been resolved for a first time for the extent of a large urban area. Most strikingly, complete reversals in predicted fluid flow patterns and connected advective heat transport are results of these models. The thermal perturbations of these modifications are on the order of interest for shallow geothermal installations and also connect to a shift in areas most promising for exploitation.
4. Groundwater production wells and their effect on groundwater circulation can only be approximated crudely by a fixed hydraulic boundary condition (Dirichlet) since predicted flow rates are several orders of magnitude lower than observed production rates. Therefore, the implementation of wells as active elements (Well boundary condition) produces more realistic flow rates, also showcasing modifications of fluid pathways which are in accordance with observations at an exemplary site in Berlin (Karolinenhöhe).
5. Reconstructing a "natural" state before the commissioning of the wells depicts a complete replenishment of the depression cones in a time-framing close to that of the activity of the wells. The results show the expected shift of recharge and discharge areas to a typical setting for the area where rivers and lakes display gaining conditions only.
6. Model results are highly sensitive to the parameters under study, which highlights the amount of caution that should be given to any planned change in the utilization of the

subsurface. This relates to any planned geothermal utilization of the different groundwater compartments which should be studied in depth using the models of this thesis as starting conditions.

7. The geothermal potential of the deeper subsurface shows nominally promising results, depicting up to $\sim 10\,MW_{th}$ for a single virtual power plant. Integrating these estimates over the entire modeling area results in a theoretically possible production of $11.4\,GW_{th}$. However these results do not regard the economical and legal feasibility of such a project. A further development of the estimation tool is envisaged and could also be expanded to different regions world-wide. Uncertainties related to the prediction of possible utilization scenarios also relate to the paucity of in situ measurements. The most important of these lies in the permeability of the reservoirs under study and models should therefore be updated as soon as new data become available.

9. References

Published

Books and Book Chapters

Anderson, M. P., Woessner, W. W., and Hunt, R. J. (2015). *Applied Groundwater Modeling: Simulation of Flow and Advective Transport*. Academic press.

Bjørlykke, K. (2015). "Heat Transport in Sedimentary Basins." In: *Petroleum Geoscience*. Springer, pp. 273–277.

Breisig, V., Claudy, P., Kohlmorgen, P., Tillner, S., Uhr, P., and Zein, M. (2015). "Energiewende-Outlook: Kurzstudie Wärme." In: *Energiewende-Outlook*. PricewaterhouseCoopers Aktiengesellschaft Wirtschaftsprüfungsgesellschaft.

Clauser, C. (2006). "Geothermal Energy." In: *Landolt-Börnstein, Group VIII: Advanced Materials and Technologies, Vol. 3: Energy Technologies, Subvol. C: Renewable Energies Chapter: 8*. Ed. by K. Heinloth. Heidelberg-Berlin: Springer Verlag, pp. 493–604. DOI: 10.1007/b83039.

Clauser, C. (2011). "Radiogenic Heat Production of Rocks." In: *Encyclopedia of Solid Earth Geophysics*. Springer, pp. 1018–1024.

Das, B. M. (2013). *Advanced Soil Mechanics*. CRC Press.

Diersch, H. J. (2014). *FEFLOW - Finite Element Modeling of Flow, Mass and Heat Transport in Porous and Fractured Media*. Berlin: Springer.

Griebler, C., Kellermann, C., Stumpp, C., and Hegler, F. (2015). *Auswirkungen Thermischer Veränderungen Infolge Der Nutzung Oberflächennaher Geothermie Auf Die Beschaffenheit Des Grundwassers Und Seiner Lebensgemeinschaften: Empfehlungen Für Eine Umweltverträgliche Nutzung*. Umweltbundesamt.

Holzbecher, E. O. (1998). *Modeling Density-Driven Flow in Porous Media: Principles, Numerics, Software*. Vol. 1. Springer Science & Business Media.

Hoth, P., Seibt, A., Kellner, T., and Potsdam, G. (1997). *Geothermie Report 97-1: Geowissenschaftliche Bewertungsgrundlagen Zur Nutzung Hydrogeothermaler Ressourcen in Norddeutschland*. Scientific Technical Report. Geoforschungszentrum. URL: https://books.google.de/books?id=nF1LnQEACAAJ.

Huenges, E. and Ledru, P. (2011). *Geothermal Energy Systems: Exploration, Development, and Utilization*. John Wiley & Sons.

Jarmersted, C. (1992). *Hydraulische Und Hydrochemische Aspekte Der Uferfiltration an Der Unterhavel in Berlin*. Vol. 140. Berliner Geowissenschaftliche Abhandlungen. Berlin: Selbstverlag Fachbereich Geowissenschaften, FU Berlin.

Kuttler, W., Oßenbrügge, J., and Halbig, G. (2017). "Städte." In: *Klimawandel in Deutschland*. Ed. by G. P. Brasseur, D. Jacob, and S. Schuck-Zöller. Berlin, Heidelberg: Springer Berlin Heidelberg, pp. 225–234. DOI: 10.1007/978-3-662-50397-3_22.

Maystrenko, Y, Bayer, U, Brink, H.-J., and Littke, R (2008). "The Central European Basin System–an Overview." In: *Dynamics of Complex Intracontinental Basins*. Springer, pp. 16–34.

Nield, D. A. and Bejan, A. (2006). *Convection in Porous Media*. Vol. 3. Springer.

Squillacote, A. H., Ahrens, J., Law, C., Geveci, B., Moreland, K., and King, B. (2007). *The Paraview Guide*. Vol. 366. Kitware.

Twidell, J. and Weir, T. (2015). *Renewable Energy Resources*. Routledge.

VDI (2010). *Thermische Nutzung Des Untergrundes: Grundlagen, Genehmigungen, Umweltaspekte*. Thermische Nutzung Des Untergrundes VDI 4640. Düsseldorf: Verein Deutscher Ingenieure e.V.

Zech, A. and Stoltmann, N. (2012). "Geologische Schnitte Ost-West; Panketal." In: *Geologischer Atlas von Berlin*. Ed. by A. LIMBERG. Red. by S. D. for Urban Development. Senate Department for Urban Development and the Environment.

Articles

Bayer, U., Scheck, M., and Koehler, M. (1997). "Modeling of the 3D Thermal Field in the Northeast German Basin." In: *Geologische Rundschau* 86.2, pp. 241–251.

Beyer, W. and Banscher, E. (1975). "Zur Kolmation Der Gewässerbetten Bei Der Uferfiltratgewinnung." In: *Zeitschrift für Angewandte Geologie* 21, pp. 565–569.

Bianchi, M. and Pedretti, D. (2017). "Geological Entropy and Solute Transport in Heterogeneous Porous Media." In: *Water Resources Research*.

Blöcher, G., Regenspurg, S., Kranz, S., Henninges, J., Norden, B., Saadat, A., and Huenges, E. (2018). "Hydraulic Performance of a Scientific Aquifer-Thermal-Energy-Storage (ATES) Site in Berlin (Germany)." In: *EGU General Assembly Conference Abstracts*. Vol. 20, p. 12831.

Blöcher, M. G., Zimmermann, G., Moeck, I., Brandt, W., Hassanzadegan, A., and Magri, F. (2010). "3D Numerical Modeling of Hydrothermal Processes during the Lifetime of a Deep Geothermal Reservoir." In: *Geofluids* 10.3, pp. 406–421. DOI: 10.1111/j.1468-8123.2010.00284.x.

Boothroyd, I. K. (2009). "Ecological Characteristics and Management of Geothermal Systems of the Taupo Volcanic Zone, New Zealand." In: *Geothermics* 38.1, pp. 200–209.

Brielmann, H., Griebler, C., Schmidt, S. I., Michel, R., and Lueders, T. (2009). "Effects of Thermal Energy Discharge on Shallow Groundwater Ecosystems." In: *FEMS Microbiology Ecology* 68.3, pp. 273–286.

Brielmann, H., Lueders, T., Schreglmann, K., Ferraro, F., Avramov, M., Hammerl, V., Blum, P., Bayer, P., and Griebler, C. (2011). "Oberflächennahe Geothermie Und Ihre Potenziellen Auswirkungen Auf Grundwasserökosysteme." In: *Grundwasser* 16.2, p. 77.

Brühl, H. (1975). "Grundwasser Im Baugrund in Berlin, Eine Einführung." In: *Zeitschrift der Deutschen Geologischen Gesellschaft*, pp. 207–210.

Brühl, H. and Trapp, C. (1983). "Eigenschaften Des Tieferen Grundwassers Im Nördlichen Stadtgebiet von Berlin (West)." In: *Zeitschrift der Deutschen Geologischen Gesellschaft*, pp. 923–941.

Cacace, M., Kaiser, B. O., Lewerenz, B., and Scheck-Wenderoth, M. (2010). "Geothermal Energy in Sedimentary Basins: What We Can Learn from Regional Numerical Models." In: *Chemie der Erde - Geochemistry* 70, Supplement 3, pp. 33–46. DOI: 10.1016/j.chemer.2010.05.017.

Cai, J., Taute, T., and Schneider, M. (2014). "Saltwater Upconing below a Pumping Well in an Inland Aquifer: A Theoretical Modeling Study on Testing Different Scenarios of Deep Saline-Groundwater Pathways." In: *Water, Air, & Soil Pollution* 225.11, p. 2203.

Cai, J., Taute, T., and Schneider, M. (2015). "Recommendations of Controlling Saltwater Intrusion in an Inland Aquifer for Drinking-Water Supply at a Certain Waterworks Site in Berlin (Germany)." In: *Water Resources Management* 29.7, pp. 2221–2232. DOI: 10.1007/s11269-015-0937-7.

Cherubini, Y., Cacace, M., Scheck-Wenderoth, M., Moeck, I., and Lewerenz, B. (2013). "Controls on the Deep Thermal Field: Implications from 3-D Numerical Simulations for the Geothermal Research Site Groß Schönebeck." In: *Environmental earth sciences* 70.8, pp. 3619–3642.

Devlin, J. F. (2017). "Reply to Comment on "HydrogeoSieveXL: An Excel-Based Tool to Estimate Hydraulic Conductivity from Grain-Size Analysis": Technical Note Published in Hydrogeology Journal (2015) 23: 837–844, by J. F. Devlin." In: *Hydrogeology Journal* 25.2, pp. 593–596. DOI: 10.1007/s10040-016-1510-z.

Devlin, J. (2015). "HydrogeoSieveXL: An Excel-Based Tool to Estimate Hydraulic Conductivity from Grain-Size Analysis." In: *Hydrogeology Journal* 23.4, pp. 837–844.

Doytsher, Y., Kelly, P., Khouri, R., McLaren, R., and Müller, H. (2010). "Rapid Urbanization and Mega Cities: The Need for Spatial Information Management." In: *XXIV FIG International Congress Proceedings*. XXIV FIG International Congress. Ed. by C. Potsiou. Sydney, Australia. URL: https://fig.net/pub/fig2010/papers/ts01b%5Cts01b_potsiou_doytsher_et_al_4709.pdf.

Engeler, I., Hendricks Franssen, H. J., Müller, R., and Stauffer, F. (2011). "The Importance of Coupled Modelling of Variably Saturated Groundwater Flow-Heat Transport for Assessing River–Aquifer Interactions." In: *Journal of Hydrology* 397.3, pp. 295–305. DOI: 10.1016/j.jhydrol.2010.12.007.

Freymark, J., Sippel, J., Scheck-Wenderoth, M., Bär, K., Stiller, M., Fritsche, J.-G., and Kracht, M. (2017). "From 3D Gravity to Coupled Fluid and Heat Transport Modelling-a Case Study from the Upper Rhine Graben." In: *EGU General Assembly Conference Abstracts*. Vol. 19, p. 8651.

Frick, M., Scheck-Wenderoth, M., Sippel, J., and Cacace, M. (2015). "Sensitivity of a 3D Geothermal Model of Berlin with Respect to Upper Boundary Conditions." In: *Energy Procedia* 76, pp. 291–300. DOI: 10.1016/j.egypro.2015.07.864.

Frick, M., Sippel, J., Cacace, M., and Scheck-Wenderoth, M. (2016a). "Influence of Geological Structure and Geophysical Parameters on the Geothermal Field below the City of Berlin, Germany." In: *European Geothermal Congress Proceedings*.

Frick, M., Sippel, J., Cacace, M., and Scheck-Wenderoth, M. (2016b). "The Geothermal Field Below the City of Berlin, Germany: Results from Structurally and Parametrically Improved 3D Models." In: *Energy Procedia*. European Geosciences Union General Assembly 2016, EGU

Division Energy, Resources & the Environment (ERE) 97, pp. 334–341. DOI: 10.1016/j.egypro.2016.10.011.

Frick, M., Scheck-Wenderoth, M., Cacace, M., and Schneider, M. (2017). "3D Thermohydraulic Modeling of the Coupling of Surface Water Bodies to the Subsurface below the Major Urban Center of Berlin." In: *EGU General Assembly Conference Abstracts*. EGU General Assembly Conference Abstracts. Vol. 19. Vienna, Austria, p. 14624. URL: http://adsabs.harvard.edu/abs/2017EGUGA..1914624F.

Frick, M., Scheck-Wenderoth, M., Schneider, M., and Cacace, M. (2018a). "Surface to Groundwater Interactions beneath the City of Berlin - Results from 3D Models." In: *Geofluids* In Press.

Frick, M., Cacace, M., Scheck-Wenderoth, M., and Schneider, M. (2018b). "Transient Effects of Groundwater Pumping on the 3D Hydrothermal Configuration of Berlin." In: *EGU General Assembly Conference Abstracts*. EGU General Assembly. Vienna, Austria.

Graupner, B. J., Koch, C., and Prommer, H. (2014). "Prediction of Diffuse Sulfate Emissions from a Former Mining District and Associated Groundwater Discharges to Surface Waters." In: *Journal of Hydrology* 513, pp. 169 –178. DOI: 10.1016/j.jhydrol.2014.03.045.

Haacke, N., Frick, M., Scheck-Wenderoth, M., Schneider, M., and Cacace, M. (2018). "3-D Simulations of Groundwater Utilization in an Urban Catchment of Berlin, Germany." In: *Advances in Geosciences*. European Geosciences Union General Assembly 2018, EGU Division Energy, Resources & Environment (ERE) - EGU General Assembly 2018, Vienna, Austria, 8–13 April 2018. Vol. 45. Copernicus GmbH, pp. 177–184. DOI: 10.5194/adgeo-45-177-2018.

Hähnlein, S., Bayer, P., Ferguson, G., and Blum, P. (2013). "Sustainability and Policy for the Thermal Use of Shallow Geothermal Energy." In: *Energy Policy* 59, pp. 914–925. DOI: 10.1016/j.enpol.2013.04.040.

Hannapel, S, Hermsdorf, A, Pohl, S, Rietz, C, and Koseck, R (2007). "Aufbau von Sondermessnetzen Zur Überwachung Der Geogenen Grundwasserversalzung in Brandenburg." In: *Brandenburg Geowiss Beitr* 14.1, pp. 5–14.

Hannappel, S. and Asbrand, M. (2002). "Entwicklung Eines Hydrogeologischen Modells Im Unterirdischen Einzugsgebiet Eines Wasserwerks Im Lockergestein." In: *Schriftenreihe der Deutschen Geologischen Gesellschaft* 24, pp. 55–68.

Hebig, K. H., Ito, N., Scheytt, T., and Marui, A. (2012). "Review: Deep Groundwater Research with Focus on Germany." In: *Hydrogeology Journal* 20.2, pp. 227–243. DOI: 10.1007/s10040-011-0815-1.

Henning, A. and Limberg, A. (2012). "Variation of the Subsoil Temperature Field in Berlin as a Result of Climate Change and Urbanization." In: *Brandenburgische Geowissenschaftliche Beiträge, Cottbus* 19.1, pp. 81–92.

Henning, A. and Limberg, A. (1995). "Das Grundwasser-Temperaturfeld von Berlin." In: *Brandenburgische Geowissenschaftliche Beiträge* 2.1, pp. 97–104. URL: http://www.geobasis-bb.de/geodaten/lbgr/pdf/1_95_Henning_97-104.pdf.

Hirschl, B., Aretz, A., Dunkelberg, E., Neumann, A., and Weiß, J. (2011). "Potenziale Erneuerbarer Energien in Berlin 2020 Und Langfristig–Quantifizierung Und

Maßnahmengenerierung Zur Erreichung Ambitionierter Ausbauziele." In: *Schriftenreihe des IÖW* 198, p. 11.

Huenges, E., Kohl, T., Kolditz, O., Bremer, J., Scheck-Wenderoth, M., and Vienken, T. (2013a). "Geothermal Energy Systems: Research Perspective for Domestic Energy Provision." In: *Environmental Earth Sciences* 70.8, pp. 3927–3933. DOI: 10.1007/s12665-013-2881-2.

Huenges, E., Liebscher, A., Kastner, O., Kranz, S., and Zunft, S. (2013b). "Thermische, Mechanische Und Stoffliche Speicherung Im Geologischen Untergrund–Konzepte, Technologien Und Betriebserfahrungen." In: *Speichertechnologien • Speicherung Im Geologischen Untergrund*. Jahrestagung 2013 Des Forschungsverbundes Erneuerbare Energien (FVEE).

Ingerle, K. (1991). "Über Die Flussbettdurchlässigkeit Und Die Sauerstoffzehrung Des Uferfiltrats Im Staubereich von Donaukraftwerken." In: *Wasserwirtschaft* 81.9, pp. 415–422.

Jaupart, C., Mareschal, J. C., and Watts, A. B. (2007). "Heat Flow and Thermal Structure of the Lithosphere." In: *Treatise on geophysics* 6, pp. 217–252.

Jensen, P. K. (1990). "Analysis of the Temperature Field around Salt Diapirs." In: *Geothermics* 19.3, pp. 273–283.

Kaiser, B. O., Cacace, M., Scheck-Wenderoth, M., and Lewerenz, B. (2011). "Characterization of Main Heat Transport Processes in the Northeast German Basin: Constraints from 3-D Numerical Models." In: *Geochemistry, Geophysics, Geosystems - G3* 12.7. DOI: 10.1029/2011GC003535.

Kaiser, B. O., Cacace, M., and Scheck-Wenderoth, M. (2013a). "3D Coupled Fluid and Heat Transport Simulations of the Northeast German Basin and Their Sensitivity to the Spatial Discretization: Different Sensitivities for Different Mechanisms of Heat Transport." In: *Environmental Earth Sciences*, p. 17.

Kaiser, B. O., Cacace, M., and Scheck-Wenderoth, M. (2013b). "Quaternary Channels within the Northeast German Basin and Their Relevance on Double Diffusive Convective Transport Processes: Constraints from 3-D Thermohaline Numerical Simulations." In: *Geochemistry, Geophysics, Geosystems* 14, pp. 3156–3175. DOI: 10.1002/ggge.20192.

Kastner, O., Sippel, J., Scheck-Wenderoth, M., and Huenges, E. (2013). "The Deep Geothermal Potential of the Berlin Area." In: *Environmental Earth Sciences*, p. 20. DOI: 10.1007/s12665-013-2670-y.

Kastner, O., Sippel, J., and Zimmermann, G. (2015). "Regional-Scale Assessment of Hydrothermal Heat Plant Capacities Fed from Deep Sedimentary Aquifers in Berlin/Germany." In: *Geothermics* 53, pp. 353–367. DOI: 10.1016/j.geothermics.2014.06.002.

Kloppmann, W., Négrel, P., Casanova, J., Klinge, H., Schelkes, K., and Guerrot, C. (2001). "Halite Dissolution Derived Brines in the Vicinity of a Permian Salt Dome (N German Basin). Evidence from Boron, Strontium, Oxygen, and Hydrogen Isotopes." In: *Geochimica et Cosmochimica Acta* 65.22, pp. 4087–4101.

Kolditz, O., Ratke, R., Diersch, H.-J. G., and Zielke, W. (1998). "Coupled Groundwater Flow and Transport: 1. Verification of Variable Density Flow and Transport Models." In: *Advances in water resources* 21.1, pp. 27–46.

Krawczyk, C. M., Rabbel, W., Willert, S., Hese, F., Götze, H. J., and Gajewski, D. (2008). "Crustal Structures and Properties in the CEBS from Geophysical Evidence." In: *Dynamics of Complex Sedimentary Basins. The Example of the Central European Basin System.* Pp. 67–95.

Krems, G. (1975). "Die Grundwassersituation in Berlin (West) Und Die Auswirkungen von Grundwasserabsenkungen Im Rahmen von Baumaßnahmen Auf Den Grundwasserhaushalt." In: *Zeitschrift der Deutschen Geologischen Gesellschaft*, pp. 215–222.

Lampe, C. and Person, M. (2002). "Advective Cooling within Sedimentary Rift Basins—Application to the Upper Rhinegraben (Germany)." In: *Marine and petroleum geology* 19.3, pp. 361–375.

Limberg, A. and Thierbach, J. (1997). "Gliederung Der Grundwasserleiter in Berlin." In: *Brandenburgische Geowiss. Beitr.* 4.2, pp. 21–26.

Limberg, A and Thierbach, J (2002). "Hydrostratigrafie von Berlin-Korrelation Mit Dem Norddeutschen Gliederungsschema." In: *Brandenburgische Geowiss. Beitr* 9.1, p. 2.

Limberg, A., Jonas, O., and Kolberg, A. (2016). "Detektion Möglicher Fehlstellen Im Rupelton Durch Messung Der Spezifischen Elektrischen Leitfähigkeit in Tiefen Grundwassermessstellen Im Land Berlin." In: *Brandenburgische Geowiss. Beitr* 23, pp. 11–15.

Lior, N. (2010). "Sustainable Energy Development: The Present (2009) Situation and Possible Paths to the Future." In: *Energy* 35.10, pp. 3976–3994.

Lüders, V., Plessen, B., Romer, R. L., Weise, S. M., Banks, D. A., Hoth, P., Dulski, P., and Schettler, G. (2010). "Chemistry and Isotopic Composition of Rotliegend and Upper Carboniferous Formation Waters from the North German Basin." In: *Chemical Geology* 276.3–4, pp. 198–208. DOI: 10.1016/j.chemgeo.2010.06.006.

Lund, H., Werner, S., Wiltshire, R., Svendsen, S., Thorsen, J. E., Hvelplund, F., and Mathiesen, B. V. (2014). "4th Generation District Heating (4GDH): Integrating Smart Thermal Grids into Future Sustainable Energy Systems." In: *Energy* 68, pp. 1–11.

Maeng, S. K., Ameda, E., Sharma, S. K., Gruetzmacher, G., and Amy, G. L. (2010). "Organic Micropollutant Removal from Wastewater Effluent-Impacted Drinking Water Sources during Bank Filtration and Artificial Recharge." In: *Water Research* 44.14, pp. 4003–4014. URL: http://www.sciencedirect.com/science/article/pii/S004313541000223X.

Magri, F. (2004). "Derivation of the Coefficients of Thermal Expansion and Compressibility for Use in FEFLOW." In: *WASY White papers* 3, pp. 13–23.

Magri, F., Bayer, U., Jahnke, C., Clausnitzer, V., Diersch, H. J., Fuhrman, J., Möller, P., Pekdeger, A., Tesmer, M., and Voigt, H. J. (2005). "Fluid-Dynamics Driving Saline Water in the North East German Basin." In: *International Journal of Earth Sciences*, p. 14. DOI: DOI\\%002010.1007/s00531-005-0497-9.

Magri, F., Bayer, U., Tesmer, M., Möller, P., and Pekdeger, A. (2008). "Salinization Problems in the NEGB: Results from Thermohaline Simulations." In: *International Journal of Earth Sciences* 97.5, pp. 1075–1085.

Manhenke, V., Reutter, E., Hübschmann, M., Limberg, A., Lückstedt, M., Nommensen, B., Peters, A., Schlimm, W., Taugs, R., and Voigt, H. J. (2001). "Hydrostratigrafische Gliederung Des Nord-Und Mitteldeutschen Känozoischen Lockergesteinsgebietes." In: *Zeitschrift für*

angewandte Geologie 47.3, p. 4. URL: http://www.stadtentwicklung.berlin.de/umwelt/wasser/wasserrecht/pdf/hydrostratigrafie2001.pdf.

Marklund, L. and Wörman, A. (2011). "The Use of Spectral Analysis-Based Exact Solutions to Characterize Topography-Controlled Groundwater Flow." In: *Hydrogeology Journal* 19.8, pp. 1531–1543.

Massmann, G., Pekdeger, A., Heberer, T., Grützmacher, G., Dünnbier, U., Knappe, A., Meyer, H., and Mechlinski, A. (2007). "Drinking-Water Production in Urban Environments – Bank Filtration in Berlin." In: *Grundwasser* 12.3, pp. 232–245. DOI: 10.1007/s00767-007-0036-7.

Massmann, G., Knappe, A., Richter, D., and Pekdeger, A. (2004). "Investigating the Influence of Treated Sewage on Groundwater and Surface Water Using Wastewater Indicators in Berlin, Germany." In: *Acta hydrochimica et hydrobiologica* 32.4-5, pp. 336–350. DOI: 10.1002/aheh.200400543.

Massmann, G., Sültenfuß, J., Dünnbier, U., Knappe, A., Taute, T., and Pekdeger, A. (2008). "Investigation of Groundwater Residence Times during Bank Filtration in Berlin: A Multi-Tracer Approach." In: *Hydrological Processes* 22.6, pp. 788–801. DOI: 10.1002/hyp.6649.

Maystrenko, Y. P. and Scheck-Wenderoth, M. (2013). "3D Lithosphere-Scale Density Model of the Central European Basin System and Adjacent Areas." In: *Tectonophysics* 601, pp. 53–77.

Menberg, K., Bayer, P., Zosseder, K., Rumohr, S., and Blum, P. (2013). "Subsurface Urban Heat Islands in German Cities." In: *Science of the total environment* 442, pp. 123–133.

Menberg, K., Blum, P., Rivera, J., Benz, S., and Bayer, P. (2015). "Exploring the Geothermal Potential of Waste Heat Beneath Cities." In: *Proceedings World Geothermal Congress 2015*. International Geothermal Association.

Mercer, J. W. and Pinder, G. F. (1974). "Finite Element Analysis of Hydrothermal Systems." In: *Finite element methods in flow problemsanalysis of hydrothermal systems. University of Alabama Press, Huntsville, AL*, pp. 401–414.

Moeck, I., Stiller, M., Pussak, M., Meinert, P., Bauer, K., Schurmann, S. B., and Hauptmann, M. (2015). "Geothermal Exploration in Megacities: Results from Reflection Seismic Surveying in Berlin (Germany)." In: *Proceedings World Geothermal Congress, Melbourne, Australia*. URL: https://pangea.stanford.edu/ERE/db/WGC/papers/WGC/2015/11071.pdf.

Möller, P., Weise, S. M., Tesmer, M., Dulski, P., Pekdeger, A., Bayer, U., and Magri, F. (2007). "Salinization of Groundwater in the North German Basin: Results from Conjoint Investigation of Major, Trace Element and Multi-Isotope Distribution." In: *International Journal of Earth Sciences* 97.5, pp. 1057–1073. DOI: 10.1007/s00531-007-0211-1.

Noack, V., Cherubini, Y., Scheck-Wenderoth, M., Lewerenz, B., Höding, T., Simon, A., and Moeck, I. (2010). "Assessment of the Present-Day Thermal Field (NE German Basin)—Inferences from 3D Modelling." In: *Chemie Der Erde-Geochemistry* 70, pp. 47–62.

Noack, V., Scheck-Wenderoth, M., and Cacace, M. (2012). "Sensitivity of 3D Thermal Models to the Choice of Boundary Conditions and Thermal Properties: A Case Study for the Area of Brandenburg (NE German Basin)." In: *Environmental Earth Sciences* 67.6, pp. 1695–1711.

Noack, V., Scheck-Wenderoth, M., Cacace, M., and Schneider, M. (2013). "Influence of Fluid Flow on the Regional Thermal Field: Results from 3D Numerical Modelling for the Area of

Brandenburg (North German Basin).” In: *Environmental Earth Sciences* 70, pp. 3523–3544. DOI: 10.1007/s12665-013-2438-4.

Norden, B., Förster, A., and Balling, N. (2008). “Heat Flow and Lithospheric Thermal Regime in the Northeast German Basin.” In: *Tectonophysics* 460, pp. 215–229.

Norden, B., Förster, A., Behrends, K., Krause, K., Stecken, L., and Meyer, R. (2012). “Geological 3-D Model of the Larger Altensalzwedel Area, Germany, for Temperature Prognosis and Reservoir Simulation.” In: *Environmental Earth Sciences* 67.2, pp. 511–526. DOI: 10.1007/s12665-012-1709-9.

Norden, B. (2011). “Modelling of the Near-Surface Groundwater Flow System at the CO2SINK Site Ketzin, Germany.” In: *Zeitschrift der Deutschen Gesellschaft für Geowissenschaften* 162.1, pp. 63–77.

Norden, B. and Förster, A. (2006). “Thermal Conductivity and Radiogenic Heat Production of Sedimentary and Magmatic Rocks in the Northeast German Basin.” In: *AAPG Bulletin* 90, pp. 939–962.

Nützmann, G., Levers, C., and Lewandowski, J. (2014). “Coupled Groundwater Flow and Heat Transport Simulation for Estimating Transient Aquifer–Stream Exchange at the Lowland River Spree (Germany).” In: *Hydrological Processes* 28.13, pp. 4078–4090. DOI: 10.1002/hyp.9932.

Otto, R. (2012). “Zur Abschätzung von Wärmeleitfähigkeiten Der Oberflächennahen Lockergesteinsschichtenfolge in Norddeutschland.” In: *Grundwasser* 17.4, pp. 219–229. DOI: 10.1007/s00767-012-0205-1.

Person, M., Banerjee, A., Hofstra, A., Sweetkind, D., and Gao, Y. (2008). “Hydrologic Models of Modern and Fossil Geothermal Systems in the Great Basin: Genetic Implications for Epithermal Au-Ag and Carlin-Type Gold Deposits.” In: *Geosphere* 4.5, pp. 888–917.

Pöppelreiter, M., Borkhataria, R., Aigner, T., and Pipping, K. (2005). “Production from Muschelkalk Carbonates (Triassic, NE Netherlands): Unique Play or Overlooked Opportunity?” In: *Geological Society, London, Petroleum Geology Conference series* 6, pp. 299–315. DOI: 10.1144/0060299.

Racz, A. J., Fisher, A. T., Schmidt, C. M., Lockwood, B. S., and Huertos, M. L. (2012). “Spatial and Temporal Infiltration Dynamics during Managed Aquifer Recharge.” In: *Groundwater* 50.4, pp. 562–570.

Ragnarsson, A. (2003). “Utilization of Geothermal Energy in Iceland.” In: *ICG 2003 Proceedings*. International Geothermal Conference. Reykjavík.

Reusswig, F., Hirschl, B., Lass, W., Becker, C., Bölling, L., and Clausen, W. (2014). “Machbarkeitsstudie Klimaneutrales Berlin 2050.” In: *Potsdamer institut für Klimafolgenforschung (PIK), Institut für Ökologische Wirtschaftsforschung (IÖW) und Andere, Berlin und Potsdam, Machbarkeitsstudie*.

Saar, M. O. (2011). “Review: Geothermal Heat as a Tracer of Large-Scale Groundwater Flow and as a Means to Determine Permeability Fields.” In: *Hydrogeology Journal* 19.1, pp. 31–52. DOI: 10.1007/s10040-010-0657-2.

Sanner, B., Kabus, F., Seibt, P., and Bartels, J. (2005). “Underground Thermal Energy Storage for the German Parliament in Berlin, System Concept and Operational Experiences.” In:

Proceedings World Geothermal Congress. Vol. 1, pp. 1–8. URL: http://sanner-geo.de/media/1438.pdf.

Scheck, M. and Bayer, U. (1999). "Evolution of the Northeast German Basin - Inferences from a 3D Structural Model and Subsidence Analysis." In: *Tectonophysics* 313, pp. 145–169.

Scheck, M., Bayer, U., and Lewerenz, B. (2003). "Salt Movement in the Northeast German Basin and Its Relation to Major Post-Permian Tectonic Phases - Results from 3D Structural Modelling, Backstripping and Reflection Seismic Data." In: *Tectonophysics* 361.3-4, pp. 277–299.

Scheck-Wenderoth, M., Maystrenko, Y., Hübscher, C., Hansen, M., Mazur, S., Littke, R., Bayer, U., Gajewski, D., and Nelskamp, S. (2008). "Dynamics of Salt Basins." In: *Dynamics of complex intracratonic basins: The Central European Basin System. XXIV*.

Scheck-Wenderoth, M. and Lamarche, J. (2005). "Crustal Memory and Basin Evolution in the Central European Basin System—New Insights from a 3D Structural Model." In: *Tectonophysics* 397.1, pp. 143–165.

Scheck-Wenderoth, M. and Maystrenko, Y. P. (2013). "Deep Control on Shallow Heat in Sedimentary Basins." In: *Energy Procedia* 40, pp. 266–275. DOI: http://dx.doi.org/10.1016/j.egypro.2013.08.031.

Scheck-Wenderoth, M., Cacace, M., Maystrenko, Y. P., Cherubini, Y., Noack, V., Kaiser, B. O., Sippel, J., and Björn, L. (2014). "Models of Heat Transport in the Central European Basin System: Effective Mechanisms at Different Scales." In: *Marine and Petroleum Geology* 55, pp. 315–331.

Scheck-Wenderoth, M., Frick, M., Cacace, M., and Sippel, J. (2017). "Overcoming Spatial Scales in Geothermal Modeling for Urban Areas." In: *Energy Procedia* 125, pp. 98–105. DOI: 10.1016/j.egypro.2017.08.080.

Sellner, D. and Fellenberg, F. (2011). "Atomausstieg Und Energiewende 2011–Das Gesetzespaket Im Überblick." In: *Neue Zeitschrift für Verwaltungsrecht (NVWZ)*, pp. 1025–1035.

Sippel, J., Fuchs, S., Cacace, M., Kastner, O., Huenges, E., and Scheck-Wenderoth, M. (2013). "Deep 3D Thermal Modelling for the City of Berlin (Germany)." In: *Environmental Earth Scienes* 70.8, pp. 3545–3566. DOI: 10.1007/s12665-013-2679-2.

Sippel, J., Scheck-Wenderoth, M., Noack, V., Moeck, I., Kastner, O., Stiller, M., Bredel-Schürmann, S., Kaden, R., and Krüger, A. (2012). "Exploration of Geothermal Reservoirs in the City of Berlin - a Pilot Study." In: *Unearthing Our Past and Future - Resourcing Tomorrow*. 34th International Geological Congress - IGC. Brisbane, Australia.

Sonntag, A. (2005). "Geologische Übersichtskarte 1:100000: Karte Der an Der Oberfläche Anstehenden Bildungen Mit Darstellung Ausgewählter Geotope Und Geologischer Objekte." In: *Brandenburgische Geowissenschaftliche Beiträge* 1.2. Ed. by G. u.R. L. Brandenburg. Landesamt für Bergbau.

Stephenson, R., Egholm, D. L., Nielsen, S. B., and Stovba, S. M. (2009). "Role of Thermal Refraction in Localizing Intraplate Deformation in Southeastern Ukraine." In: *Nature geoscience* 2.4, p. 290.

Taniguchi, M., Uemura, T., and Jago-on, K. (2007). "Combined Effects of Urbanization and Global Warming on Subsurface Temperature in Four Asian Cities." In: *Vadose Zone Journal* 6.3, pp. 591–596. DOI: 10.2136/vzj2006.0094.

Taylor, C. A. and Stefan, H. G. (2009). "Shallow Groundwater Temperature Response to Climate Change and Urbanization." In: *Journal of Hydrology* 375.3–4, pp. 601–612. DOI: 10.1016/j.jhydrol.2009.07.009.

Tesmer, M., Möller, P., Wieland, S., Jahnke, C., Voigt, H., and Pekdeger, A. (2007). "Deep Reaching Fluid Flow in the North East German Basin: Origin and Processes of Groundwater Salinisation." In: *Hydrogeology Journal* 15.7, pp. 1291–1306.

Van Balen, R. T., Verweij, J. M., Van Wees, J. D., Simmelink, H., Van Bergen, F., and Pagnier, H. (2002). "Deep Subsurface Temperatures in the Roer Valley Graben and the Peelblock, the Netherlands-New Results." In: *Netherlands Journal of Geosciences* 81.1, pp. 19–26.

Westaway, R. and Younger, P. L. (2016). "Unravelling the Relative Contributions of Climate Change and Ground Disturbance to Subsurface Temperature Perturbations: Case Studies from Tyneside, UK." In: *Geothermics* 64, pp. 490–515. DOI: 10.1016/j.geothermics.2016.06.009.

Yalcin, T. and Yetemen, O. (2009). "Local Warming of Groundwaters Caused by the Urban Heat Island Effect in Istanbul, Turkey." In: *Hydrogeology Journal* 17.5, pp. 1247–1255. DOI: 10.1007/s10040-009-0474-7.

Zhu, K., Blum, P., Ferguson, G., Balke, K.-D., and Bayer, P. (2010). "The Geothermal Potential of Urban Heat Islands." In: *Environmental Research Letters* 5.4, p. 044002. DOI: 10.1088/1748-9326/5/4/044002.

Zlotnik, V. A., Cardenas, M. B., and Toundykov, D. (2011). "Effects of Multiscale Anisotropy on Basin and Hyporheic Groundwater Flow." In: *Groundwater* 49.4, pp. 576–583.

Zlotnik, V. A., Toundykov, D., and Cardenas, M. B. (2015). "An Analytical Approach for Flow Analysis in Aquifers with Spatially Varying Top Boundary." In: *Groundwater* 53.2, pp. 335–341.

Thesis

Cai, J. (2014). "An Integrated Study of Hydraulic Anisotropy and Its Impact on Saltwater Intrusion in an Inland Aquifer." Ph.D. Dissertation. Freie Universität Berlin.

Karpf, C. (2012). "Modellierung Der Interaktion Zwischen Grundwasser Und Kanalisation." Ph.D. Dissertation. TU Dresden.

Ruf, W. (2007). "Numerical Modelling of Distributed River–Aquifer Coupling in an Alpine Floodplain." Ph.D. Dissertation. Universität Freiburg.

Verleger, H. (1988). "Zur Hydrogeochemischen Infiltrationsdynamik Im Bereich Der Unterhavel in Berlin (West)." Ph.D. Dissertation. Berlin: Freie Universität Berlin.

Viszkok, J. (2000). "Subsurface Fluid Flow Simulation with Finite Element Method in the East Pannonian Basin." Ph.D. Dissertation. Genève, Italia: Univ. Genève.

Zhu, K. (2013). "Urban Heat Island in the Subsurface and Geothermal Potential in Urban Areas." Ph.D. Dissertation. Eberhard Karls Universität Tübingen.

Unpublished

Technical and Institutional Reports

BBergG (2016). *Bundesberggesetz Vom 13. August 1980 (BGBI. I S. 1310), Das Zuletzt Durch Artikel 4 Des Gesetzes Vom 30. November 2016 (BGBI. I S. 2749) Geändert Worden Ist*. Bill BGBI. I S. 1310, BGBI. I S. 2749.

DWD (2015). *Mittelwerte 30-Jähriger Perioden Für Das Gebiet Berlin*. Offenbach, Germany: DWD.

Geodäsie, B. für Kartographie und (2012). *Digitales Geländemodell Gitterweite 10 m DGM10*. Bundesamt für Kartographie und Geodäsie.

Hasch, B. (2014). *Nachnutzungskonzept Rieselfelder Karolinenhöhe - Integriertes Gesamptkonzept*. Berlin: p2m berlin GmbH.

Lange, C., Klebsch, R., Faber, A., Schönewolf, J., Thur, M., Laakmann, C., Hollandt, F., Türkowsky, S., Weyer, G., Knorr, A., Haag, L., and Brehme, M. (2017). *Teilstudie Potenziale der Nutzung von Umweltwärme in der LHP*. Potsdam: Landeshaupt Potsdam Koordinierungsstelle Klimaschutz, p. 72.

Limberg, A. (2018). *Auswirkungen der Urbanisierung und des Klimawandels auf die Grundwasserleiter-Temperatur in Berlin*. Seminar Talk. Berlin: Senate Department for Urban Development and Housing.

Möller, K. and Burgschweiger, J. (2008). *Wasserversorgungskonzept Für Berlin Und Für Das von Den BWB Versorgte Umland (Entwicklung Bis 2040)*. Berlin: Berliner Wasserbetriebe.

S. Berlin-Brandenburg, A. f. (2016). *Energie Und CO2-Bilanz in Berlin 2013*. Amt für Statistik Berlin-Brandenburg.

S. Berlin-Brandenburg, A. f. (2018a). *Bevölkerungsentwicklung und Bevölkerungsstand im Land Brandenburg November 2017*. A I 7 – m 11/17. Amt für Statistik Berlin-Brandenburg. URL: https://www.statistik-berlin-brandenburg.de/publikationen/stat_berichte/2018/SB_E04-04-00_2015j01_BE.xlsx.

S. Berlin-Brandenburg, A. f. (2018b). *Bevölkerungsentwicklung und Bevölkerungsstand in Berlin November 2017*. A I 7 – m 11/17. Amt für Statistik Berlin-Brandenburg. URL: https://www.statistik-berlin-brandenburg.de/publikationen/stat_berichte/2018/SB_E04-04-00_2015j01_BE.xlsx.

S. Berlin-Brandenburg, A. f. (2018c). *Energie und CO2-Bilanz in Berlin 2015*. E IV 4 – j / 15. Amt für Statistik Berlin-Brandenburg. URL: https://www.statistik-berlin-brandenburg.de/publikationen/stat_berichte/2018/SB_E04-04-00_2015j01_BE.xlsx.

S. Berlin-Brandenburg, A. f. (2018d). *Energie und CO2-Bilanz in Brandenburg 2015*. E IV 4 – j / 15. Amt für Statistik Berlin-Brandenburg. URL: https://www.statistik-berlin-brandenburg.de/publikationen/stat_berichte/2018/SB_E04-04-00_2015j01_BE.xlsx.

Schälchli, U. (1993). *Die Kolmation von Fliessgewässersohlen: Prozesse Und Berechnungsgrundlagen*. Zürich: Technische Hochschule Zürich, p. 266.

Senate Department for Urban Development and Housing (2001). *Map: 04.02 Long-Term Mean Air Temperatures 1961-1990 (Edition 2001)*. Berlin: Senate Department for Urban

Development and Housing. URL: http://www.stadtentwicklung.berlin.de/umwelt/umweltatlas/ka402.htm.

Senate Department for Urban Development and Housing (2013). *02.13 Surface Runoff, Percolation, Total Runoff and Evaporation from Precipitation (Edition 2013)*. Berlin: Senate Department for Urban Development and Housing. URL: https://fbinter.stadt-berlin.de/fb/index.jsp?loginkey=showMap&mapId=wmsk02_13_02vers2012@senstadt.

SenStadtUm (2013a). *01.17 Geological Outline (Edition 2013)*. Berlin: Senate Department for Urban Development and the Environment.

SenStadtUm (2013b). *02.12 Groundwater Levels of the Main Aquifer and Panke Valley Aquifer (Edition 2013)*. Berlin: Senate Department for Urban Development and the Environment.

SenStadtUm (2014). *02.14 Groundwater Temperature (Edition 2014)*. Berlin: Senate Department for Urban Development and the Environment. Chap. 02 Water.

Wasserwirtschaft, B. e. V. Bundesverband der Energie-und (2015). *"Wie Heizt Berlin¿' – Studie Zum Heizungsmarkt. Berlin.* Berlin: B. e. V. Bundesverband der Energie- und Wasserwirtschaft.

Wedewardt, M. (2017). *Genehmigungsrechtliche Aspekte bei der Zulassung von Erdwärmeanlagen in Berlin.* Forum Presentation. Dresden, Germany.

Thesis

Frick, M. (2015). "Influence of Shallow Flow on the Deep Geothermal Field of Berlin - Results from 3D Models." Master's Thesis. Universität Potsdam.

Haacke, N. (2018). "Numerische 3D-Modellierung Der Komplexen Hydraulischen Verhältnisse Zwischen Der Unter-Havel Und Angrenzender Grundwasserleiter, Berlin." Master's Thesis. Berlin: Freie Universität Berlin.

Jaroch, A. (2006). "Stratifizierung Des Hydrogeologischen 3D Modells von Berlin Unter Berücksichtigung Qualifizierter Bohrungsinformationen." Master's Thesis. Technische Universität Berlin.

Liu, J. (2017). "Die Grundwasserdynamik im Grunewald - Aufbau eines numerischen Strömungsmodells." Master's Thesis. Berlin: Freie Universität Berlin.

Przybycin, A. M. (2011). "Sensitivity Study on Mesh Dependence for 3D Coupled Fluid- and Heat-Transport-Simulations- an Example from the North East German Basin." Master's Thesis. Freie Universität Berlin.

Manuscript

Frick, M., Lewerenz, B., Kastner, O., Scheck-Wenderoth, M., Schneider, M., and Cacace, M. (In Preparation). "The Geothermal Potential of the Subsurface of Berlin."

Appendix A.

Glossary

Different heat transport mechanisms and other topic specific terms are referenced frequently in this thesis. To assist the reader, who may not be familiar with these terms and mechanisms, brief definitions are provided.

A.1. Heat Transport Mechanisms

A.1.1. Heat conduction

Heat conduction is defined as the transfer of energy (heat) caused by temperature differences between or within bodies. The transfer of potential and kinetic energy (internal energy) is defined by microscopic collisions of particles and the movement of electrons and takes place in all phases of matter. The rate at which energy is then transferred is dependent of the difference in temperature between the two bodies and the properties of the conductive medium, for this thesis most relevant, the different rock types. Hence, in absence of any fluid motion within a closed system a thermal equilibrium will be established. Under steady state conditions this translates to a bodies conductivity being defined by a linear relationship between temperature gradient and the heat flux through a units cross sectional area as given by Fourier's law.

A.1.2. Advection (forced convection)

Advection is defined as the transfer of heat or mass by bulk fluid motion. This bulk motion is caused by an external active force leading to pressure (hydraulic head) gradients. The motion of the fluid is from areas of higher pressure to areas of lower pressure. In a typical hydrogeological setting, where the groundwater table mimics the topographic distribution to some extent, flow will then be parallel to gradients in topographic relief, that is from areas of high topography (recharge areas) to areas of low topography (discharge areas). In an anthropogenically overprinted setting these relationships might not hold true, thus a close examination of pressure distributions and flow directions is necessary to understand advective heat transport phenomena.

In this regime, the heat and/or mass is then transported by the bulk motion of the fluid, wherein a linear relationship between fluid velocities and temperature or mass gradients develops. Therefore, this mode of heat and mass transport is directly linked to the ease with which water might flow through the subsurface, represented by the hydraulic conductivity of the geological units. Due to this process being caused by pressure gradients, it is usually referred to as forced convection.

A.1.3. Free Convection

Free convection is a mode of heat or mass transfer which is not driven by any external forcing, that is the existence of pressure gradients. This mechanism is caused by intrinsic density differences in the fluid due to temperature or mass concentration gradients.

Free thermal convection relies of the principle of thermal expansion of a fluid if heated up. Due to its expansion it becomes less dense and will tend to rise. The rising body of hot fluid with then slowly lose its heat due to exchange with its surroundings (colder fluids) either directly or dispersively. Due to the heat loss the fluid contracts, becoming denser than the hotter fluid beneath, but cannot sink due to the rising fluid. The result is a lateral escape from the ascending column until reaching a distance where the gravitational forces of the cold fluid surpass the buoyant forces of the rising hot fluids. The resulting decent then leads to a repetition of warming, concluding the cycle. This circular motion is then referred to as a convection cell, whose size and velocity depend on the geological configuration of the subsurface. This process is rarely observed in nature due to the more prominent forced convectional heat transport mechanism overprinting the signature.

Free solute convection works in a similar way, where more saturated fluids are more dense, thus tending to descend, while less saturated fluids are less dense and therefore tend to rise. In a situation where those two fluid would be stacked on top of each other (e.g. infiltration of a saturated brine) fingers of dense fluid would descend parallel to fingers of less dense fluid rising. Therefore the denser fluid is displaced gravitationally downward and the less dense fluid is displaced upward. The sinking fluid will loose mass on its descend to the surrounding fluid through diffusive and dispersive phenomena.

A.2. Numerics

A.2.1. Hydraulic Head Boundary Condition

The hydraulic head boundary condition is a way of prescribing fixed hydraulic potentials to 3D (thermo)hydraulic models. It stands representative for a pressure [Pa] relative to the elevation [m] of the node it is prescribed to, the two of which are hard linked in the modeling software FEFLOW©. Instead of recalculating pressure (hydraulic head) for these nodes, they are fixed throughout the simulation. This results in either inflow at this node if the surrounding pressure or head is lower, or outflow if their potentials are higher. This boundary condition is applied if one knows the hydraulic potential of the area beforehand, like for surface water bodies or given a high data density for groundwater heads. A shortcoming of this approach is the possibility of the creation of infinite water source nodes, given extreme gradients between two nodes. This was checked and does not occur in the models of this thesis.

A.2.2. Well Boundary Condition

A well boundary condition refers to a node that features a predefined extraction or injection rate (volumetric flux, $\left[\frac{m^3}{s}\right]$). It is commonly used if the amount of water injected of abstracted is

priorly known. The most common use is to represent groundwater production wells (extraction) or geothermal doublets (injection and extraction).

A.2.3. Quasi Steady State

Due to the high non-linearity of the coupled problems presented in this thesis, all models were run in transient state for both, fluid and heat transport. Here, rapidly changing temperatures and pressures of all model nodes slowly stabilize (no change in both parameters over simulation time), to arrive at a stable solution called quasi-steady-state conditions. The latter was typically reached after approximately 250k yrs simulation time.

A.3. Hydrogeology

A.3.1. Hydraulic Properties

Permeability and porosity combined describe the ease which which water can pass through a volume of rock and can be used to define three classes: (1) aquifer, (2) aquitard, (3) aquiclude. Herein, an aquifer is a unit with both, high porosity and high permeability and is therefore promising for any kind of groundwater utilization. An aquitard is represented by a porosity and permeability high enough to allow leakage, but too low for any utilization. An aquiclude displays even lower permeabilities and porosities, has therefore no yield, thus effectively separating the former two types hydraulically form above or below.

A.3.2. Water Chemistry

In terms of water chemistry, the most important parameter discussed in this thesis is the saturation with dissolved halite. Here a four classes are separated: (1) fresh water $\left(0-5\frac{kg}{m^3}\right)$, (2) brackish water $\left(5-30\frac{kg}{m^3}\right)$, (3) saline water $\left(30-50\frac{kg}{m^3}\right)$, (4) briny water $\left(50-345\frac{kg}{m^3}\right)$.

A.3.3. Depression Cone

A depression cone is an areal drop in hydraulic heads developing during groundwater production from wells. The size of such a (semi)circular drop in hydraulic head depends on the hydraulic properties of the aquifer from which groundwater is produced from. If the depression of more than one groundwater well coincide, large areal extents of such depressions might develop as is exemplified in Berlin.

A.3.4. Rupelian Clay

The Rupelian Clay is a local aquitard of Oligocene age in the Northeast German Basin system. Since its deposition it has been massively restructured due to piercing from salt diapirs from below or glacial erosion from above. Therefore it displays a highly heterogeneous thickness distribution with numerous discontinuities called hydrogeological windows. This structural configuration is of high importance since this unit separates the brackish to saline aquifers below form the fresh

water aquifers above, its capability in doing so being a matter of ongoing discussions. An upconing of the saline water from below represents a major threat to the freshwater compartment from which Berlin produces all of its freshwater resources.

A.4. Anthropogenic Overprinting

Anthropogenic overprinting in the context of the subsurface mainly refers to all modifications of a natural relationships between surficial parameters and subsurface observables. In detail, this refers to increased subsurface temperatures due to artificial surface sealing (urbanization) or artificial heat sources (waste heat from buildings etc.). Another example is large scale groundwater abstraction leading to a drop in groundwater heads for extensive areas. These artificial modifications lead to a redistribution of groundwater circulation patterns as well as groundwater temperature. These are then also connected to changes in groundwater quality and ecology.

Another major source of anthropogenic overprinting is represented by groundwater contamination. Here, contaminants could have diverse sources, including riverine load, wastewater farming or anthropogenically mobilized geogenic salt.

A.5. Geothermal Potential

The term geothermal potential unfortunately does not have a clear cut definition. In this thesis I use the term referring to two main parameters of the modeling results. On the one hand, predicted temperatures of the models are used to identify above average temperature areas likely linking to a high geothermal potential, if being above a certain threshold. A more advanced definition is the physics based potential of producible heating energy. Here, the geothermal potential is defined by the maximum energy extractable from a reservoir in a production scenario. To identify the geothermal potential even more clear cut, considerations of the technical and economical feasibility of geothermal utilization should be investigated.

Appendix B.

Publications related to this Thesis

Frick, M., Scheck-Wenderoth, M., Schneider, M., and Cacace, M. (2018a). "Surface to Groundwater Interactions beneath the City of Berlin - Results from 3D Models." In: *Geofluids* In Press

Haacke, N., Frick, M., Scheck-Wenderoth, M., Schneider, M., and Cacace, M. (2018). "3-D Simulations of Groundwater Utilization in an Urban Catchment of Berlin, Germany." In: *Advances in Geosciences*. European Geosciences Union General Assembly 2018, EGU Division Energy, Resources & Environment (ERE) - EGU General Assembly 2018, Vienna, Austria, 8–13 April 2018. Vol. 45. Copernicus GmbH, pp. 177–184. DOI: 10.5194/adgeo-45-177-2018

Scheck-Wenderoth, M., Frick, M., Cacace, M., and Sippel, J. (2017). "Overcoming Spatial Scales in Geothermal Modeling for Urban Areas." In: *Energy Procedia* 125, pp. 98–105. DOI: 10.1016/j.egypro.2017.08.080

Frick, M., Lewerenz, B., Kastner, O., Scheck-Wenderoth, M., Schneider, M., and Cacace, M. (In Preparation). "The Geothermal Potential of the Subsurface of Berlin"